PTEN REGULATES THE DEVELOPMENT OF THE STEREOTYPED DENDRITIC ARBORS OF THE STARBURST AMACRINE CELL

By

Teva Wu Bracha

A DISSERTATION

Presented to the Neuroscience Graduate Program and the
Oregon Health & Science University School of Medicine
in partial fulfillment of the requirements for the degree of

Doctor of Philosophy

June 2025

Advisor, Kevin Wright, PhD

Member and Chair, Benjamin Sivyer, PhD

Member, John Brigande, PhD

Member, Anthony Barnes, PhD

Member, Renee Ryals, PhD

Table of Contents

Acknowledgements

This dissertation was a huge undertaking that would not have been possible without the help of many individuals. I have been incredibly lucky in life to have met these people and receive their support. Though I cannot reasonably acknowledge everyone individually, I hope you all know who you are. Thank you.

I was very fortunate to have my first real scientific experience joining the lab of Gulcin Pekkurnaz at UCSD. In that lab, I got my first taste of neuroscience by contaminating western blot paper, sabotaging neuronal cultures, and making many other mistakes. I must thank Gulcin for her patience and commitment to the growth and development of her lab members. I would not be doing graduate school without her. I also need to thank the lab who taught me and grew into scientists alongside me. In particular, Nathalie Djaja, Haoming Wang, and Blenda Yu were all amazing mentors and role models.

My undergraduate experiences prepared me well for graduate school, where joining the lab of Kevin Wright was probably one of the most important decisions I had the privilege of making. Kevin and the lab have created such an amazing environment for graduate research, and my PhD would not be the same without them. I want to thank Kevin in particular for being an incredibly supportive mentor, providing immense technical and project guidance while also trusting in me the independence to perform scientific research. For all the people in the lab I overlapped and interacted with, in no particular order: Patrick Kerstein, Daniel Miller, Matthew Pomaville, Jennifer Jahncke, Marissa Co, Alejandra Fernandez, Yessica Santana Agreda, Arielle Isakharov, Nina Luong, Frederika Sullivan, and Olivia Hougham --- Thank you for your help and insight as scientists, as well as creating a lab environment that is truly special to work in. Work

just wouldn't be the same without the spicy snacks, the chatter and laughter between lab members, and of course the incredible pieces of art that adorn the lab.

I was very fortunate to have a dissertation committee filled with both brilliant scientists and kind, considerate people. Thank you, Ben Sivyer, John Brigande, and Paul Barnes. Each of you provided important lessons to me along the way of my PhD. Thank you, Ben for being a supportive committee chair and helping coordinate the MEA experiments which allowed to expand my scientific horizons. Thank you, John for being so passionate about me and my science. I will always remember the times we got coffee and chatted about life and science. Thank you, Paul for continuing to stay involved and present even after leaving OHSU. My dissertation and scientific journey would be very different without the three of you advising me.

I would like to thank the ALMC for their support in the technical imaging and quantification of my project, as it is the fundamental basis of my findings. Thank you to core staff (Stefanie Kaech Petrie, Brian Jenkins, Hannah Bronstein, Felice Kelly) and in particular, Brian Jenkins, who helped me establish my confocal imaging paradigm and subsequent quantification in Imaris. Thank you for working with me and sending me so many Imaris remote licenses.

I am very lucky to have many friends to thank, from high school to college to graduate school, for keeping life fun even while working hard pursuing a PhD. It's unreasonable to name you all individually, so I would like to thank the group activities I have the pleasure of being in. I would like to thank my video game book club for keeping me connected with my friends and my love talking about video games alive. I would like to thank my commander group for

keeping me in touch with my love of Magic: the Gathering. I would like to thank my DnD group for creating a fun and safe space to slay some goblins, get casually gaslit, and, of course, save the world. Finally, I would like to thank the co-hosts of my very casual podcast, We Should Hangout More, Luke and Erik. Every time we record, I'm reminded of the year we lived together and how much fun it was to just be around you both. We really should hangout more.

There are two very important people I need to thank, which are my parents. Their support has been instrumental in my ability to go through graduate school and maintain a happy existence. They have always been there for me and that means more to me than words could ever express. Mom and Dad, thank you for everything.

Lastly, I want to thank my partner, Milana. I think the most important part of my PhD was meeting you. We've done so much in Portland and been able to create so many cherished memories. I love the moments we've created together, whether it be going to the Oregon Zoo Brew, getting $10 student tickets to the Oregon Symphony, going to OMSI afterdark, walking around the international rose test garden, hiking in the arboretum, going to the PSU farmer's market, getting coffee every Sunday, or any of the other experiences we got to have together. You bring so much color into my life, so thank you ☺.

List of Figures and Tables

Figure 4.1 Working model of *Pten* function and deletion in SACs

List of Abbreviations

AAV	Adeno-associated virus
ACh	Acetylcholine
AIY	Anterior interneuron Y
AKT	Protein kinase B
AMIGO2	Adhesion molecule with Ig like domains 2
ChAT	Choline acetyltransferase
cHet	Conditional heterozygous
CK2	Casein kinase 2
cKO	Conditional knockout
Cre	Cre recombinase
Da	Dendritic Arborization
DG	Dentate granule
DMA-1	LRRCT domain-containing protein
DSGC	Direction-selective ganglion cell
DSI	Direction-selective index
EPSC	Excitatory postsynaptic current
FLEx	Flip-Excision
FLRT2	Fibronectin leucine rich transmembrane protein 2
GABA	Gamma-Aminobutyric Acid
GAL4-UAS	Regulatory protein GAL4-upsteam activating sequence
GCL	Ganglion cell layer
GSK3β	Glycogen synthase kinase β
INBL	Inner Neuroblast Layer
INL	Inner nuclear layer
IPL	Inner plexiform layer
J-RGC	JAM-B retinal ganglion cell
LECT-2	Leukocyte cell-derived chemotaxin-2 homolog
MARCM	Mosaic analysis with a repressible cell marker

MEA	Multielectrode array
MEGF10	Multiple EGF like domains 10
MNR-1	Menorin
MORF	Mononucleotide repeat frameshift
MORF	Mononucleotide repeat frameshift
mTOR	Mammalian target of rapamycin
mTORC1	Mammalian target of rapamycin complex 1
mTORC2	Mammalian target of rapamycin complex 2
Pcdhg	Clustered g-protocadherins
PHTS	PTEN hamartoma tumor syndromes
PI3K	Phosphoinositide 3-kinase
PlexA2	Class A plexin receptor 2
pS6	Phosphorylated ribosomal protein S6
PTEN	Phosphatase and tensin homologue
PVD	Posterior Ventral D-Type
RasGAP	Ras GTPase-activating protein
S2	Sublamina 2
S4	Sublamina 4
SAC	Starburst Amacrine Cell
SAX-7	Neuroglian
Sema6A	Semaphorin 6A
SIX3	SIX homeobox 3
SYP	Synaptophysin
TSC1	Hamartin
TSC2	Tuberin
TSC2	Tuberous sclerosis complex 2
UNC5	Uncoordinated-5
WT	Wildtype

Abstract

Over the course of development, neurons form unique dendritic morphologies through discrete regulation of elongation, retraction, and branching. The starburst amacrine cell (SAC) is one such neuron that forms a stereotyped radially symmetric dendritic arbor with a "firework-like" branching pattern. SAC morphology is evolutionarily conserved across mammals and requires the activity of several transmembrane proteins to achieve its mature form. These transmembrane proteins control different aspects of SAC morphological development, including self-avoidance, arbor size, contacts between homotypic neighbors, and lamination of the inner plexiform layer. However, several other mechanisms must be involved to explain the stereotyped development of the SAC dendritic arbor, and in this dissertation I explore how the activity of an intracellular signaling protein, PTEN, regulates the branching architecture of SACs. I show that PTEN activity is essential for regulating SAC arborization, as the number of dendritic branches nearly doubles in *Pten-null* SACs. This phenotype arises in mice during the second postnatal week of SAC development and maintains at two months of age. Following *Pten* deletion, downstream activation of pS6 occurs at two weeks of age. Together, this suggests PTEN activity is critical by the second postnatal week to repress levels of pS6, and failure to do so leads to an increase of dendritic branching. Despite nearly doubling their branching, SACs show intact synaptic compartmentalization and their function in generating direction-selectivity in the retina appears intact. These findings present a novel role for PTEN in regulating SAC branching architecture during development. Collectively, these results advance our understanding of the mechanisms that guide neuronal morphological development.

Chapter 1: Introduction

Neurons are the building blocks that compose our minds and identities. Therefore, understanding the formation and preservation of neurons is of special interest to the field of neuroscience and the general public. A fundamental question yet to be answered is: "How does a neuron decide what it's going to be when it grows up?" I chose to address one aspect of this question by focusing on how a specific protein, phosphatase and tensin homologue (PTEN), regulates the decisions one neuronal subtype, starburst amacrine cells (SACs), makes during its development to achieve its mature form and function. This research contributes to a larger body of knowledge that is collectively working towards understanding what rules govern how a neuron determines its identity and the form it takes. This project stems from decades of research encompassing cellular and molecular neuroscience, neuronal morphology, SACs, and PTEN signaling—the histories of which I will briefly cover here.

The Birth of the Neuron and Modern Neuroscience

The field of modern-day cellular neuroscience began with the discoveries of Santiago Ramón y Cajal, who, in 1888, asserted and provided compelling evidence that neurons were in fact individual cellular entities, and not a connected reticulum (Ramón y Cajal 1888; López-Muñoz et al. 2006). Ramón y Cajal employed the newly invented Golgi stain, which allowed sparse labeling of neurons, to show that neurons had independent processes which were contiguous, rather than continuous, with one another (Golgi 1873; Mariotto et al. 2018). This theory, titled "the neuron doctrine," and the surrounding scientific discourse gave birth to and solidified the term "neuron" referring to what were formerly "nerve cells" or "nervous units"

(Waldeyer 1891). The processes of these neurons were also formalized into dendrites and axons, the areas of information input and output, respectively (His 1889). In 1897, the neuron doctrine lead to the conceptualization of the synapse, the site of chemical transmission and cornerstone of how neurons integrate information (Sherrington 1906; López-Muñoz et al. 2006). It wasn't until 1955 however, through the advent of electron microscopy, that the existence of the synapse was definitively confirmed, and the neuron doctrine proved irrefutably correct (Palade and Palay 1954; De Robertis and Bennett 1955). These fundamental discoveries are now the basis of modern cellular neuroscience.

Since then, our understanding of neuronal complexity has grown tremendously, and to draw meaningful conclusions from our work, the categorization of neurons into subtypes is critical (Armañanzas and Ascoli 2015; Zeng and Sanes 2017). The idea that neurons have different "types" also originates from Ramón y Cajal, as his drawings depicted a fraction of the incredible morphological diversity among neurons (Ramón y Cajal 1888). Today, we know that neurons have different cellular subtypes to perform vastly different functions (Azeredo da Silveira and Roska 2011). To define neuronal subtypes, we reference their molecular, electrophysiological, and morphological identities; i.e. the proteins they express, the electrical impulses they produce, and their physical structure/appearance (Zeng and Sanes 2017). The morphological information Ramón y Cajal used to deduce that neurons come in different types is still utilized today as a core aspect of neuronal identity.

The Study of Neuronal Morphology

For over a century, neuroscientists have sought to understand the principles that guide and direct neuronal morphology, the shape, structure and anatomical features of a neuron (Ramón y Cajal 1923; Jan and Jan 2003; Lefebvre et al. 2015). Neurons form circuits to process different types of information, such as motion and color, but can only form synaptic connections with circuit partners whose processes physically overlap. Where neurons localize their dendrites and axons is therefore critical to their function. Additionally, to adapt to the broad range of information processing needed in the nervous system, different neuronal subtypes developed type-specific morphological properties. For example, the JAM-B retinal ganglion cell (J-RGC) within the retina have an asymmetric, ventrally oriented dendrite which is specific for upwards motion (Kim et al. 2008; Figure 1.1F).

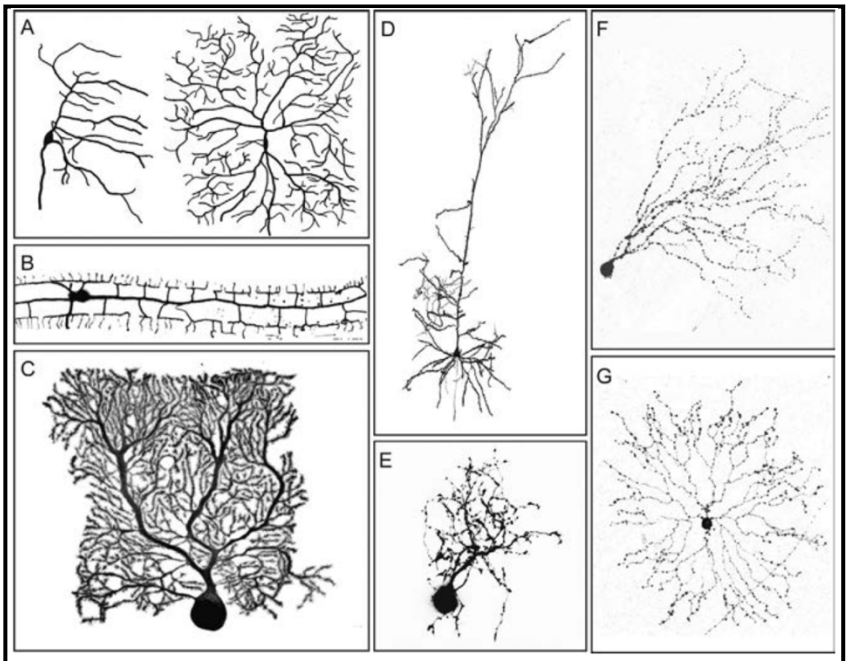

1.1 Models to Study Neuronal Morphology.
Neurons with stereotyped morphological features that are easy to target and manipulate have become excellent models to understand the principles that guide neurodevelopment. The cells shown are: (A) Class I (left) and Class IV (right) dendritic arborization (da) neurons from *D. melanogaster*, (B) Posterior ventral type D (PVD) neuron from *C. elegans*, (C) Purkinje neuron from *M. musculus*, (D) Pyramidal neuron from *M. musculus*, (E) Tectal neuron from *Xenopus* (F) J-retinal ganglion cell from *M. musculus*, and (G) Starburst amacrine cell from *M. musculus*. Figure from Lefebvre 2021 with the following acknowledgements: *Panel B: Adapted from Zou, W., Shen, A., Dong, X., Tugizova, M., Xiang, Y. K., & Shen, K. (2016). A multi-protein receptor-ligand complex underlies combinatorial dendrite guidance choices in C. elegans. eLife, 5, e18345. Panel D: Image courtesy of M. Scofield, Medical University of South Carolina. Panel E: Image courtesy of K. Haas, University of British Columbia. Some images are from Lefebvre, J. L., & Marocha, J. (2020). Chapter 12—Dendrite development: Vertebrates. In Rubenstein, J., Rakic, P., Chen, B., Kwan, K. Y., Kolodkin, A., & Anton, E. (Eds.), Cellular migration and formation of axons and dendrites (2nd ed.) (pp. 257–286). Academic Press*.

Given the functional importance of unique morphologies, understanding how they consistently arise during development is a fundamental question in the field of neurobiology.

The ability of scientists to dissect out the governing principles of neuronal morphology is wholly dependent on the tools available to visualize them. Technical innovations in microscopy, genetic targeting of cells, and sparse labeling methods have been critical in understanding what factors dictate a neuron's morphology (Fire 1986; Perrimon 1993; Minksy 1988; Gu et al. 1993; Lee and Luo 1999; Branda and Dymecki 2004). A few neuronal subtypes have emerged as quintessential models for the study of neuronal morphology due to their stereotyped morphological features and technical accessibility (Lefebvre 2021; Figure 1.1). Some of the key regulators of neuronal morphology are: (1) Transcription factors, proteins which bind to and regulate expression of genes; (2) Cell surface proteins/receptors, proteins which reside on the cell membrane and respond to extracellular cues; (3) Signaling pathways, proteins that engage in signaling cascades intracellularly to effect changes in cellular processes; and (4) Cytoskeletal effectors, proteins that actively shape and remodel the cytoskeleton (Lefebvre et al. 2015; Lefebvre 2021). Clear examples of how these fundamental mechanisms function to direct neuronal morphology can be seen in studies from simpler model organisms, notably the posterior ventral D-type (PVD) neurons from *C. elegans* (Figure 1.1B) and the dendritic arborization (da) neurons from *D. melanogaster* (Figure 1.1A) (Jan and Jan 2010).

PVD Neuron: Fundamental Mechanisms of Morphological Development

In 1982, Horvitz and Sternberg elegantly explained the value of studying simpler model organisms through three general principles: (1) Simpler organisms will facilitate better

understanding; (2) Many biological mechanisms will likely be universal and broadly applicable; and (3) "A detailed understanding of any biological phenomenon is likely to be interesting" (Horvitz and Sternberg 1982). During this time, the *C. elegans* field had just achieved the monumental feat of mapping out the complete post-embryonic lineages of all 959 somatic cells of the free-living nematode (Sulston and Horvitz 1977; Horvitz and Sternberg 1982; White et al. 1982). Combined with the development of *C. elegans* transgenics, the field now had a genetically tractable model organism to study basic biological principles (Fire 1986).

With its entire neuronal cell lineage mapped out, *C. elegans* has been a potent model organism to study the mechanisms that guide neurodevelopment. The PVD mechanosensory neuron in particular has been well-characterized due to its stereotyped morphology (Albeg et al. 2011). PVD neuron dendrites have a well-defined "candelabra-like" projection pattern, with their primary and tertiary branches extending laterally, and their secondary and quaternary branches extending vertically (Tsalik et al. 2003; Oren-Suissa et al. 2010; Figure 1.1B). These neurons extend their fourth order projections between muscle and hypodermis and are polymodal nociceptors responsive to harsh mechanical stimuli (Way and Chalfie 1989; Oren-Suissa et al. 2010; Albeg et al. 2011). Forward genetic screens, a method for determining relevant genes by causing random mutations then screening for phenotypes, have enabled the identification several proteins that are required for normal PVD dendrite development (Sundararajan et al. 2019). The proteins DMA-1 (LRRCT domain-containing protein), SAX-7 (Neuroglian), and MNR-1 (Menorin) were all identified to be extracellular adhesion proteins necessary for PVD dendrite development (Liu and Shen 2012; Dong et al. 2013). Cell-autonomous targeting, performing the manipulation specifically in the cell type of interest, of

PVD neurons and the surrounding muscle and hypodermis enabled scientists to build an accurate model for how these three proteins interact to form an adhesion complex between PVD neuron fourth order dendrites and the hypodermis, while requiring secreted LECT-2 (Leukocyte cell-derived chemotaxin-2 homolog) from nearby muscle cells (Dong et al. 2013; Díaz-Balzac et al. 2016; Zou et al. 2016). Many individual proteins with a broad range of functions required for normal PVD neuron dendrite development have been identified, including but not limited to: transcription factors, fusogens, proteases, endonucleases, GTPases, transporters, motors, and cytoskeletal regulators (Sundararajan et al. 2019). Additionally, because *C. elegans* is relatively transparent, time-lapse imaging of the real time development and dynamics of PVD neuron dendrites have been established (Smith et al. 2010) This study showed that first order dendrites extend initially, followed sequentially by second, third, and fourth order projections. PVD neuron dendritic growth is dynamic with several iterations of extension and retraction. These dynamics have been recapitulated in other neuronal subtypes as well showing this is likely a conserved biological mechanism (Palavalli et al. 2021; Shree et al. 2022; Wit and Hiesinger 2023; Ing-Esteves and Lefebvre 2024). In studying the PVD neuron, scientists have unveiled how several classes of protein, interaction with the local environment, and iterative extension/retraction events control a neuron's morphological fate.

Dendritic Arborization Neurons: Transcriptional Control of Morphology

The da neurons were first identified in 1987 through HRP immunostaining and were named based on the observation that they "gave rise to elaborate dendritic arborizations."

(Bodmer and Jan 1987). Despite this initial characterization, it would not be until 15 years later, in 2002, that the individual morphologies of the four da neuronal subtypes were visualized (Grueber et al. 2002). Key innovations in fly genetics and individual cell labeling through the GAL4-UAS (regulatory protein GAL4-upsteam activating sequence) system and MARCM (mosaic analysis with a repressible cell marker) allowed scientists to sparsely target and label distinct populations of cells in the fly (Brand and Perrimon 1993; Lee and Luo 1999). Upon visualization of the da neurons, it became clear that there were four distinct morphological subtypes of increasing complexity, with Class I having a small arbor with few dendritic branches and Class IV being the most densely branched and arborized. This sparked the question: "What mechanisms make these four related mechanosensory neurons so morphologically distinct?"

Fortunately, scientists uncovered a clue in 1990, when their studies showed that different da neurons expressed either no, low, medium, or high levels of a putative transcriptional regulator, Cut (Blochlinger et al. 1990). Uncoincidentally, each class of da neuron corresponded to a different level of Cut expression (Grueber et al. 2003). When *Cut* was selectively deleted from the da neurons, each class showed a reduction in dendritic complexity except for Class I da neurons, which already had no detectable levels of Cut. Conversely, ectopic expression of Cut in Class I neurons greatly increased their morphological complexity. This landmark study revealed how specific expression of a transcription factor can influence neuronal morphology. In similar studies, a Class I specific transcription factor, Abrupt, was shown to reduce arbor complexity in a Cut independent manner, while a Class IV specific transcription factor, Knot, was shown to increase arbor complexity synergistically with Cut (Sugimura et al. 2004; Li et al. 2004; Jinushi-Nakao et al. 2007). These three transcription

factors alone were able to explain the relative complexity of the da neurons and clarified the role of transcription factors in shaping dendritic arborization. RNAi knockdown of several different transcription factors in the da neurons identified 78 genes responsible for dendritic patterning and their roles in either increasing or decreasing dendritic arborization (Parrish et al. 2006). Importantly, this study implicated multiple different genetic programs in regulating the morphology of the da neurons, and the role of transcriptional programs in controlling discrete aspects of morphology, such as extension or branching, independently. The da neurons continue to be a tractable model to study and understand the regulation of dendritic morphology and have provided fundamental insights into the transcriptional control of neuronal shape (Parrish et al. 2006; Jan and Jan 2010; Kilo et al. 2021). Lessons from the PVD and da neurons have affirmed Horvitz and Sternberg's original assertion: simpler model organisms have provided a deeper understanding of the mechanisms underlying neuronal morphology.

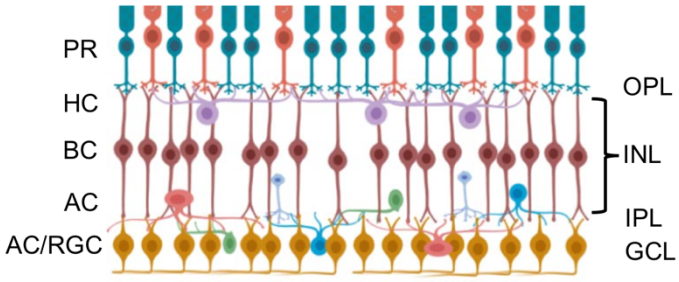

Figure 1.2 Schematic of the Retina.
The retina is a highly laminar and organized structure which functions to convert light into signals which can be processed for vision. Photoreceptors (PR) that transduce light into electrical signals and synapse with bipolar cells (BC) and horizontal cells (HC) in the outer plexiform layer (OPL). These BCs reside in the inner nuclear layer (INL) alongside amacrine cells (AC) and synapse with retinal ganglion cells (RGC) in the inner plexiform layer (IPL). RGCs are the primary output neuron of the retina and have axons which form the optic nerve and synapse in retinorecipient areas of the brain. RGCs themselves reside in the ganglion cell layer (GCL) alongside the displaced ACs. Starburst amacrine cells (SAC) are one of the many subtypes of amacrine cells which reside in both the INL and GCL.

Starburst Amacrine Cells: A Model for Morphological Analysis

The SAC is an excellent model to study neurodevelopment in a mammalian system, as they are well-characterized morphologically, functionally, and transcriptionally (Masland 2005; Taylor and Smith 2012; Yan et al. 2020). SACs

were named after their stereotyped radially symmetric, planar arbor with a “starburst” branching pattern (Famiglietti and Siegfried 1980; Famiglietti 1983a; Famiglietti 1983b; Figure 1.1G). This characteristic morphology is evolutionarily conserved and largely identical in cat, mouse, rat, rabbit, macaque, and humans (Tauchi and Masland 1984; Voigt 1986; Schmidt et al. 1987; Rodieck 1989; Wässle and Boycott 1991). SACs reside in two cell layers within the retina, the inner nuclear layer (INL) and ganglion cell layer (GCL), and stratify their entirely dendritic arbors in the inner plexiform layer (IPL) (Famiglietti 1987; Figure 1.2). SACs in the INL are responsive to the offset of light (OFF SACs) and stratify in sublamina 2 (S2) of the IPL, while SACs in the GCL are responsive to the onset of light (ON SACs) and stratify in sublamina 4 (S4) (Famiglietti 1983a). Functionally, SACs have a well-defined role in conferring direction-selectivity in visual processing (Yoshida et al. 2001; Amthor et al. 2002). SACs accomplish this by providing GABAergic inhibition to direction-selective ganglion cells (DSGCs) to stimuli in the null-direction, preventing DSGCs from firing (Fried et al. 2002; Taylor and Smith 2012). SACs also contribute to DS processing via co-release of acetylcholine (ACh) alongside Gamma-Aminobutyric Acid (GABA) to help improve DSGC responses under low contrast conditions (Sethuramanujam et al. 2016). SAC dendritic arbors are highly compartmentalized, receiving input from bipolar cells and other amacrine cells in the proximal two thirds of their arbor and providing GABAergic and cholinergic output to DSGCs in the distal third (Briggman et al. 2011). This structured organization makes a SAC intrinsically responsive to the direction of light as it passes across its arbor and innately ties the morphology of a SAC to its function (Morrie and Feller 2018). Crucially, SACs are genetically tractable as they are the only cholinergic neuron in

the retina and can be specifically targeted using a *ChAT*^{Cre} (Choline acetyltransferase Cre recombinase) mouse line (Hayden et al. 1980; Rossi et al. 2011).

Though the rough timeline of SAC morphological development in the mouse is well characterized, a comprehensive understanding of the molecular signaling driving SAC development remains elusive (Ford and Feller 2012; Lefebvre 2021). EdU labeling has revealed that progenitors fated to be SACs undergo their final cell division and become post-mitotic from E10.5-E12.5 (embryonic day 10.5-12.5) (Voinescu 2009). From there, SACs must first migrate radially to arrive at the nascent inner neuroblast layer (INBL) and then migrate tangentially to mosaically arrange their soma and achieve even coverage of the retina (Galli-Resta et al. 1997). Fezf1 expression in ON SACs mediates the differential migration of ON and OFF SACs, separating the two populations into the GCL and INL, respectively (Peng et al. 2020). By P0 SAC migration is complete, and they have begun to sprout their dendrites (Ray et al. 2018; Ing-Esteves and Lefebvre 2024). Elegant live-imaging studies have shown that from P2 to P14, SAC dendrites form an interconnected, spiderweb-like lattice that is dynamic, extending and retracting their arbors much like the PVD neurons of *C. elegans* (Ing-Esteves and Lefebvre 2024; Smith et al. 2010). This seemingly stochastic process is required for SACs to develop their final "starburst" morphology with little variation between cells.

Mechanisms of SAC Morphological Development

While the molecular mechanisms that regulate SAC morphology are not fully known, a few studies have shown that transmembrane proteins are critical for individual aspects of this process (Lefebvre et al. 2012; Sun et al. 2013; Ray et al. 2018; Soto et al. 2019; Prigge et al.

2023; Figure 1.3). The Pcdhgs (clustered g-protocadherins) are essential for SAC dendritic self-avoidance and self/non-self-recognition (Lefebvre et al. 2012). Loss of all *Pcdhg* isoforms causes SAC dendrites to co-fasciculate, resulting in uneven coverage of their dendritic field and the formation of autapses (Lefebvre et al. 2012; Kostadinov and Sanes 2015). During development SACs lacking the *Pcdhgs* show changes in their dynamics, accumulating stable self-contacting protrusions compared to controls due to reduced retraction events (Ing-Esteves and Lefebvre 2024). Adding back a single isoform is sufficient to rescue mature SAC morphology, but leads to increased avoidance

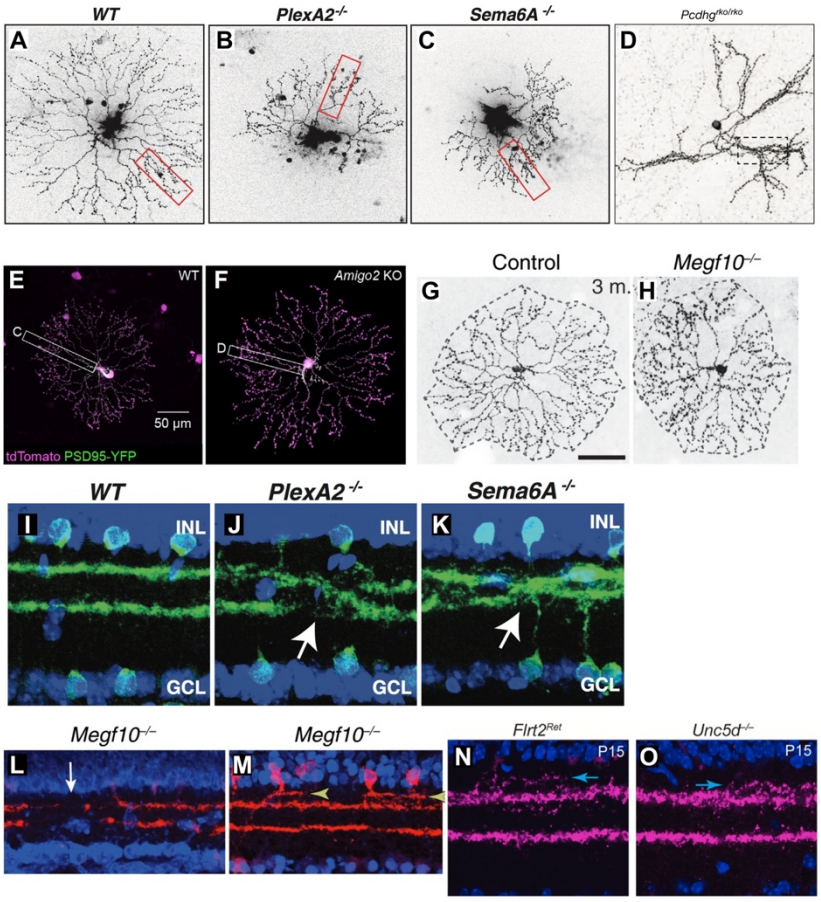

Figure 1.3 Known Transmembrane Proteins Important for SAC Morphology. Prior studies of SAC morphology have revealed a handful of transmembrane proteins that differentially affect the development of SAC morphology and lamination of the IPL. **A.** A wildtype SAC with a radially symmetric arbor and "firework-like" branching pattern. **B, C.** SACs lacking *PlexA2* and *Sema6A* show increased self-crossing of their dendritic arbor and disruptions to symmetry. **D.** *Pcdhg-null* SACs lack the ability to recognize self and fasciculate their dendritic arbors, causing a loss of dendritic coverage and symmetry. **E, F.** Loss of *Amigo2* causes SACs to expand their arbors 1.5 fold while maintaining their relative branch spacing and structure. **G, H.** SACs lacking *Megf10* appear mostly normal, but have reduced dendritic field area. **I-K.** In the absence of either *PlexA2* or *Sema6A* show crossovers between the dendrites of the INL and GCL SACs. **L, M.** *Megf10-null* SACs display gaps in their S2 and S4 bands, as well as ectopic projections into S1. **N, O.** Deletion of either *Flrt2* or *Unc5d* (Unc-5 Netrin Receptor D) causes SACs to misproject into S1. Figure is adapted from data from the following publications: Panels A-C and I-K: Sun et al. 2013; Panel D: Lefebvre et al 2012; Panels E-F: Soto et al. 2019; Panels G-H and L-M: Ray et al. 2018; Panels N-O: Prigge et al. 2023.

between neighboring SACs, emphasizing the necessity of multiple isoforms for heteroneuronal SAC interactions (Lefebvre et al. 2012).

PlexA2 (Class A plexin receptor 2) and its transmembrane ligand Sema6A (semaphorin 6A) are critical for defining the boundary between INL and GCL SACs (Sun et al. 2013). SACs in mice lacking PlexA2 or Sema6A show crossovers between their S2 and S4 bands. The phenotype differs between INL and GCL SACs, with the GCL SACs being much more profoundly impacted in their total dendrite length, field area, and symmetry. Notably, Sema6A is not required cell-autonomously in SACs for proper lamination of the IPL, but is required for normal SAC morphology (James et al. 2024). Differential expression levels of PlexA2 and Sema6A may explain the divergence between INL and GCL SACs and stands out as a mechanistic distinction in dendritic assembly between the two populations.

MEGF10 (multiple EGF like domains 10) is a transmembrane protein that acts as both a receptor and ligand to mediate SAC homotypic contacts which are required for proper innervation of the IPL (Ray et al. 2018). MEGF10 turns on in SACs once they have finished their radial migration to the INBL and is necessary for the tangential migration SACs undergo to form their somal mosaic (Kay et al. 2012). The homotypic contacts that occur during this time also mediate stratification in the IPL, and, when *Megf10* is deleted, SACs have gaps in their S2 and S4 bands and ectopic projections in S1 (Ray et al. 2018). Interestingly, *Megf10* deficient SACs have reduced dendritic field areas, but otherwise appear morphologically similar to controls. This suggests a primary role in dendrite stratification for MEGF10 in SAC development (Kay et al. 2012).

FLRT2 (fibronectin leucine rich transmembrane protein 2) and UNC5 (uncoordinated-5) are part of a receptor-ligand system which generates repulsive cues that refine targeting of SAC dendrites to S2 and S4 of the IPL (Prigge et al. 2023). When *Flrt2* or *Unc5d* are deleted from the retina, SACs show ectopic stratification in S1. FLRT2 is expressed in SACs while UNC5 is expressed in neighboring amacrine cells that stratify in S1, S3, and S5. These bands of expression are important for stratification of the IPL and ensure SACs and other neurons in the retina form a uniform laminar plexus (Prigge et al. 2023).

AMIGO2 (Adhesion molecule with Ig like domains 2) is a cell surface protein that regulates the size of the SAC dendritic field area (Soto et al. 2019). When *Amigo2* is deleted, SACs have an increased arbor size of approximately 50%, but their branching structure remains unchanged, simply scaling with the arbor increase. *Amigo2* deletion does not change the connectivity of SACs with its synaptic partners but does enhance the direction-selectivity of SACs (Soto et al. 2019). While the mechanism is unknown, *Amigo2* deletion in SACs delineates the regulation of arbor size and branching structure.

These studies have provided valuable insights into the regulation of SAC dendritic architecture by cell surface/transmembrane proteins; however, it remains unclear what downstream intracellular signaling is occurring. PlexA2 requires its cytoplasmic RasGAP (Ras GTPase-activating protein) activity to properly coordinate SAC lamination. When only the RasGAP domain is deleted from PlexA2 the disruption is much weaker compared to *PlexA2* knockouts, indicating the importance of other PlexA2 functions (James et al. 2024). Grasping how proteins involved in intracellular signaling pathways regulate specific aspects of SAC morphology would allow the field to match effects from transmembrane proteins to their

downstream signaling partners and build a more mechanistic understanding of SAC development, similar to the PVD and da neurons.

PTEN Signaling and Morphology

One such protein that seems to underlie neuronal morphology and many other aspects of cell biology is phosphatase and tensin homologue (PTEN). First discovered in 1997 as a putative tumor suppressor gene, PTEN has been widely studied for its role in cancer, cellular homeostasis, and regeneration (Li et al. 1997; Steck et al. 1997; Worby and Dixon 2014). PTEN's canonical function is a lipid phosphatase in the PI3K-AKT (Phosphoinositide 3-kinase-Protein kinase B) Pathway, where it serves as the primary inhibitor by opposing the activity of PI3K to prevent AKT signaling (Worby and Dixon 2024; Figure 1.4). AKT itself is a kinase that regulates several downstream signaling pathways, such as mTOR (mammalian target of rapamycin) and GSK3β (Glycogen synthase kinase 3-beta) (Manning and Toker 2017). The PI3K-

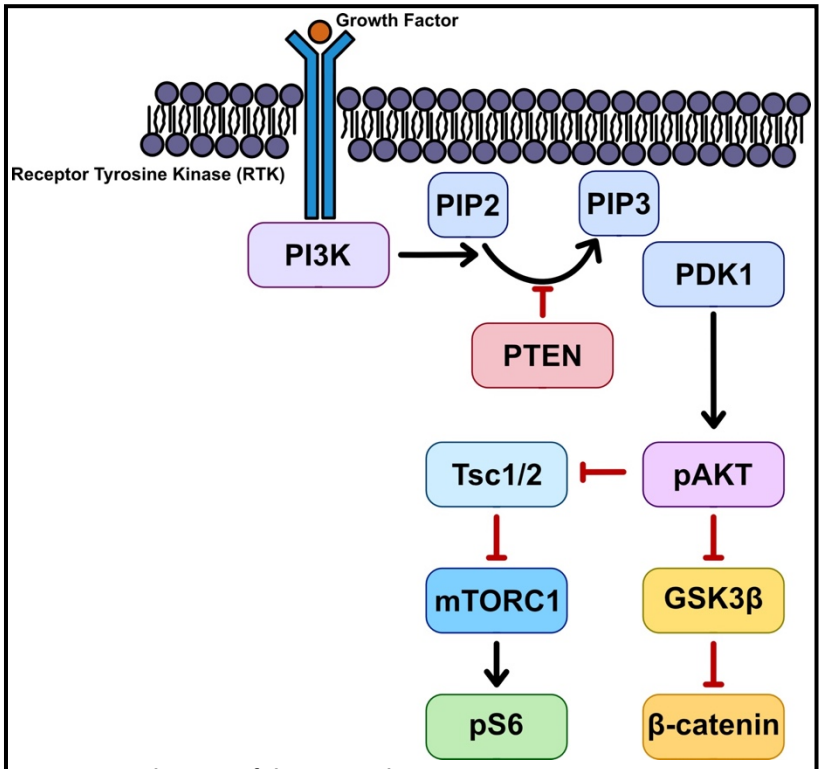

Figure 1.4 Schematic of the PI3K Pathway.
PTEN functions as the primary negative regulator of the PI3K pathway by dephosphorylating PIP3 to PIP2, preventing the generation of phosphorylated AKT and subsequent mTORC1 activation and GSK3β inhibition. mTORC1 activity can be specifically targeted through manipulations of TSC2. The downstream consequences of this regulation can be assessed by measuring levels of pS6 and β-catenin, respectively.

AKT pathway is a major signaling cascade that is implicated in several intracellular processes, including cell survival and apoptosis, cell cycling, proliferation, protein synthesis, cellular growth, and metabolism (Fruman et al. 2017). PTEN additionally has protein phosphatase activity and localizes to many specific subcellular compartments, such as the mitochondria, ER, and growth cone (Kreis et al. 2014; Bononi and Pinton 2015). PTEN is primarily a cytoplasmic protein with non-canonical roles in epigenetic regulation within the nucleus (Misra et al. 2021; Gupta et al. 2022).

PTEN regulates a multitude of cellular processes and is implicated in several neurodevelopmental disorders (Skelton et al. 2020). Cowden, Bannayan-Riley-Ruvalcaba, and Proteus syndrome are PTEN hamartoma tumor syndromes (PHTS) that have been described in patients with autism-spectrum disorder caused by heterozygous loss of *Pten* function (Zori et al. 1998; Goffin et al. 2001; Butler et al. 2005; Spinelli et al. 2015; Rademacher and Eickholt 2019). Genome-wide association studies and exome sequencing have shown PTEN to be a predominant autism-risk gene, and significant effort has gone into understanding the molecular mechanisms that result in the PHTS phenotypes of macrocephaly and learning disability (Grove et al. 2019; Satterstrom et al. 2020; Rademacher and Eickholt 2019). Mice heterozygous for PTEN show deficits in the migration of neural stem cells to the olfactory bulb, specification and development of inner and outer hair cells in the organ of Corti, and specification of dorsal root ganglion neurons in the spinal cord (Li et al. 2002; Dong et al. 2010; Fernandez et al. 2025). To further dissect out *Pten's* neurodevelopmental functions, *Pten* has been conditionally deleted in select neuronal populations, including dentate granule neurons, Purkinje neurons, inner ear neurons, motor neurons, and retinal neurons (Luikart et al. 2011; Cupolillo et al. 2016; Kim et

al. 2013; Reckendorf et al. 2022; Sakagami et al. 2012; Cantrup et al. 2012). These neurons typically show severe defects in the key developmental processes of proliferation, specification, migration, and lamination (Skelton et al. 2020). Functionally, neurons lacking *Pten* show changes in excitability and synaptic activity (Luikart et al. 2011; Cupolillo et al. 2016). Neurons also show broad morphological changes in the growth, caliber, and branching of their soma, axon, and dendrites (Kwon et al. 2001; Kwon et al. 2006; Luikart et al. 2011; Cupolillo et al. 2016; Reckendorf et al. 2022).

PTEN's effect on morphology has been characterized in several model organisms and neuronal subtypes (Kwon et al. 2006; Cupolillo et al. 2016; Gallent and Steward 2018; Chen et al. 2021). Conditional *Pten* deletion typically results in broad increases of neurite growth and arborization. This has been relatively well-studied in dentate granule (DG) neurons of the hippocampus, where loss of *Pten* causes both axonal and dendritic hypertrophy. Specifically, DG neuron axon outgrowth is increased while dendrites show ectopic growth alongside increases in length, branching, caliber, and spine density (Kwon et al. 2006; Santos et al. 2017). These cells show a high degree of dendritic overlap and perturbed self-avoidance. Neuronal activity modulates the degree of branching in DG neurons lacking *Pten*, but not their dendritic length (Skelton et al. 2020). Mechanistically, dynamic instability of microtubules seems critical for this phenotype, as reduction of microtubule polymerization with vinblastine reduces dendritic overgrowth (Getz et al. 2022). PTEN deletion in other neuronal subtypes exhibits a more specific morphological phenotype (Christiansen et al. 2011; Urwyler et al. 2019). The AIY (anterior interneuron Y) interneuron of *C. elegans* requires PTEN to control its neurite length, but loss of PTEN causes an unusual reduction in length through dysregulated downstream

FOXO signaling (Christiansen et al. 2011). In the dorsocentral neurons of *Drosophila*, RNAi knockdown of *Pten* causes a localized dramatic increase in branching, while minimally affecting other regions of the arbor (Urwyler et al. 2019). More studies in stereotyped neuronal subtypes (Figure 1.1) are needed to reconcile how PTEN regulates neuronal morphology in different contexts.

The role of PTEN in SAC Development

PTEN has been studied in SAC development, but its cell-autonomous role remains unclear (Sakagami et al. 2012; Cantrup et al. 2012; Jo et al. 2012; Tachibana et al. 2016). Two groups have utilized pan-retinal deletion of *Pten* in retinal progenitor cells to study retinal and SAC development (Sakagami et al. 2012; Cantrup et al. 2012). These deletions take effect by E9.5, before SACs are born, and impact every class of retinal neuron (Liu et al. 1994; Liu and Cvekl 2017). In this context, SACs show many developmental defects; SAC density is decreased, their mosaic arrangement is impacted, and some SACs migrate into the IPL. SACs fail to form laminar bands in S2 and S4 of the IPL, instead generating a diffuse wave of dendrite that bleeds more into S1 and S5 (Sakagami et al. 2012, Cantrup et al. 2012). These phenotypes are not unique to SACs, as the total number of amacrine cells and broad organization of the IPL are also disrupted (Tachibana et al. 2016). A follow up study using the same pan-retinal *Pten* deletion found SACs had defects in endocytic trafficking of cell surface proteins, including MEGF10, an important protein for SAC lamination (Touahri et al. 2024; Ray et al. 2018). While not directly investigated or quantified in any of these studies, SAC morphology is likely affected as well. However, these findings come from a retina whose development has been profoundly

disrupted beginning at E9.5. Every neuron in the retina has been perturbed, making it unclear if the effects on SACs are based on cell-autonomous loss of *Pten* or from downstream non-cell autonomous consequences of developing in a *Pten-null* retina.

Dissertation Overview and Findings

My dissertation aims to answer the question of how PTEN cell-autonomously regulates the morphological development of SACs. To accomplish this, I combined techniques from mouse genetics, immunohistochemistry, viral labeling, morphometric analysis, and multielectrode array (MEA) data analysis. I deleted *Pten* specifically from SACs within the retina using a $ChAT^{Cre}$ line (Backman et al. 2001; Rossi et al. 2011). This deletion of *Pten* begins at P1, just as dendritic arborization is beginning and allows for the study of PTEN's role in regulating morphology without prior developmental deficits (Ray et al. 2018). I sparsely labeled SACs using either intravitreal viral injections or a Tigre-MORF genetic reporter and reconstructed these cells in Imaris (Chapter 2; Veldman et al. 2020). Through these reconstructions, I was able to obtain morphometric data and discern discrete aspects of morphology that PTEN regulates in SACs. I evaluated the effects of PTEN deletion at multiple developmental timepoints to build a timeline of phenotypic development and align it with changes in downstream mTOR signaling. Finally, I analyzed multielectrode array (MEA) data to determine whether the morphological changes caused by *Pten* loss resulted in functional changes to direction-selectivity.

My work resulted in the following conclusions:

1. *ChAT*^{Cre}-mediated *Pten* deletion causes robust loss of PTEN specifically in SACs within the retina.
2. Cell-autonomous deletion of *Pten* via *ChAT*^{Cre} does not impact SAC proliferation, specification, and migration.
3. PTEN does not cell-autonomously regulate gross SAC lamination of the IPL.
4. PTEN cell-autonomously regulates SAC branch number and organization.
5. *ChAT*^{Cre}-mediated *Pten* deletion impacts SAC dendritic development between P14 and P21.
6. SACs lacking PTEN preferentially upregulate mTOR rather than GSK3β signaling.
7. *Pten* deletion-mediated upregulation of mTOR signaling in SACs precedes dendritic changes.
8. Despite morphological changes, SACs lacking PTEN have preserved synaptic compartmentalization and downstream DSGC (direction-selective ganglion cell) activity appears normal.
9. PTEN signaling does not appear to be primarily responsible for the phenotypes seen in previous studies that have investigated SAC morphology.
10. *ChAT*^{Cre}; *Tsc2*$^{f/f}$ (Tuberin) mice show inconsistent activation of mTOR signaling.

Chapter 2: Results

PTEN regulates starburst amacrine cell dendrite morphology during development

Teva W. Bracha[1], Nina Luong[1], Joseph Leffler[3], Benjamin Sivyer[3], Kevin M. Wright[2]

Affiliations:
1 – Neuroscience Graduate Program, Oregon Health & Science University, Portland, Oregon 97239
2 – Vollum Institute, Oregon Health & Science University, Portland, Oregon 97239
3 – Casey Eye Institute, Oregon Health & Science University, Portland, Oregon 97239

Abstract: Neurons are subject to extensive developmental regulation to ensure precise subtype-specific morphologies that are intimately tied to their function. Starburst amacrine cells (SACs) in the mammalian retina have a highly stereotyped, radially symmetric dendritic arbor that is essential for their role in direction-selective circuits in the retina. We show that PTEN, the primary negative regulator of the PI3K-AKT-mTOR pathway that is highly implicated in neurodevelopmental disorders, regulates SAC morphology in a cell-autonomous manner. *Pten*-deficient SACs show a nearly twofold increase in the number of dendritic branches, while other morphological properties remain largely unchanged. These morphological changes arise late in SAC development after dendrite development is largely complete and persist into adulthood. Mechanistically, excessive dendritic branching appears to arise from dysregulated mTOR activity. Despite this dramatic increase in dendritic branches, *Pten*-deficient SACs maintain a normal population number, organization of synaptic outputs, and intact direction-selectivity in the retina. Collectively, these results show that PTEN is essential for the normal development of highly stereotyped neuronal morphology.

INTRODUCTION

Since the time of Ramón y Cajal, neuroscientists have appreciated the complexity of the nervous system and the vast array of neuronal shapes and sizes. This morphological diversity underlies the computational power of the nervous system, as neurons acquire specific morphologies that are uniquely adapted to support their function [1]. Specific morphological features can be used in conjunction with molecular profiles and functional properties to classify neurons into discrete subtypes [2]. Neuronal morphology is influenced by the interplay between intrinsic factors and extrinsic cues in the extracellular environment. Cell type-specific transcription factors control the expression of effectors that in turn regulate the morphological development of a given neuronal subtype [3]. A neuron's complement of cell surface receptors allows it to organize its dendritic arbors and identify synaptic partners in response to extrinsic cues. These cell surface receptors converge on intracellular signaling cascades that modulate cytoskeletal dynamics, leading to differences in neurite elongation, branch initiation, and stabilization [4].

Many insights about the development of neuronal morphology come from highly stereotyped neuronal subtypes in a wide range of model organisms. PVD sensory neurons in *C. elegans* have a defined pitchfork-like projection pattern that line the body wall and are fundamental to mechanosensation and proprioception [5]. Forward genetic screens have identified transcription factors, cell surface receptors, and intracellular signaling molecules that are required for the stereotyped PVD neuron projection pattern [6-9]. The dendritic arborization (da) neurons in *Drosophila* larvae can be easily distinguished into four morphologically distinct subtypes based on the degree of dendrite branching [10]. The

morphological complexity of the four da neuron subtypes is determined by relative levels of three transcription factors: abrupt, cut, and knot [11-13]. Purkinje neurons in the mammalian cerebellar cortex have large, planar dendritic arbors with extensive branching patterns that maintain a high degree of self-avoidance. Multiple molecular pathways govern the development of these arbors, including repulsive Slit/Robo signaling, protocadherin-mediated self-avoidance, and actin regulators Daam1 and MTSS [14-16].

Starburst amacrine cells (SACs) in the mammalian retina are an excellent model for studying the development of neuronal morphology due to their stereotyped radially symmetric branching pattern, defined circuit function, and the established link between their dendritic form and neuronal function [17, 18]. SAC somas reside in two neuronal layers in the retina, the inner nuclear layer (INL) and ganglion cell layer (GCL), and project their dendrites to the inner plexiform layer (IPL), where they form planar dendritic arbors that stratify in sublamina 2 (S2) and 4 (S4), respectively (Figure 2.1A). Over the past several years, work from multiple labs has identified cell surface receptors that direct SAC morphology and stratification in the IPL. MEGF10 regulates the mosaic spacing of SACs through mediation of homotypic contacts during development [19-21]. Repulsive signaling mediated by FLRT2/UNC5 regulates SAC dendrite stratification [22]. Bidirectional PlexinA2/Semaphorin6A signaling is critical for SAC radial morphology and dendrite stratification [23, 24]. Other studies have identified molecules that disrupt SAC dendrite morphology without affecting stratification, suggesting that these are separate processes. g-protocadherins (g-Pcdhs) undergo extensive alternative splicing to generate hundreds of isoforms, with homophilic matching between isoforms mediating self-recognition in SAC dendrites. Genetic deletion of all *g-Pcdh* isoforms causes SAC dendrites to

fasciculate into bundles, disrupting their radial morphology; expression of a single *g-Pcdh* isoform in *g-Pcdh* deficient SACs is sufficient to restore self-recognition and normal radial morphology [15]. Loss of the cell surface protein AMIGO2 results in a 1.5-fold increase in the size of SAC dendritic arbors, but does not affect their stereotyped branching, symmetry, or stratification [25]. While these cell surface proteins are critical for regulating SAC morphology, little is known about the downstream intracellular signaling pathways that govern SAC morphology.

PTEN (phosphatase and tensin homologue) is a protein and lipid phosphatase that canonically functions as the primary negative regulator of the PI3K-AKT-mTOR pathway [26]. This pathway functions downstream of several cell surface receptors to regulate neuronal differentiation, migration, neurite outgrowth, and survival [27]. PTEN has a well-established role in regulating neurite growth and branching in mammalian neurons *in vivo*. Deletion of *Pten* results in neuronal hypertrophy and increased dendrite branching in cortical pyramidal neurons, hippocampal dentate granule cells, serotonergic raphe neurons, and cerebellar Purkinje neurons [28-31]. This can ultimately lead to altered synaptic connectivity and neuronal hyperexcitability [32, 33].

Whether PTEN plays a role in regulating the highly stereotyped dendritic morphology of SACs remains an open question. Deletion of *Pten* from retinal progenitors results in widespread defects in neuronal differentiation, migration, cellular lamination, mosaic spacing, and dendrite stratification throughout the retina, precluding any analysis of SAC morphology [34-37]. We therefore used a $ChAT^{Cre}$ line to delete *Pten* specifically from post-migratory SACs ($ChAT^{Cre};Pten^{cKO}$) to address its cell-autonomous role in regulating SAC morphology. SACs in

ChAT^{Cre}*;Pten*^{cKO} mice had a >1.5-fold increase in dendritic branching without affecting the overall length or field area of their dendritic arbors. We found that these branching phenotypes arose gradually during the later phase of SAC dendrite development and persist into adulthood. Analysis of signaling pathways downstream of PI3K-AKT suggests that increased dendrite branching is likely due to increased mTOR activity. Finally, we show that loss of *Pten* does not affect the compartmentalization of synaptic outputs in SACs or the function of the direction-selective circuit in the retina.

RESULTS

SAC-specific deletion of *Pten* does not affect cell density, somal lamination, mosaic spacing, or dendrite stratification

Pan-retinal deletion of *Pten* from retinal progenitors causes widespread abnormal somal lamination, mosaic spacing, and dendrite stratification in retinal neurons, including SACs [34, 35]. Subsequent work identified a role for PTEN in regulating the vesicular trafficking of cell adhesion molecules that are involved in establishing retinal neuron mosaics and dendrite stratification [37]. However, it is unclear whether these defects reflect a SAC-autonomous effect or are due to the overall disorganization of the retina. To circumvent this confound, we used a *ChAT*^{Cre} line to selectively drive recombination in SACs, the only cholinergic neurons in the retina, beginning at postnatal day 1 (P1) [20]. This timing coincides with the end of SAC laminar migration and the initiation of their dendritic stratification in the nascent IPL.

To better understand which aspects of SAC development require cell-autonomous PTEN function, we conducted a side-by-side comparison of pan-retinal (*Six3*^{Cre}) and SAC-specific

(*ChAT*^{Cre}) *Pten* conditional knockouts. Using retinal flat mount preparations from P28 *Six3*^{Cre}*;Pten*^{cHet} and *Six3*^{Cre}*;Pten*^{cKO} mice, we confirmed that while all cells in the GCL were positive for PTEN in *Six3*^{Cre}*;Pten*^{cHet} retinas, staining was completely absent in *Six3*^{Cre}*;Pten*^{cKO} retinas (Figure 2.1B-C'). We next analyzed P28 *ChAT*^{Cre}*;Pten*^{cHet} and *ChAT*^{Cre}*;Pten*^{cKO} retinas (Figure 2.1D-E'). In contrast to the complete loss of PTEN staining in pan-retinal mutants, the PTEN staining was selectively lost from ChAT^{+} SAC somas but retained in all other GCL neurons in *ChAT*^{Cre}*;Pten*^{cKO} retinas (Figure 2.1D-E'). As an additional confirmation of functional PTEN loss from SACs, we measured soma size, as neuronal hypertrophy is consistently seen after *Pten* deletion. In both *Six3*^{Cre}*;Pten*^{cKO} and *ChAT*^{Cre}*;Pten*^{cKO} retinas SAC soma sizes were significantly increased compared to their respective controls (Figure 2.1F-I).

We next compared the early developmental processes of differentiation, migration, and mosaic spacing in *Six3*^{Cre}*;Pten*^{cKO} and *ChAT*^{Cre}*;Pten*^{cKO}*;Ai9* retinas. Since loss of a single *Pten* allele can affect neuronal differentiation in certain contexts, we included both wildtype and heterozygous controls [38-40]. Consistent with previous studies using pan-retinal deletion of *Pten*, we found reduced cellular density and mosaic regularity of SACs in *Six3*^{Cre}*;Pten*^{cKO} retinas compared to controls (Figure 2.2A-E) [34, 35]. In contrast, there was no difference in cellular density or mosaic spacing of SACs in either the GCL or INL following *ChAT*^{Cre}-mediated *Pten* deletion (Figure 2.2F-J). The lack of differentiation or migration phenotypes in *ChAT*^{Cre}*;Pten*^{cKO}*;Ai9* retinas in which SACs are genetically labeled with tdTomato is likely due to *Pten* deletion occurring after these developmental processes are nearly complete and allows us to examine its cell-intrinsic role during dendrite development without these confounds.

To examine how deletion of *Pten* affects SAC dendrite stratification in the IPL, we stained retinal cross-sections at P28. Similar to previous studies that examined pan-retinal deletion of *Pten*, we observed a gross disruption of SAC lamination, with highly disorganized S2 and S4 bands which appeared to bleed into S1 and S5 in *Six3^{Cre};Pten^{cKO}* retinas (Figure 2.2K-N)[34, 35]. In contrast, we observed two well-defined tdTomato^{+} bands corresponding to S2 and S4 in *ChAT^{Cre};Pten^{cKO};Ai9* retinas (Figure 2.2O-R). While these bands appeared slightly less compact in *ChAT^{Cre}; Pten^{cKO};Ai9* retinas compared to littermate controls, there was no statistical difference between genotypes when quantified. Therefore, PTEN is not required for SAC dendrite stratification in the IPL.

Loss of *Pten* causes increased dendritic branching in SACs

SACs have a high degree of dendritic overlap with their neighbors, preventing analysis of individual cell dendrites at a population level. To perform comprehensive morphometric analysis of individual SACs, we induced sparse labeling with a *Cre*-dependent AAV (*AAV8-FLEx-tdTomato-CAAX*) injected into the vitreous of the eye at P1-P2. We analyzed *ChAT^{Cre};Pten^{WT}*, *ChAT^{Cre};Pten^{cHet},* and *ChAT^{Cre};Pten^{cKO}* SACs from both the GCL and INL at P21 when dendrite morphology is largely mature (Figure 2.3A-C") [23]. We quantified total dendritic length, number of branch points, dendritic field area, and dendritic self-crossings (Figure 2.3D-G). While we did not detect any differences between *ChAT^{Cre};Pten^{WT}* and *ChAT^{Cre};Pten^{cHet}* SACs, there were significant changes in *ChAT^{Cre};Pten^{cKO}* SACs. There was a small increase in total dendritic length in GCL SACs but not INL SACs in *ChAT^{Cre};Pten^{cKO}* retinas (Figure 2.3D). The total number of branch points was significantly increased in both INL and GCL SACs in *ChAT^{Cre};Pten^{cKO}*

retinas, nearly doubling in number (Figure 2.3E). Despite the increase in dendrite branching, *ChAT^{Cre};Pten^{cKO}* SACs show no changes in their dendritic field size (Figure 2.3F). We also found that *ChAT^{Cre};Pten^{cKO}* SACs have a significant increase in dendritic self-crossings compared to control SACs (Figure 2.3G). Using a Sholl analysis to measure local changes in dendritic density we found that *ChAT^{Cre};Pten^{cKO}* GCL SACs showed relatively localized increases in dendritic density in the distal 50% of their dendritic arbor (Figure 2.3H), whereas *ChAT^{Cre};Pten^{cKO}* INL SACs showed a generalized increase in dendritic density across their entire arbor (Figure 2.3I). These results show that while PTEN is not required for establishing arbor size in SACs, it regulates proper dendrite branching. These local changes in density are significant as SACs are purely dendritic neurons with spatially segregated synaptic inputs and outputs [41, 42]. Therefore, local increases in dendritic density could lead to a biased recruitment of specific pre- and post-synaptic partners.

Alterations in dendrite branching arise late in the development of *ChAT^{Cre};Pten^{cKO}* SACs and persist into adulthood

SACs undergo extensive dendritic arborization during the first two postnatal weeks, increasing their arbor territory and number of terminal branches [43]. To address when dendritic branching alterations arise in *ChAT^{Cre};Pten^{cKO}* SACs, we selected two developmental time points, one prior to eye opening (P7) and one after (P14), to assess SAC morphology. To label P7 SACs, we used a genetic approach, crossing the *ChAT^{Cre};Pten* line with a *TIGRE-MORF* (*Ai166*) reporter line, which stochastically expresses EGFP in 1-5% of *Cre* positive cells [44]. At P7, SAC dendrites are in a highly dynamic state, constantly extending and retracting branches,

which is critical for establishing their stereotyped radially symmetric morphology [43]. Since there were no differences between *ChAT^{Cre};Pten^{WT}* and *ChAT^{Cre};Pten^{cHet}* SACs at P21, we opted to include both genotypes as controls (*ChAT^{Cre};Pten^{Ctrl}*). We focused our analysis on GCL SACs, as the imaging resolution of individual cells was better than INL SACs. Reconstruction and quantification of SACs identified no significant changes in total dendrite length, number of branch points, dendritic field area, or soma size between *ChAT^{Cre};Pten^{Ctrl}* and *ChAT^{Cre};Pten^{cKO}* SACs at P7 (Figure S2.1A-F). By P14, SACs have a much sparser dendritic arbor, with a morphology that nearly recapitulates their mature morphology. Using our sparse viral labeling approach to quantify morphology at P14, we found that total dendritic length, branch number, and dendritic field area remain unchanged in *ChAT^{Cre};Pten^{cKO}* SACs compared to littermate controls (Figure S2.1G-K). However, we did detect a significant increase in soma size in *ChAT^{Cre};Pten^{cKO}* SACs, suggesting that somal hypertrophy precedes changes in the dendritic arbor (Figure S2.1L). Taken together, our results indicate that loss of PTEN from SACs drives excess dendritic branching between P14 and P21.

To assess whether the increased dendritic branching seen at P21 would resolve, persist, or worsen in adulthood we injected *AAV8-FLEx-tdTomato-CAAX* at P28 and examined sparsely labeled *ChAT^{Cre};Pten^{Ctrl}* and *ChAT^{Cre};Pten^{cKO}* SACs at P60 (Figure 2.4A-B). Similar to SACs at P21, adult *ChAT^{Cre};Pten^{cKO}* SACs showed a near doubling of dendrite branching across their arbor despite no change in total dendrite length (Figure 2.4D, E). Sholl analysis at P60 largely recapitulated the phenotypes at P21 as well, showing increased branch density in the outer 50% of the dendritic arbor (Figure 2.4G). However, we did identify distinctions between P21 and P60; notably, *ChAT^{Cre};Pten^{Ctrl}* SACs had 3-5 proximal dendrites of similar sizes, whereas

ChAT^{Cre}*;Pten*^{cKO} SACs frequently had a prominent single hypertrophic dendrite (Figure 2.4A'-B'). We defined any dendrite >1mm in caliber as a "hypertrophic dendrite" and found that these were present in 13/16 of *ChAT*^{Cre}*; Pten*^{cKO} SACs, compared with 1/12 in controls (Figure 2.4C). *ChAT*^{Cre}*;Pten*^{cKO} SACs also had slightly smaller dendritic field areas compared to *ChAT*^{Cre}*;Pten*^{Ctrl} SACs (Figure 2.4F). Despite these changes, SACs at P60 showed no changes in cell density, indicating that cell death was not occurring (Figure S2.2A-C). These results show that the long-term loss of *Pten* in SACs results in a persistent alteration in their dendritic arbor morphology.

Loss of *Pten* in SACs results in increased mTOR signaling over the course of development

PTEN serves as the primary negative regulator of the PI3K-AKT signaling pathway, which in turn activates mTOR signaling and inhibits GSK3β signaling (Figure 2.5K) [26]. Both mTOR and GSK3β alter the growth capacities of neurons and are likely candidates to regulate SAC branching [45]. We therefore examined how the loss of *Pten* from SACs affects these pathways using an antibody to pS6 as a readout of mTOR activity [35] and a genetically-encoded β-catenin:GFP reporter (*TCF/Lef:H2B-GFP*) as a proxy for GSK3β signaling (Figure 2.5A-H) [46]. In the GCL of P28 *ChAT*^{Cre}*;Pten*^{cHet} retinal flat mounts, pS6 was undetectable in SACs, while it was present in a subset of RGCs. In contrast, all GCL SACs in P28 *ChAT*^{Cre}*;Pten*^{cKO} retinas showed elevated pS6 levels, indicating activation of mTOR signaling (Figure 2.5I). Quantification of GFP signal in *ChAT*^{Cre}*;Pten*^{cHet}*;TCF/Lef:H2B-GFP* and *ChAT*^{Cre}*; Pten*^{cKO}*;TCF/Lef:H2B-GFP* retinas showed minimal fluorescence in SACs in both genotypes, suggesting that GSK3β signaling is unaffected by the absence of *Pten* (Figure 2.5J). Together, these results suggest that the

morphological changes in *ChAT^{Cre};Pten^{cKO}* SACs arise at least in part due to increased mTOR activity (Figure 2.5K-L).

Since SACs did not show any changes in dendritic branching during the most dynamic time of dendritic growth (P7-P14), we assessed pS6 at these ages in *ChAT^{Cre};Pten^{cKO}* SACs. At P7, *ChAT^{Cre};Pten^{cHet}* SACs showed high levels of pS6 immunoreactivity, which was not further elevated in *ChAT^{Cre};Pten^{cKO}* SACs (Figure 2.6A-B, G, H). By P14 most SACs in *ChAT^{Cre};Pten^{cHet}* mice had pS6 levels that were barely above background (Figure 2.6C-C', G, H), whereas pS6 was significantly increased in *ChAT^{Cre};Pten^{cKO}* SACs (Figure 2.6D-D', G, H). Elevated pS6 levels were maintained in *ChAT^{Cre};Pten^{cKO}* SACs at P60 (Figure 2.6E-F', G, H). These results suggest that the lack of a dendritic branching phenotype in *ChAT^{Cre};Pten^{cKO}* SACs at P7 may be because mTOR is already elevated at this age and loss of PTEN cannot drive further mTOR activity. In contrast, from P14 onwards mTOR activity has decreased in *ChAT^{Cre};Pten^{cHet}* SACs, and deletion of *Pten* results in persistently elevated mTOR activity which maintains the branching and arborization process, leading to an increase in branch number by P21 and dendrite caliber by P60 (Figure 2.6I).

SAC synaptic outputs and direction-selective circuit function are unaffected by loss of *Pten*

SACs have a highly compartmentalized synaptic organization, with presynaptic inputs from bipolar cells localized to the inner two thirds of their dendritic arbor, and their synaptic outputs localized to the outer third [47]. To examine whether the loss of *Pten* affected the number or compartmentalization of SAC synapses we intravitreally injected *AAV1-FLEx-mGFP-2A-Synaptophysin-mRuby* at P2 [48]. SACs transduced with this construct have a membrane-

bound GFP that labels their dendritic arbor and synaptophysin (Syp) fused to mRuby to label synaptic outputs [49] (Figure 2.7A-B). Both *ChAT^{Cre};Pten^{cHet}* and *ChAT^{Cre};Pten^{cKO}* SACs showed robust localization of Syp:mRuby to the outer third of their dendritic arbor at P28 (Figure 2.7A'-B'). We quantified the number, volume, and spatial distribution of Syp:mRuby puncta and saw no differences between *ChAT^{Cre};Pten^{cKO}* SACs and controls (Figure 2.7C-F). Therefore, even though SAC dendrite branching is dysregulated by P28 in *ChAT^{Cre};Pten^{cKO}* SACs, synaptic outputs appear largely intact.

SACs have a conserved and well-characterized function of providing GABAergic inhibition and cholinergic excitation onto direction-selective ganglion cells (DSGCs) to tune direction selectivity [50, 51]. Genetic deletion of either *Sema6A* or *g-Pcdhs* dramatically alters SAC morphology and degrades the direction selectivity of postsynaptic DSGCs [23, 52]. Therefore, we used multielectrode array (MEA) recordings to assess whether SAC-specific deletion of *Pten* influences downstream DSGCs. We isolated recordings from individual cells and computed their direction-selective index (DSI) in response to bars of light moving in 30-degree increments (Fig 7G-H). A von Mises goodness of fit test was performed to determine if a cell matched established DSGC response properties [53]. Cells with a DSI greater than 0.37 and a von Mises fit greater than 0.5 were classified as DSGCs. There was no significant difference in the distribution of DSIs of all RGCs between *ChAT^{Cre};Pten^{cHet}* and *ChAT^{Cre};Pten^{cKO}* retinas (Figure 2.7I). The average DSI, von-Mises fit, average number of spikes per epoch, average spikes in preferred direction, and tuning width in cells classified as DSGCs were unaffected in *ChAT^{Cre};Pten^{cKO}* retinas compared to controls (Fig 7J-N). Taken together, these data show that

while *Pten*-deficient SACs have significant morphological changes at P60, the function of the direction-selective circuit is unaffected.

DISCUSSION

The process by which neurons develop stereotyped morphologies necessary to perform subtype-specific computations must be highly regulated to ensure consistency across each cell population. Here, we show that PTEN is required for SACs to adopt their precise branching patterns. By deleting *Pten* selectively from post-migratory SACs beginning at early postnatal ages, we were able to isolate PTEN's cell-autonomous function and uncover its role in regulating dendrite branching at later stages of development. Mechanistically, this appears to result from elevated mTOR signaling, which normally decreases as SAC development progresses, but remains elevated in *Pten*-deficient SACs. Finally, we show despite altering the branching patterns of SAC dendrites, the loss of PTEN does not appear to disrupt the precise organization of synaptic outputs or the function of downstream retinal circuitry.

Refining the cell-autonomous function of PTEN in SAC development

The environment in which cells develop plays a critical role in regulating their mature morphological features. Manipulating the pathways involved in regulating neuronal morphological development in intact preparations that maintain the extracellular environment can present challenges, as genetic deletions can lead to widespread anatomical changes that could affect neuronal morphology non-cell-autonomously. For example, pan-retinal *Pten* deletion broadly affects retinal progenitor proliferation, differentiation of multiple neuronal

classes, somal lamination, and dendrite stratification of inner retinal neurons [34-36]. The SAC somal organization and dendrite stratification phenotypes in these *Pten*-deficient retinas resemble defects seen in mice lacking specific transmembrane adhesion proteins important for various aspects of SAC development, suggesting that PTEN could regulate the function of these proteins. Furthermore, deletion of *Pten* from retinal progenitors results in abnormal endocytic trafficking of cell surface proteins and signaling molecules important for SAC migration, mosaic spacing, and dendrite development [37]. However, it is equally possible that some of the SAC developmental phenotypes seen following pan-retinal *Pten* mutants are indirect and due to the profoundly disrupted extracellular environment surrounding them.

To address this issue, we compared the effects of pan-retinal (*Six3^{Cre};Pten^{cKO}*) and SAC-specific (*ChAT^{Cre};Pten^{cKO}*) deletion of *Pten* side-by-side to disentangle its non-cell and cell-autonomous roles in SAC development. Like prior studies, we observed profound disruptions in SAC somal lamination and dendrite stratification after pan-retinal deletion of *Pten*. In contrast, when this deletion was restricted to post-migratory SACs, we observed normal mosaic spacing and dendrite stratification in the IPL, suggesting PTEN is not required for these processes. This could be due to the timing of *Pten* deletion; pan-retinal deletion of *Pten* occurs in retinal progenitors between E8.5 and E9.5, whereas recombination in *ChAT^{Cre};Pten^{cKO}* mice begins at P1 as these cells are tangentially migrating to space their somas and beginning to stratify their dendrites in the nascent IPL [20, 54-56]. However, mice in which *Megf10* or *PlexA2* are deleted using *ChAT^{Cre}* still show defects in SAC mosaic arrangement and dendrite stratification, respectively [20, 23]. Therefore, the most likely explanation for our results is that PTEN is not essential for the function of the molecular pathways that regulate SAC somal positioning or

dendrite stratification, while it is required for proper SAC dendrite branching. We also attempted to selectively delete *Pten* earlier from migrating SACs using *Megf10*^{Cre} to examine SACs migration and mosaic spacing; however, these mice die immediately after birth, precluding these analyses.

PTEN's function in regulating neuronal morphology

PTEN has been highly studied in the nervous system due to its identification as an autism risk gene [57]. In cultured mammalian hippocampal neurons, knockdown of *Pten* increases dendrite branching through the PI3K-AKT-mTOR pathway [58]. *In vivo* deletion of *Pten* also causes generalized increases in dendritic growth and branching in hippocampal dentate granule cells, cortical neurons, and raphe serotonergic neurons [28, 29, 31, 33, 59, 60]. However, in *Drosophila* dorsocentral neurons, RNAi knockdown of *Pten* primarily caused localized branching as opposed to widespread neuronal hypertrophy, suggesting that PTEN's role in regulating dendrite branching can differ depending on the neuronal subtype [61]. Similarly, we found while that *Pten*-deficient SACs displayed somal hypertrophy and nearly double the number of dendrite branches, they maintained their overall dendritic arbor size. It is unclear why deletion of *Pten* from SACs does not result in increased dendritic arbor size like it does in many other neuronal subtypes. Arbor size is tightly regulated in SACs, allowing them to create an even coverage factor of 30x across the retina. However, SACs do have the capacity to grow larger dendritic arbors, as constitutive deletion of the transmembrane protein *Amigo2* causes SAC dendrite length and overall dendritic arbor size to scale 50% larger, while branching is unaffected [25]. Based on the normal overall dendritic arbor size in *Pten*-deficient SACs, we conclude that PTEN is not required for the regulation of dendritic length by AMIGO2. Instead,

these findings reinforce that the molecular mechanisms that modulate SAC dendritic field size and the branching of their dendritic arbor are discrete processes. *Pten* deletion from SACs also did not significantly affect dendrite lamination in the IPL, suggesting it is not essential for the transmembrane proteins shown to regulate this process [22, 23].

Both g-Pcdhs and Sema6A/PlexinA2 are required cell-autonomously within SACs to regulate dendrite self-avoidance [15, 23, 24, 43]. *g-Pcdh* mutant SACs have a normal number of terminal branches and overall arbor size, while *Sema6A/PlexinA2* mutant SACs show reduced branching and arbor size. The dendrite morphology phenotypes that arise from mutations in these genes are much more severe that what we observed following deletion of *Pten*. Therefore, while it is possible that PTEN can function in the same molecular pathway as g-Pcdhs and Sema6A/PlexinA2, there are clearly additional signaling pathways required. For PlexinA2, Rac1 GTPases are likely candidates, as SACs in mice with a point mutation that abolishes PlexinA2 RasGAP activity show significant dendritic self-avoidance phenotypes [24].

Dysregulation of the PI3K-AKT-mTOR pathway following *Pten* deletion in SACs

Deletion of *Pten* from SACs is likely to have multiple effects, including dysregulation of the PI3K-AKT-mTOR pathway [26]. mTOR activation is a potent enhancer of neuronal growth, and deletion of its upstream inhibitor *Tsc1* causes dendritic hypertrophy that largely recapitulates *Pten* deficiency in cortical and olfactory bulb neurons [45, 62]. Conversely, inhibition of mTOR via rapamycin is sufficient to rescue overgrowth phenotypes from *Pten* loss in dentate granule neurons [63]. Our results showing elevated pS6 levels following the deletion of *Pten* suggests that elevated mTOR activity increases dendritic branching in SACs. GSK3β,

another effector downstream of the PI3K-AKT pathway, can also regulate neurite outgrowth by modulating microtubule stabilization and polymerization [64, 65]. Our results using a genetic reporter of b-catenin activity as readout of GSK3β function detected no differences between control and *Pten*-deficient SACs, suggesting that this pathway may not play a major role in regulating dendrite branching in SACs.

How does the loss of *Pten* in SACs result in increased dendritic branching? Elegant live imaging studies show that most of the SAC dendritic growth occurs between P4-P14 [43]. During the early portion of this phase, dendrites contain many exuberant self-contacting interstitial protrusions that are highly dynamic and largely prune away by P14. While we did not conduct live imaging in our studies, the timing of increased pS6 and increased branching provides some clues as to PTEN's function. At P7 when SACs are undergoing extensive dendritic growth, high levels of pS6 were seen in control SACs. Deletion of *Pten* had no effect on pS6, somal hypertrophy, or dendrite branching at P7, suggesting that mTOR activity may already be near maximal levels at this age. By P14, we saw decreased levels of pS6 in control SACs, suggesting that mTOR activity normally declines coincident with when dendritic arbor growth and branching begins to slow. In contrast, *Pten*-deficient SACs show elevated pS6 and somal hypertrophy at this age, yet dendrite branching is unaffected. It is not until P21 and later that *Pten*-deficient SACs show increased dendrite branching. This suggests that loss of PTEN does not generally affect the major phase of developmental dendrite growth in SACs, but prolongs it beyond its normal plateau, resulting in excessive branching. The presence of excessive dendrite branches at P60 suggests that these branches are not unstable dynamic projections like those

seen in developing SACs but rather are persistent branches. Whether these aberrant branches are functionally integrated into retinal circuitry is unclear.

At P60, SACs in *ChAT^{Cre};Pten^{cKO}* retinas began to show a decrease in dendritic arbor size, suggesting that prolonged deletion of *Pten* could have adverse effects in neurons. In Purkinje neurons, loss of *Pten* results in the eventual apoptotic death of these neurons beginning around 6 months of age [30]. We did not observe any loss of SACs in *ChAT^{Cre};Pten^{cKO}* retinas at P60, and did not examine later ages as these mice eventually develop facial tumors [66]. However, it is important to consider the long-term consequences of *Pten* deletion in neurons, as it is widely studied for its ability to facilitate axon regeneration after injury [67-70]. While these studies rarely report the effect of *Pten* deletion on the dendrites of these cells, a recent report shows that RGC dendrites rapidly retract in response to axonal injury, and co-deletion of *Pten* and *SOCS3* exacerbates this effect, although it is unclear whether these dendritic arbors eventually recover in size [71]. Our results suggest that the long-term deletion of *Pten* in neurons can cause deleterious changes in dendritic architecture.

Functional Consequences of *Pten* Loss in SACs

At a circuit function level, SACs are crucial for the directional tuning of downstream DSGCs, as eliminating or pharmacologically silencing SACs results in a loss of direction selectivity [72-74]. SACs themselves display intrinsic direction selectivity, responding preferentially to centrifugal motion moving from the soma to the dendritic tips [75, 76]. Mutations that cause disruptions of the radial morphology of SAC dendritic arbors result in defective direction selectivity [23, 52, 77]. Loss of *Pten* in other neurons can dramatically affect

their circuit function; hippocampal dentate granule neurons and serotonergic raphe neurons lacking *Pten* are hyperactive due to changes in their intrinsic excitability and have an increased number of excitatory inputs, whereas *Pten*-deficient Purkinje neurons show reduced excitability [28, 30, 32, 33, 78]. It is therefore somewhat surprising that despite the abnormal dendritic branching in SACs, direction selectively appeared intact in $ChAT^{Cre};Pten^{cKO}$ retinas. We did not examine the intrinsic physiological properties of *Pten*-deficient SACs directly, so it is possible that there are cell-autonomous functional differences that are not sufficient to affect the downstream DSGCs. We also observed no changes in the localization, density, or size of SAC synaptic outputs in $ChAT^{Cre};Pten^{cKO}$ retinas. While the molecular mechanisms that underlie the spatial segregation of synaptic inputs and outputs in SACs remain unknown, *Pten* signaling is apparently not required.

Altogether, our study refines the role of PTEN in regulating the morphology of SACs, showing that it is critical for establishing the highly stereotyped dendritic branching pattern in these neurons. Further studies will be needed to identify additional intracellular signaling pathways that function downstream of cell surface receptors to regulate cytoskeletal dynamics in developing SACs.

FIGURES AND FIGURE LEGENDS

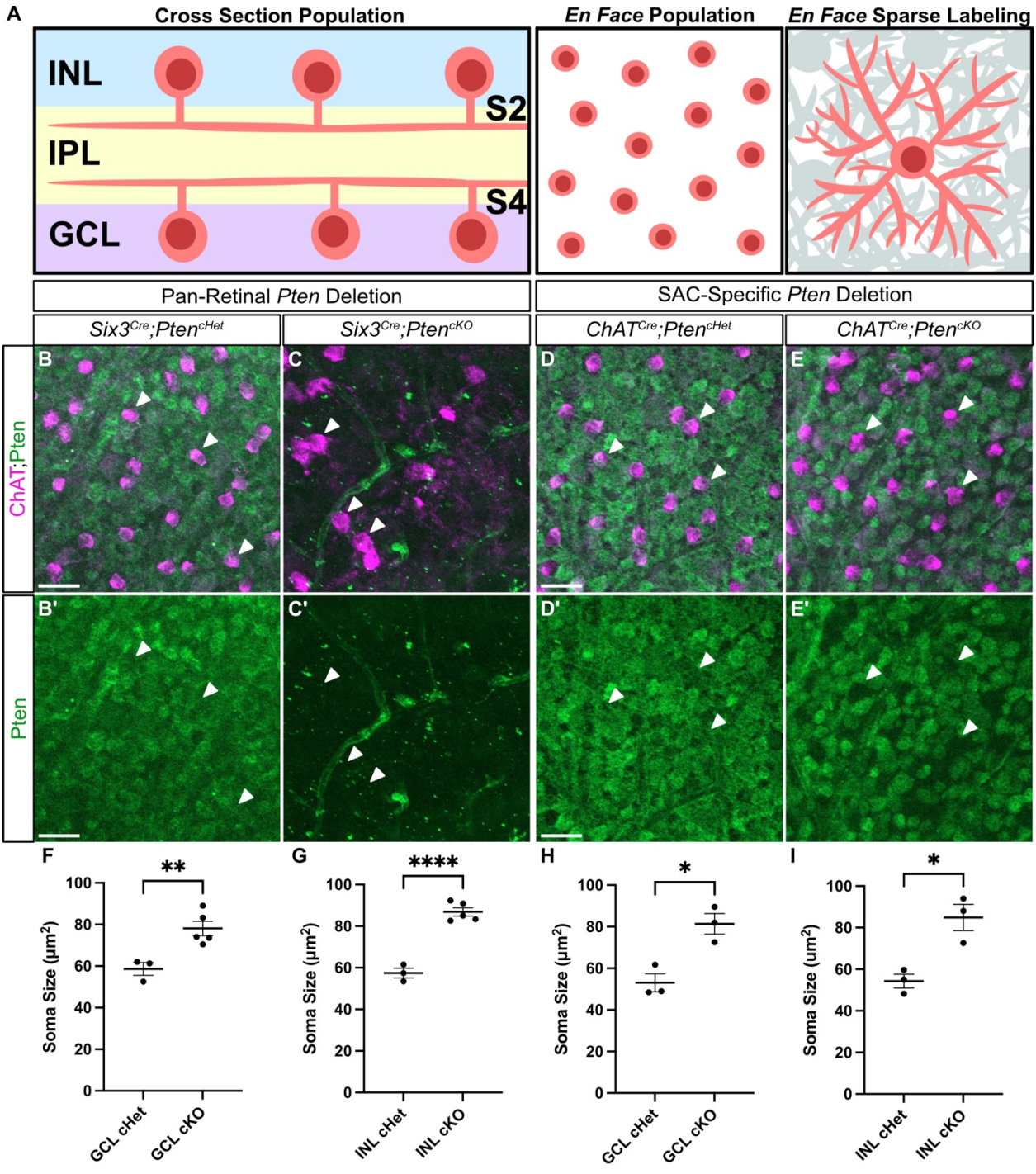

Figure 2.1. Validation of SAC specific *Pten* deletion

A. Schematic showing different retinal preparations for visualizing SACs. Retinal cross-sections (left panel) are used to analyze cellular lamination and dendrite stratification. Retinal flat mounts imaged in an *En Face* preparation are used for population measurements (middle panel) and single cell morphology (right panel). **B-E'.** P28 retinal flat mounts immunostained with ChAT (magenta) to label SAC somas and PTEN (green) shows that PTEN is present in all cells in the GCL. In *Six3^{Cre};Pten^{cKO}* retinas, PTEN is eliminated from all GCL cells (C, C'), whereas in *ChAT^{Cre};Pten^{cKO}* retinas, PTEN is selectively lost only from SACs (white arrows) (E, E'). **F-I.** Quantification of SAC soma sizes at P28 reveals somal hypertrophy, a common phenotype seen after *Pten* deletion, in both *Six3^{Cre};Pten^{cKO}* and *ChAT^{Cre};Pten^{cKO}* GCL and INL SACs ($p = 0.0433$ (F), 0.0017 (G), 0.0124 (H), 0.0307 (I)). Data reported as mean ± SEM. Scale bars = 25 µm.

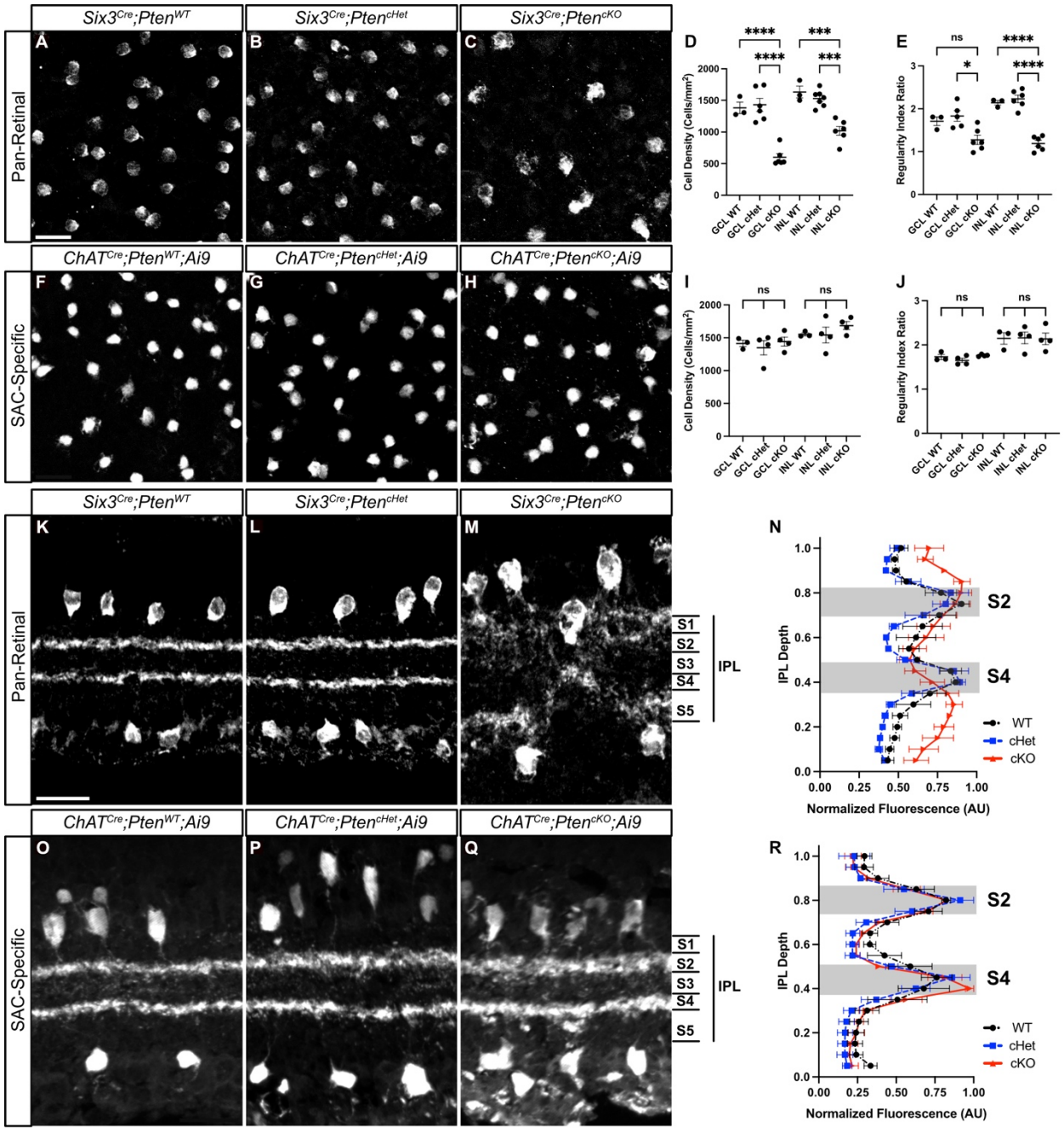
Six3Cre;PtenWT
Six3Cre;PtenCHet
Six3Cre;PtenCKO
Pan-Retinal
A
B
C
D
E
Cell Density (Cells/mm2)
Regularity Index Ratio
GCL WT
GCL cHet
GCL cKO
INL WT
INL cHet
INL cKO
ns
ChATCre;PtenWT;Ai9
ChATCre;PtenCHet;Ai9
ChATCre;PtenCKO;Ai9
SAC-Specific
F
G
H
I
J
K
L
M
S1
S2
S3
S4
S5
IPL
N
IPL Depth
Normalized Fluorescence (AU)
WT
cHet
cKO
O
P
Q
R

Figure 2.2. Selective deletion of *Pten* from SACs does not affect their cell density, mosaic spacing, or dendrite lamination

A-C. Images of P28 *Six3^{Cre};Pten^{WT}*, *Six3^{Cre};Pten^{cHet}* and *Six3^{Cre};Pten^{cKO}* retina flat mounts with GCL SACs labeled by ChAT immunostaining. **D, E.** Quantification of cell density (***GCL:*** *WT: n = 3, 1.71 ± 0.097; cHet: n = 5, 1.83 ± 0.12; n = 6, cKO: 1.27 ±0.11;* ***INL:*** *WT: n = 3, 2.14 ± 0.053; cHet: n = 6, 2.23 ± 0.085; cKO: n = 6, 1.19 ± 0.068*) and mosaic spacing (***GCL:*** *WT: n = 3, 1382 ± 90.79; cHet: n = 6, 1428 ± 103.5; n = 6, cKO: 598.6 ± 58.35;* ***INL:*** *WT: n = 3, 1633 ± 94.77; cHet: n = 7, 1530 ± 48.96; cKO: n = 6, 1019 ± 71.13*) of GCL and INL SACs shows decreased cell density and mosaic regularity in *Six3^{Cre};Pten^{cKO}* retinas following pan-retinal deletion of *Pten* ($p < 0.0001$ for GCL and INL (D), $p = 0.01$ for GCL and $p < 0.0001$ for INL (E)). **F-H.** Images of P28 *ChAT^{Cre};Pten^{WT};Ai9*, *ChAT^{Cre};Pten^{cHet};Ai9* and *ChAT^{Cre};Pten^{cKO};Ai9* retina flat mounts with GCL SACs labeled by tdTomato. **I, J.** Quantification shows normal cell density (***GCL:*** *WT: n = 3, 1415 ± 47.91; cHet: n = 4, 1349 ± 107.4; n = 4, cKO: 1442 ± 69.42;* ***INL:*** *WT: n = 3, 1553 ± 23.73; cHet: n = 4, 1542 ± 117.8; cKO: n = 4, 1686 ± 59.67*) and mosaic spacing (***GCL:*** *WT: n = 3, 1.73 ± 0.059; cHet: n = 4, 1.65 ± 0.048; n = 4, cKO: 1.76 ± 0.011;* ***INL:*** *WT: n = 3, 2.15 ± 0.13; cHet: n = 4, 2.16 ± 0.13; cKO: n = 4, 2.14 ± 0.13*) of SACs in *ChAT^{Cre};Pten^{cKO};Ai9* retinas following selective deletion of *Pten* from SACs ($p = 0.7195$ for GCL and 0.4336 INL (I), $p = 0.1871$ for GCL and 0.9901 for INL (J)). **K-M.** P28 *Six3^{Cre};Pten^{WT}*, *Six3^{Cre};Pten^{cHet}* and *Six3^{Cre};Pten^{cKO}* retina cross-sections labeled by ChAT immunostaining show abnormal SAC somal lamination and disorganized dendrites in *Six3^{Cre};Pten^{cKO}* retinas. **N.** Quantification of SAC dendrite stratification using IPLaminator shows aberrant dendrite stratification in *Six3^{Cre};Pten^{cKO}* compared to controls ($p = 0.0004$). **O-Q.** P28 *ChAT^{Cre};Pten^{WT};Ai9*, *ChAT^{Cre};Pten^{cHet};Ai9* and *ChAT^{Cre};Pten^{cKO};Ai9* retina cross-sections with SAC

somas and dendrites labeled via tdTomato. SAC somal lamination and dendrite organization are grossly normal, with two distinct bands in S2 and S4 in the IPL. **R.** Quantification of SAC dendrite stratification shows no significant changes in *ChAT^{Cre};Pten^{cKO};Ai9* SACs relative to controls ($p = 0.4638$). Data reported as mean ± SEM. Scalebars = 25 µm.

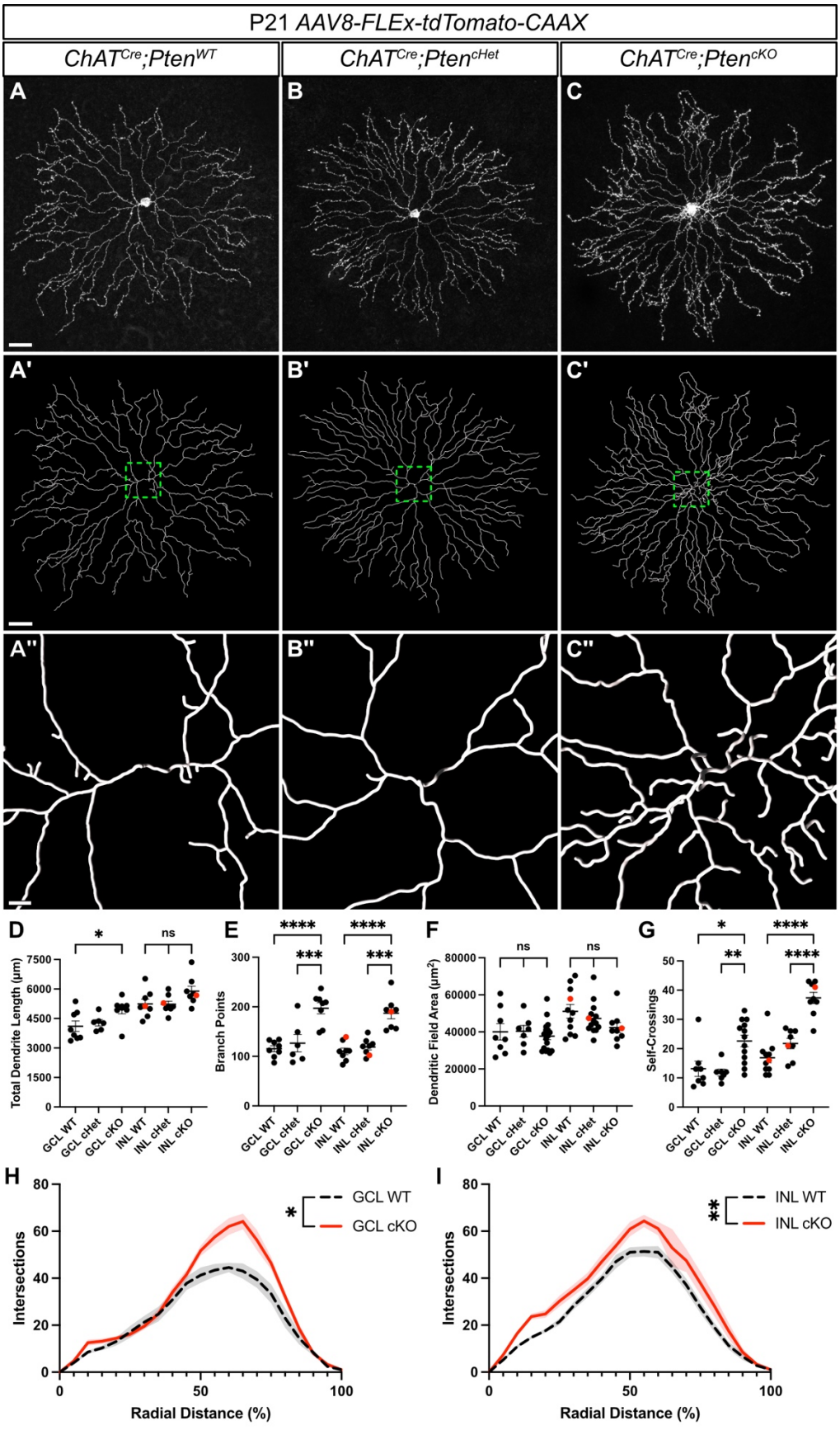
P21 AAV8-FLEx-tdTomato-CAAX
ChAT^Cre;Pten^WT
ChAT^Cre;Pten^cHet
ChAT^Cre;Pten^cKO
A
B
C
A'
B'
C'
A''
B''
C''
D
Total Dendrite Length (µm)
E
Branch Points
F
Dendritic Field Area (µm²)
G
Self-Crossings
GCL WT
GCL cHet
GCL cKO
INL WT
INL cHet
INL cKO
ns
H
Intersections
Radial Distance (%)
GCL WT
GCL cKO
I
INL WT
INL cKO

Figure 2.3. *Pten*-deficient SACs have abnormal dendritic branching patterns

A-C. SACs from P21 *ChAT^{Cre};Pten^{WT}*, *ChAT^{Cre};Pten^{cHet}*, and *ChAT^{Cre};Pten^{cKO}* retina flat mounts sparsely labeled with *AAV8-FLEx-tdTomato-CAAX*. Images show single SACs located in the INL. **A'-C'.** Imaris reconstructions of SACs in A-C. **A''-C''.** Zoomed-in view of the dendritic arbor reconstruction near the soma. **D-G.** Quantification of total dendrite length (***GCL:*** *WT: n = 8, 4106 ± 264.9; cHet: n = 6, 4280 ± 162.8; n = 8, cKO: 4953 ± 214.4;* ***INL:*** *WT: n = 8, 5243 ± 242.2; cHet: n = 8, 5219 ± 161.4; cKO: n = 8, 5890 ± 252.3)* (GCL p = 0.033; INL p = 0.076), number of branch points (***GCL:*** *WT: n = 8, 115.4 ± 5.937; cHet: n = 6, 126.7 ± 17.52; n = 8, cKO: 197.1 ± 11.16;* ***INL:*** *WT: n = 8, 110.0 ± 6.716; cHet: n = 8, 118.9 ± 5.962; cKO: n = 8, 187.1 ± 11.32)* (GCL and INL p < 0.0001), dendritic field area (***GCL:*** *WT: n = 8, 40012 ± 4399; cHet: n = 7, 40382 ± 3074; n = 17, cKO: 37723 ± 1944;* ***INL:*** *WT: n = 11, 51104 ± 3668; cHet: n = 14, 47263 ± 2269; cKO: n = 9, 42333 ± 2714)* (GCL p = 0.756; INL p = 0.152), and dendritic branch self-crossings (***GCL:*** *WT: n = 8, 13.13 ± 2.601; cHet: n = 7, 11.86 ± 1.164; n = 17, cKO: 22.62 ± 1.979;* ***INL:*** *WT: n = 11, 16.91 ± 1.781; cHet: n = 14, 21.75 ± 1.770; cKO: n = 9, 37.33 ± 1.900)* (GCL p = 0.756; INL p = 0.152) (GCL p = 0.0015; INL p < 0.0001). A significant increase in the number of branch points and self-crossings is present in both GCL and INL SACs in *ChAT^{Cre};Pten^{cKO}* retinas. Red dots indicate data from representative images. **H, I.** Sholl analysis reveals differences in local density that differ between GCL and INL SACs in *ChAT^{Cre};Pten^{cKO}* retinas (GCL p = 0.0312; INL p = 0.0011). GCL cKO SACs show increased density near their terminal arbors, while INL cKO SACs show increased density throughout their arbor. Data reported as mean ± SEM and contain cells from at least 3 animals. Scalebars in A-C and A'-C' = 25 µm. Scalebar in A"-C" = 3 µm.

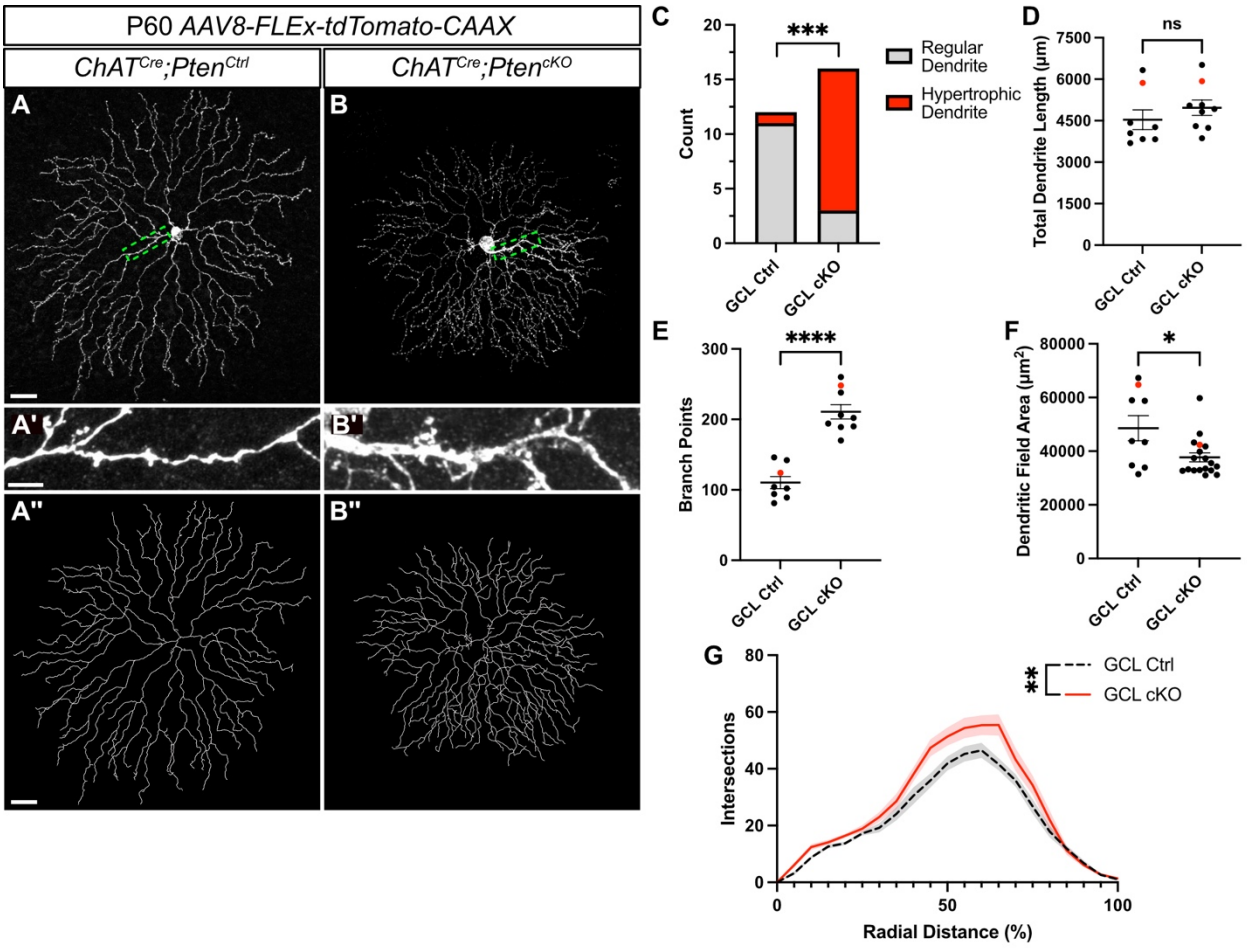
P60 AAV8-FLEx-tdTomato-CAAX
ChAT^Cre;Pten^Ctrl
ChAT^Cre;Pten^cKO
A
B
A'
B'
A"
B"
C
***
Regular Dendrite
Hypertrophic Dendrite
Count
GCL Ctrl
GCL cKO
D
ns
Total Dendrite Length (μm)
E
****
Branch Points
F
*
Dendritic Field Area (μm²)
G
**
GCL Ctrl
GCL cKO
Intersections
Radial Distance (%)

Figure 2.4. *Pten*-deficient SACs continue to show dendritic abnormalities at P60

A-B. P60 *ChAT^{Cre};Pten^{Ctrl}* and *ChAT^{Cre};Pten^{cKO}* SACs sparsely labeled by injection of *AAV8-FLEx-tdTomato-CAAX*. Images show single SACs located in the GCL. **A'-B'.** Enlargement from A-B highlighting that in *ChAT^{Cre};Pten^{cKO}* SACs one of the dendrites frequently becomes hypertrophic. **A''-B''.** Imaris reconstructions of SACs in A-B. **C.** Quantification of the number of SACs containing a hypertrophic dendrite greater than 1µm in caliber (8.33% in *Pten^{Ctrl}* and 81.25% in *Pten^{cKO}* SACs; p = 0.0003 by Fisher's exact test). **D-F.** Quantification shows that P60 cKO SACs have normal total dendritic length (*Ctrl: n = 8, 4535 ± 353.8; cKO: n = 9, 4968 ± 277.5*) (p = 0.345), an increased number of branch points (*Ctrl: n = 8, 110.3 ± 8.612; cKO: n = 9, 210.8 ± 10.21*) (p < 0.0001), and reduced dendritic field area (*Ctrl: n = 9, 48556 ± 4680; cKO: n = 18, 37693 ± 1690*) (p = 0.013). Red dots indicate data from representative images. **G.** Sholl analysis reveals increases in local dendrite branch density similar to the phenotype observed at P21. (p = 0.0043). Data reported as mean ± SEM and contain cells from at least 3 animals. Scalebars for A and A" = 25 µm. Scalebars for A' = 2 µm.

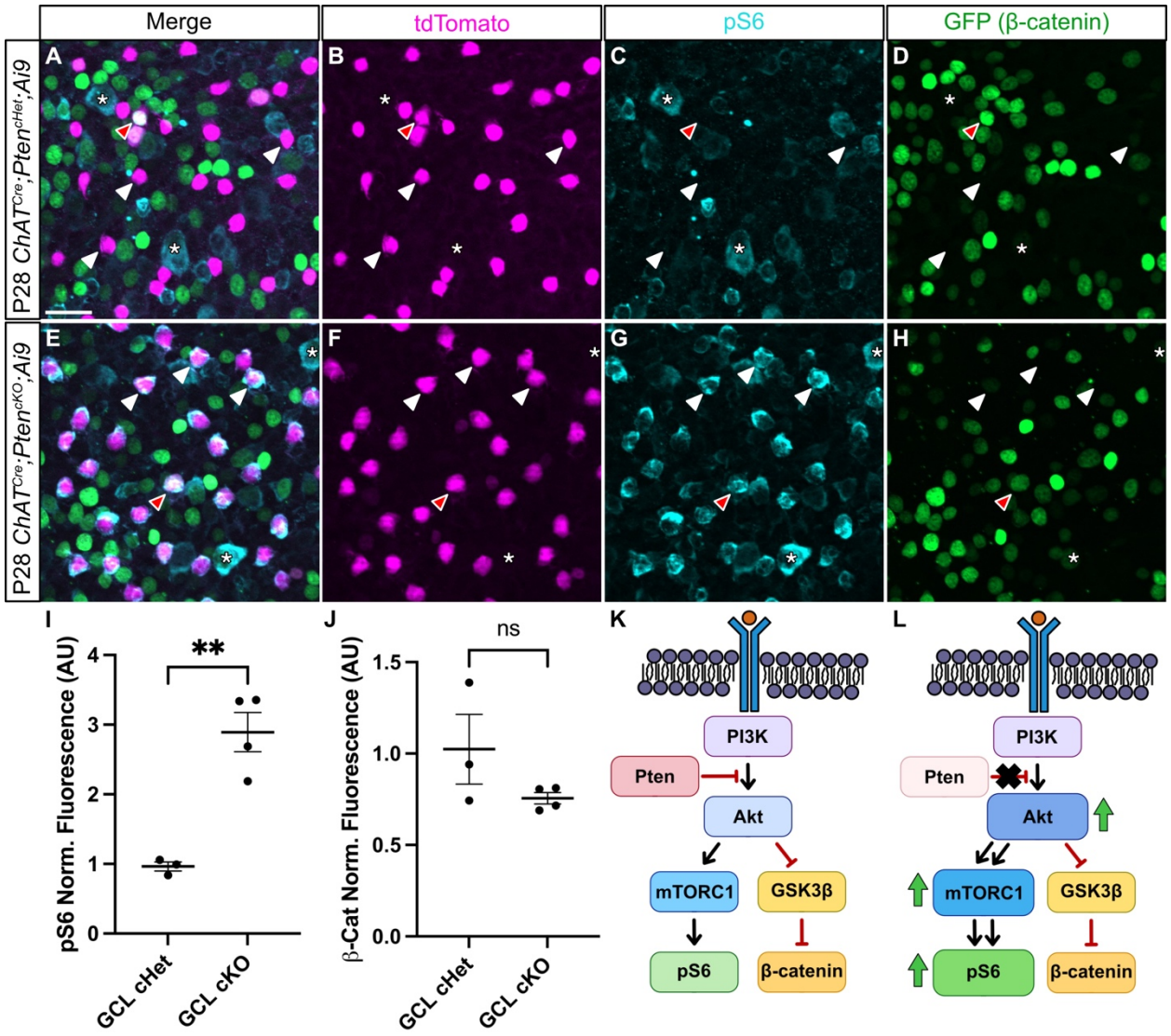
Merge
tdTomato
pS6
GFP (β-catenin)
P28 ChAT^Cre;Pten^cHet;Ai9
P28 ChAT^Cre;Pten^cKO;Ai9
A
B
C
D
E
F
G
H
I
pS6 Norm. Fluorescence (AU)
**
GCL cHet
GCL cKO
J
β-Cat Norm. Fluorescence (AU)
ns
GCL cHet
GCL cKO
K
PI3K
Pten
Akt
mTORC1
GSK3β
pS6
β-catenin
L
PI3K
Pten
Akt
mTORC1
GSK3β
pS6
β-catenin

Figure 2.5. Deletion of *Pten* from SACs upregulates mTOR but not GSK3β signaling

A-H. Flat mount preparations of P28 *ChAT^{Cre};Pten^{cHet};Ai9;Tcf/Lef:H2B-GFP* and *ChAT^{Cre};Pten^{cKO};Ai9;Tcf/Lef:H2B-GFP* retinas immunostained for tdTomato (magenta, B, F), pS6 (teal, C-G), and β-catenin reporter *Tcf/Lef:H2B-GFP* (green, D-H). White arrowheads highlight SAC cell bodies in the GCL in both *Pten* controls (A-D) and cKOs (E-H). Red arrowhead indicates a SAC with elevated levels of β-catenin reporter signal. Asterisks indicate retinal ganglion cells in both the control and cKO retinas that show elevated levels of pS6. **I, J.** Quantification of pS6 and β-catenin fluorescence intensity show a significant increase in pS6 levels (*cHet: n = 3, 0.9636 ± 0.06534; cKO: n = 4, 2.892 ± 0.2812*) (p = 0.009) but no change in β-catenin levels (*cHet: n = 3, 1.024 ± 0.1907; cKO: n = 4, 0.7556 ± 0.03099*) (p = 0.312) in cKO SACs. **K, L.** Schematic showing a simplified view of the PI3K-AKT pathway. In the absence of *Pten* in SACs, AKT appears to increase mTOR activity as measured by pS6 levels, while GSK3β signaling as measured by β-catenin activity remains unchanged. Data reported as mean ± SEM. Scalebars = 25 μm.

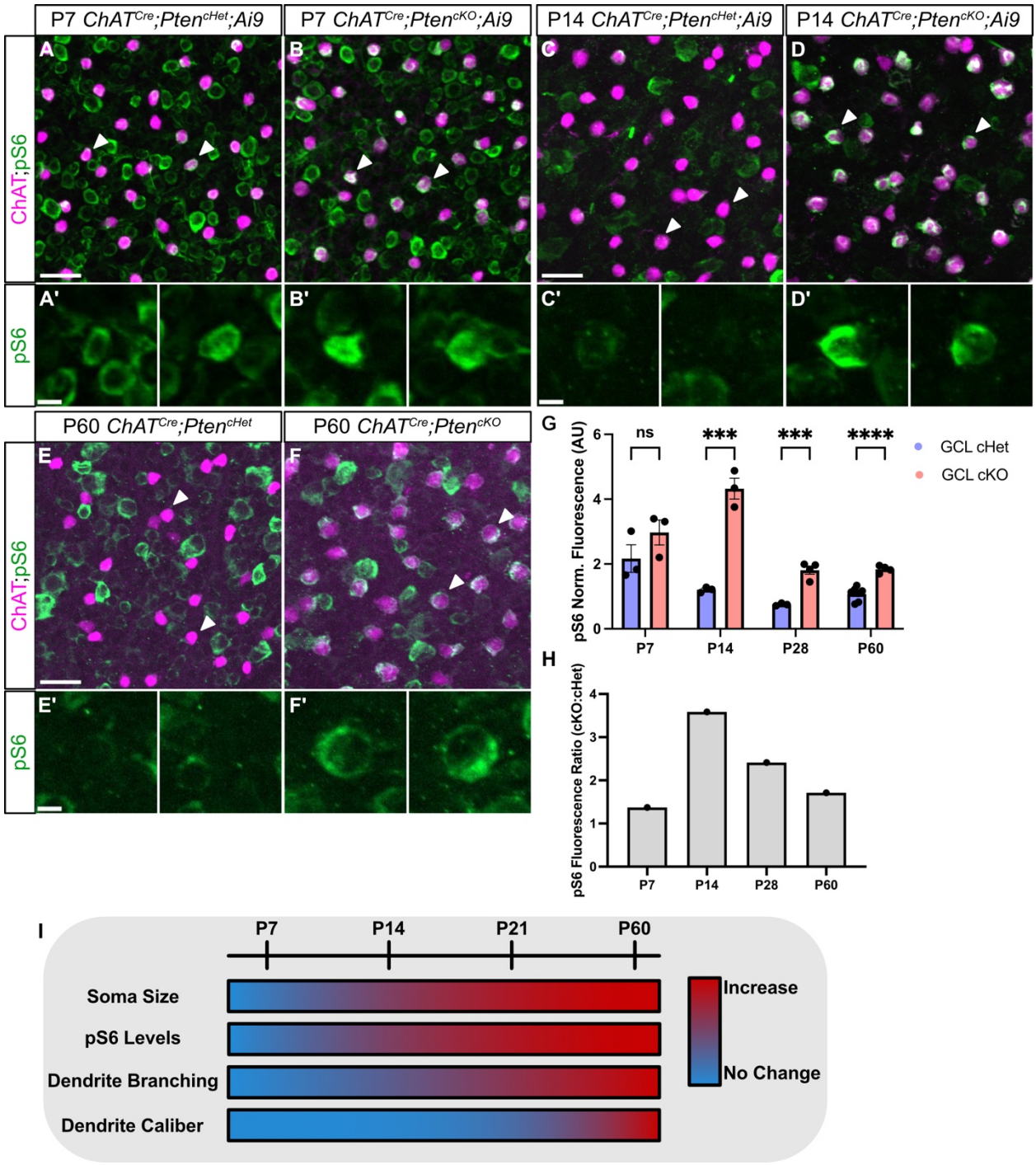
P7 ChATCre;PtencHet;Ai9
P7 ChATCre;PtencKO;Ai9
P14 ChATCre;PtencHet;Ai9
P14 ChATCre;PtencKO;Ai9
ChAT;pS6
pS6
A
B
C
D
A'
B'
C'
D'
P60 ChATCre;PtencHet
P60 ChATCre;PtencKO
E
F
E'
F'
G
pS6 Norm. Fluorescence (AU)
ns
***
***
****
GCL cHet
GCL cKO
P7
P14
P28
P60
H
pS6 Fluorescence Ratio (cKO:cHet)
I
P7
P14
P21
P60
Soma Size
pS6 Levels
Dendrite Branching
Dendrite Caliber
Increase
No Change

Figure 2.6. Increased pS6 precedes dendrite branching phenotypes in developing SACs

A-F. Retinal flat mounts of *ChAT^{Cre};Pten^{cHet}* and *ChAT^{Cre};Pten^{cKO}* SACs immunostained for ChAT (magenta) and pS6 (green) at P7 (**A-B**), P14 (C-D), and P60 (**E-F**). White arrowheads indicate SAC somas. **A'-B'.** Closeups of indicated P7 SAC somas show high levels of pS6 in both *ChAT^{Cre};Pten^{cHet}* and *ChAT^{Cre};Pten^{cKO}* retinas. **C'-D'.** At P14, pS6 levels are diminished in *ChAT^{Cre};Pten^{cHet}* SACs but elevated in *ChAT^{Cre};Pten^{cKO}* SACs. **E'-F'.** Closeups of SAC somas show that pS6 remains elevated in *ChAT^{Cre};Pten^{cKO}* SACs relative to controls at P60. **G-H.** Quantification at P7, P14, P28, and P60 shows that pS6 levels are initially high in SACs at P7 (*cHet: n = 3, 2.168 ± 0.4260; cKO: n = 3, 2.971 ± 0.3848*) (p = 0.2346) and decrease at later time points in control SACs, while pS6 levels remain significantly elevated in *ChAT^{Cre};Pten^{cKO}* SACs relative to controls at P14 (*cHet: n = 3, 1.206 ± 0.04906; cKO: n = 3, 4.325 ± 0.3233*) (p = 0.0007), P28 (*cHet: n = 5, 0.8165 ± 0.04913; cKO: n = 8, 2.351 ± 0.2493*) (p = 0.0006), and P60 (*cHet: n = 7, 1.078 ± 0.07916; cKO: n = 4, 1.839 ± 0.05409*) (p < 0.0001). **I.** Summary of cellular phenotypes in *ChAT^{Cre};Pten^{cKO}* SACs over the course of development and maturation. Increases in soma size and pS6 levels become apparent by P14, increased dendritic branching by P21, and localized increases in dendrite caliber are seen at P60. Scalebars = 25 µm in A, C, and E. Scalebars = 5 µm in A', C', and E'.

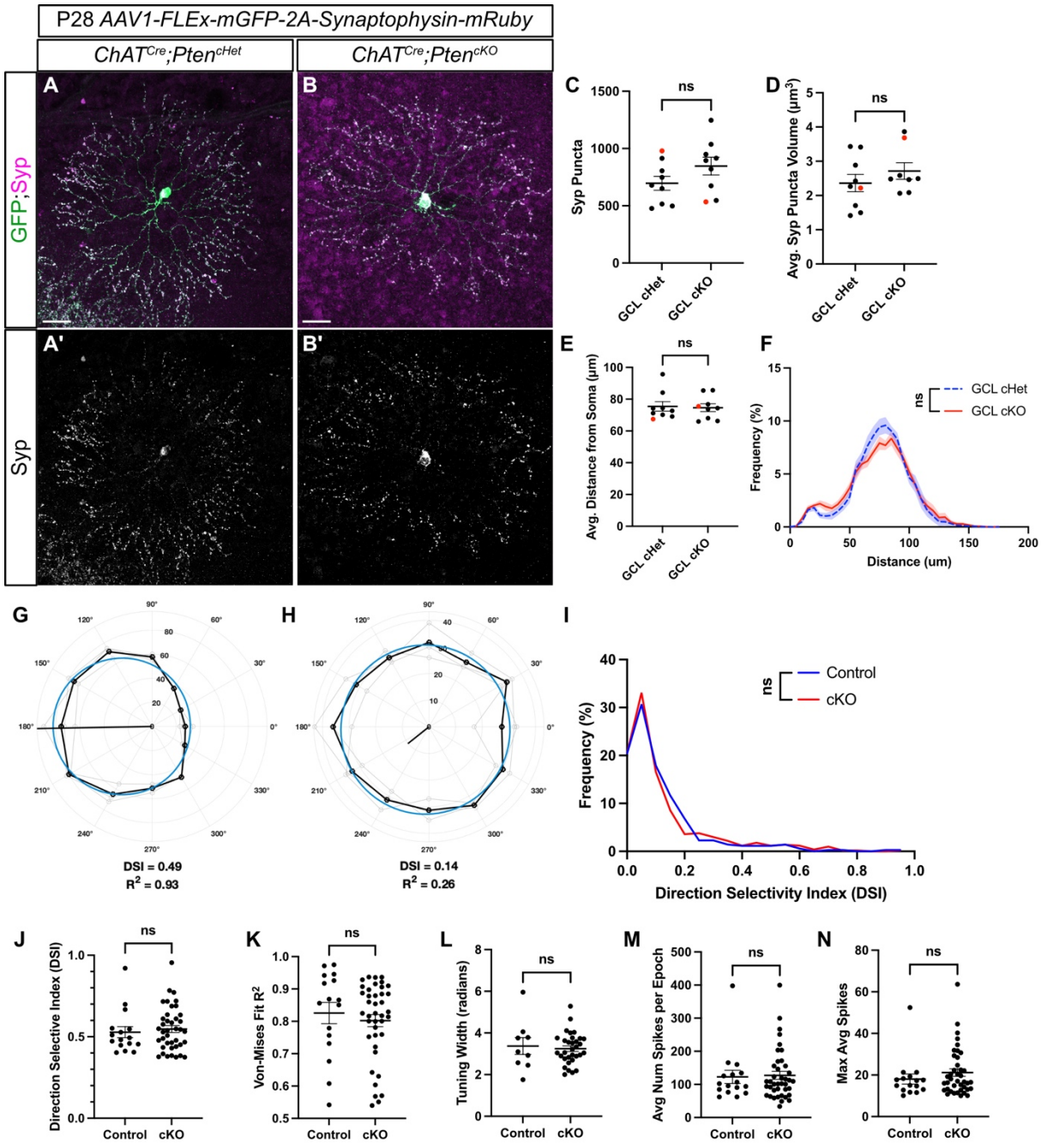
P28 AAV1-FLEx-mGFP-2A-Synaptophysin-mRuby
ChAT^Cre;Pten^cHet
ChAT^Cre;Pten^cKO
A
B
GFP;Syp
A'
B'
Syp
C
Syp Puncta
ns
GCL cHet
GCL cKO
D
Avg. Syp Puncta Volume (µm³)
E
Avg. Distance from Soma (µm)
F
Frequency (%)
Distance (um)
GCL cHet
GCL cKO
G
DSI = 0.49
R² = 0.93
H
DSI = 0.14
R² = 0.26
I
Control
cKO
Direction Selectivity Index (DSI)
J
Direction Selective Index (DSI)
K
Von-Mises Fit R²
L
Tuning Width (radians)
M
Avg Num Spikes per Epoch
N
Max Avg Spikes

Figure 2.7: Loss of *Pten* does not affect SAC synaptic outputs nor alter retinal responses to directional stimuli

A-B. P28 *ChAT^{Cre};Pten^{Ctrl}* and *ChAT^{Cre};Pten^{cKO}* retinas injected with *AAV1-FLEx-mGFP-2A-Synaptophysin-mRuby* to label SAC dendrites with membrane-bound GFP and synaptic release sites with Synaptophysin (Syp) fused to mRuby. **A'-B'.** Syp:mRuby shows highly compartmentalized localization to the outer third of SAC dendritic arbors in both *ChAT^{Cre};Pten^{cHet}* and *ChAT^{Cre} Pten^{cKO}* SACs. **C-D.** Quantification of the number (*cHet: n = 9, 696.3 ± 60.60; cKO: n = 9, 846.8 ± 77.48*) (p = 0.146) and volume (*cHet: n = 9, 2.362 ± 0.2537; cKO: n = 8, 2.716 ± 0.2415*) (p = 0.332) of Syp:mRuby puncta show no significant differences between *ChAT^{Cre};Pten^{cHet}* and *ChAT^{Cre} Pten^{cKO}* SACs. **E-F.** Quantification of the distribution of Syp:mRuby puncta reveals no significant changes in the average distance from the soma number (*cHet: n = 9, 75.46 ± 2.994; cKO: n = 9, 74.66 ± 2.452*) (p = 0.838) or the distribution along SAC dendrites (p > 0.999) in *ChAT^{Cre};Pten^{cHet}* and *ChAT^{Cre} Pten^{cKO}* SACs. Data reported as mean ± SEM and contain cells from at least 3 animals. Scalebars = 25 µm. **G, H.** Example polar plots of directional responses from individual RGCs following MEA recording of *ChAT^{Cre};Pten^{cHet}* and *ChAT^{Cre} Pten^{cKO}* retinas. Direction selective (DS) cells were identified based on their direction selective index (DSI) and their goodness of fit for the von Mises distribution. The black trace indicates the cells responses to light stimuli in different directions, while the blue circle represents the von Mises fit. **(G)** shows an example of a direction selective response, while **(H)** shows a direction insensitive response. **I.** Distribution of the DSI of all detected cells from MEA recordings shows that most cells fall below the DSI threshold for a DS cell (0.37), but a small population are direction selective (p = 0.9999). **J-N.** Quantification of DSI (p = 0.632), von Mises fit (p = 0.5179), tuning width (p = 0.6965), average

number of spikes per epoch (p = 0.8411), and average spikes (p = 0.3397) in preferred direction from DS cells; no significant differences in the response properties of DS cells were detected between *ChAT^{Cre};Pten^{cHet}* and *ChAT^{Cre} Pten^{cKO}* retinas.

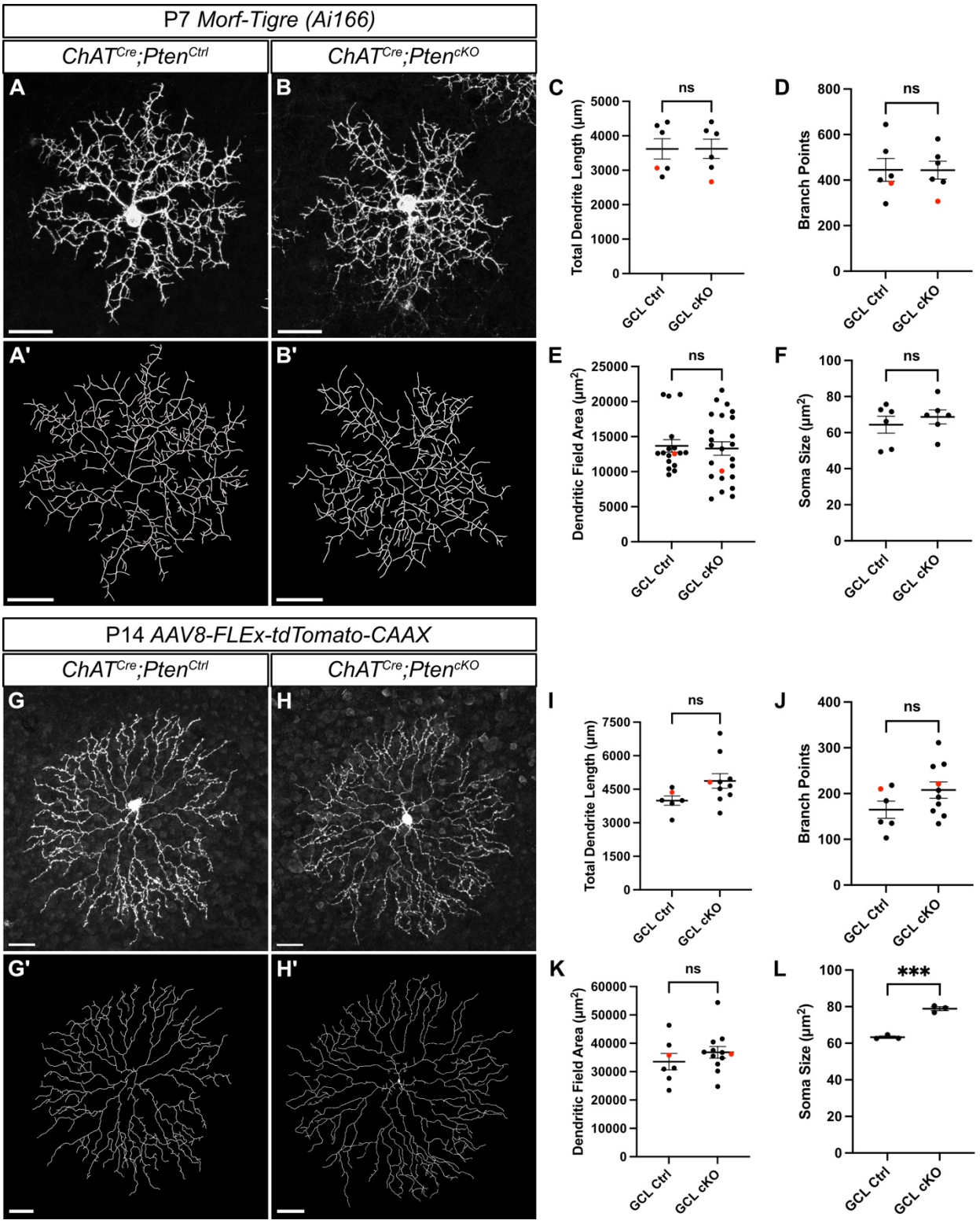
P7 Morf-Tigre (Ai166)
ChAT^Cre;Pten^Ctrl
ChAT^Cre;Pten^cKO
A
B
A'
B'
C
ns
Total Dendrite Length (µm)
5000
4000
3000
2000
1000
0
GCL Ctrl
GCL cKO
D
ns
Branch Points
800
600
400
200
0
GCL Ctrl
GCL cKO
E
ns
Dendritic Field Area (µm²)
25000
20000
15000
10000
5000
0
GCL Ctrl
GCL cKO
F
ns
Soma Size (µm²)
100
80
60
40
20
0
GCL Ctrl
GCL cKO
P14 AAV8-FLEx-tdTomato-CAAX
ChAT^Cre;Pten^Ctrl
ChAT^Cre;Pten^cKO
G
H
G'
H'
I
ns
Total Dendrite Length (µm)
7500
6000
4500
3000
1500
0
GCL Ctrl
GCL cKO
J
ns
Branch Points
400
300
200
100
0
GCL Ctrl
GCL cKO
K
ns
Dendritic Field Area (µm²)
60000
50000
40000
30000
20000
10000
0
GCL Ctrl
GCL cKO
L
***
Soma Size (µm²)
100
80
60
40
20
0
GCL Ctrl
GCL cKO

Supplementary Figure S2.1. *Pten* deletion from SACs does not affect their morphology at early developmental timepoints

A-B. P7 SACs from *ChAT^{Cre};Pten^{cHet};Ai166* and *ChAT^{Cre};Pten^{cKO};Ai166* retinas were sparsely labeled using a genetically encoded *Morf-Tigre* reporter. Images show single SACs located in the GCL. **A'-B'.** Imaris reconstructions of P7 SACs from A-B. **C-E.** Quantification of total dendrite length (*Ctrl: n = 6, 3620 ± 293.6; cKO: n = 6, 3623 ± 279.7*) (p = 0.778), number of branch points (*Ctrl: n = 6, 445.2 ± 49.84; cKO: n = 6, 443.5 ± 39.23*) (p = 0.889), and dendritic field area (*Ctrl: n = 17, 13672 ± 900.3; cKO: n = 24, 13297 ± 956.0*) (p = 0.784) from individual SACs showed no significant differences between control and cKO SACs at P7. **F.** Quantification of average soma size (*Ctrl: n = 6, 64.39 ± 4.710; cKO: n = 6, 68.73 ± 3.920*) (p = 0.495) by animal showed no changes between control and cKO SACs. **G-H.** P14 *ChAT^{Cre};Pten^{cHet}* and *ChAT^{Cre};Pten^{cKO}* SACs were sparsely labeled by injection of *AAV8-FLEx-tdTomato-CAAX*. Images show single SACs located in the GCL. **G'-H'.** Imaris reconstructions of P14 SACs from G-H. **I-K.** Quantification of total dendritic length (*Ctrl: n = 6, 3989 ± 205.5; cKO: n = 10, 4873 ± 326.4*) (p = 0.072), number of branch points (*Ctrl: n = 6, 164.7 ± 18.86; cKO: n = 10, 207.8 ± 17.82*) (p = 0.137), dendritic field area (*Ctrl: n = 7, 33546 ± 2898; cKO: n = 12, 36816 ± 2052*) (p = 0.361) from individual SACs showed no significant differences between control and cKO SACs. **L.** Quantification of average soma size revealed significant increases in cKO SACs at P14 (*Ctrl: n = 3, 63.32 ± 0.6511; cKO: n = 3, 78.88 ± 1.092*) (p = 0.0003). Red dots indicate data from representative images. Data reported as mean ± SEM and contain cells from at least 3 animals. Scalebars = 25 μm.

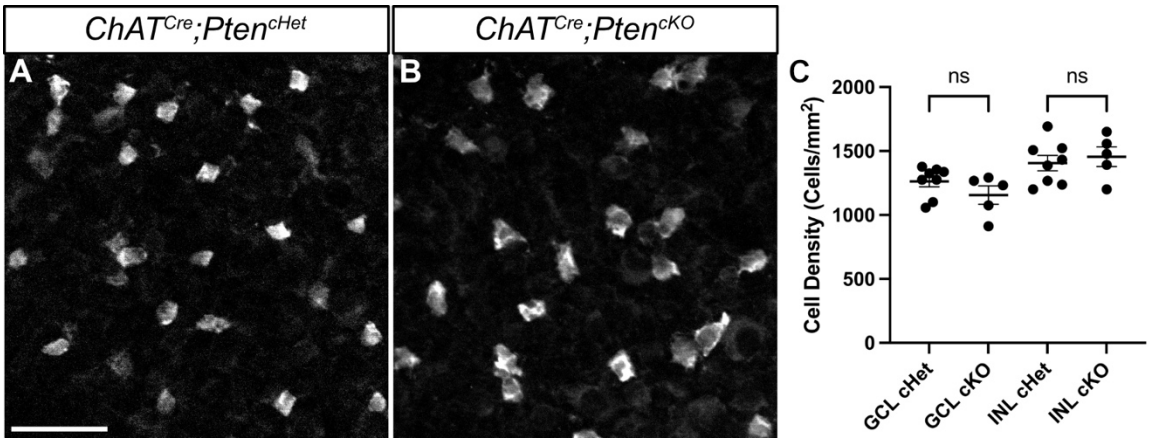

Supplementary Figure S2.2. *ChAT^{Cre}* mediated *Pten* deletion from SACs does not cause changes in cell density at P60

A, B. Representative images of P60 SACs from the GCL labeled with ChAT antibody. **C.** Quantification of cell density reveals no changes in cell density between *ChAT^{Cre};Pten^{cHet}* and *ChAT^{Cre};Pten^{cKO}* SACs at P60 in both the GCL number (*cHet: n = 8, 1263 ± 42.23; cKO: n = 5, 1156 ± 71.58*) (p = 0.1931) and INL (*cHet: n = 8, 1406 ± 59.30; cKO: n = 5, 1456 ± 76.89*) (p = 0.6171). Data reported as mean ± SEM. Scalebars = 25 µm.

References

1. Lefebvre, J.L., J.R. Sanes, and J.N. Kay, *Development of dendritic form and function.* Annu Rev Cell Dev Biol, 2015. **31**: p. 741-77.
2. Zeng, H. and J.R. Sanes, *Neuronal cell-type classification: challenges, opportunities and the path forward.* Nat Rev Neurosci, 2017. **18**(9): p. 530-546.
3. Jan, Y.N. and L.Y. Jan, *Branching out: mechanisms of dendritic arborization.* Nat Rev Neurosci, 2010. **11**(5): p. 316-28.
4. Lefebvre, J.L., *Molecular mechanisms that mediate dendrite morphogenesis.* Curr Top Dev Biol, 2021. **142**: p. 233-282.
5. Albeg, A., et al., *C. elegans multi-dendritic sensory neurons: morphology and function.* Mol Cell Neurosci, 2011. **46**(1): p. 308-17.
6. Oren-Suissa, M., et al., *The fusogen EFF-1 controls sculpting of mechanosensory dendrites.* Science, 2010. **328**(5983): p. 1285-8.
7. Tsalik, E.L., et al., *LIM homeobox gene-dependent expression of biogenic amine receptors in restricted regions of the C. elegans nervous system.* Dev Biol, 2003. **263**(1): p. 81-102.
8. Inberg, S., et al., *Lessons from Worm Dendritic Patterning.* Annu Rev Neurosci, 2019. **42**: p. 365-383.
9. Sundararajan, L., J. Stern, and D.M. Miller, 3rd, *Mechanisms that regulate morphogenesis of a highly branched neuron in C. elegans.* Dev Biol, 2019. **451**(1): p. 53-67.
10. Grueber, W.B., L.Y. Jan, and Y.N. Jan, *Tiling of the Drosophila epidermis by multidendritic sensory neurons.* Development, 2002. **129**(12): p. 2867-78.
11. Jinushi-Nakao, S., et al., *Knot/Collier and cut control different aspects of dendrite cytoskeleton and synergize to define final arbor shape.* Neuron, 2007. **56**(6): p. 963-78.
12. Sugimura, K., et al., *Development of morphological diversity of dendrites in Drosophila by the BTB-zinc finger protein abrupt.* Neuron, 2004. **43**(6): p. 809-22.
13. Grueber, W.B., L.Y. Jan, and Y.N. Jan, *Different levels of the homeodomain protein cut regulate distinct dendrite branching patterns of Drosophila multidendritic neurons.* Cell, 2003. **112**(6): p. 805-18.
14. Gibson, D.A., et al., *Dendrite self-avoidance requires cell-autonomous slit/robo signaling in cerebellar purkinje cells.* Neuron, 2014. **81**(5): p. 1040-1056.
15. Lefebvre, J.L., et al., *Protocadherins mediate dendritic self-avoidance in the mammalian nervous system.* Nature, 2012. **488**(7412): p. 517-21.
16. Kawabata Galbraith, K., et al., *MTSS1 Regulation of Actin-Nucleating Formin DAAM1 in Dendritic Filopodia Determines Final Dendritic Configuration of Purkinje Cells.* Cell Rep, 2018. **24**(1): p. 95-106.e9.
17. Morrie, R.D. and M.B. Feller, *Development of synaptic connectivity in the retinal direction selective circuit.* Curr Opin Neurobiol, 2016. **40**: p. 45-52.
18. Prigge, C.L. and J.N. Kay, *Dendrite morphogenesis from birth to adulthood.* Curr Opin Neurobiol, 2018. **53**: p. 139-145.
19. Kay, J.N., M.W. Chu, and J.R. Sanes, *MEGF10 and MEGF11 mediate homotypic interactions required for mosaic spacing of retinal neurons.* Nature, 2012. **483**(7390): p. 465-9.

20. Ray, T.A., et al., *Formation of retinal direction-selective circuitry initiated by starburst amacrine cell homotypic contact.* Elife, 2018. **7**.
21. Kozlowski, C., S.E. Hadyniak, and J.N. Kay, *Retinal neurons establish mosaic patterning by excluding homotypic somata from their dendritic territories.* Cell Rep, 2024. **43**(8): p. 114615.
22. Prigge, C.L., et al., *Rejection of inappropriate synaptic partners in mouse retina mediated by transcellular FLRT2-UNC5 signaling.* Dev Cell, 2023. **58**(20): p. 2080-2096.e7.
23. Sun, L.O., et al., *On and off retinal circuit assembly by divergent molecular mechanisms.* Science, 2013. **342**(6158): p. 1241974.
24. James, R.E., et al., *Retinal ganglion cell-derived semaphorin 6A segregates starburst amacrine cell dendritic scaffolds to organize the mouse inner retina.* Development, 2024. **151**(22).
25. Soto, F., et al., *AMIGO2 Scales Dendrite Arbors in the Retina.* Cell Rep, 2019. **29**(6): p. 1568-1578.e4.
26. Worby, C.A. and J.E. Dixon, *PTEN.* Annu Rev Biochem, 2014. **83**: p. 641-69.
27. Rademacher, S. and B.J. Eickholt, *PTEN in Autism and Neurodevelopmental Disorders.* Cold Spring Harb Perspect Med, 2019. **9**(11).
28. Chen, L., et al., *Pten is a key intrinsic factor regulating raphe 5-HT neuronal plasticity and depressive behaviors in mice.* Transl Psychiatry, 2021. **11**(1): p. 186.
29. Gallent, E.A. and O. Steward, *Neuronal PTEN deletion in adult cortical neurons triggers progressive growth of cell bodies, dendrites, and axons.* Exp Neurol, 2018. **303**: p. 12-28.
30. Cupolillo, D., et al., *Autistic-Like Traits and Cerebellar Dysfunction in Purkinje Cell PTEN Knock-Out Mice.* Neuropsychopharmacology, 2016. **41**(6): p. 1457-66.
31. Kwon, C.H., et al., *Pten regulates neuronal arborization and social interaction in mice.* Neuron, 2006. **50**(3): p. 377-88.
32. Luikart, B.W., et al., *Pten knockdown in vivo increases excitatory drive onto dentate granule cells.* J Neurosci, 2011. **31**(11): p. 4345-54.
33. Santos, V.R., et al., *PTEN deletion increases hippocampal granule cell excitability in male and female mice.* Neurobiol Dis, 2017. **108**: p. 339-351.
34. Sakagami, K., et al., *PTEN regulates retinal interneuron morphogenesis and synaptic layer formation.* Mol Cell Neurosci, 2012. **49**(2): p. 171-83.
35. Cantrup, R., et al., *Cell-type specific roles for PTEN in establishing a functional retinal architecture.* PLoS One, 2012. **7**(3): p. e32795.
36. Tachibana, N., et al., *Pten Regulates Retinal Amacrine Cell Number by Modulating Akt, Tgfβ, and Erk Signaling.* J Neurosci, 2016. **36**(36): p. 9454-71.
37. Touahri, Y., et al., *Pten regulates endocytic trafficking of cell adhesion and Wnt signaling molecules to pattern the retina.* Cell Rep, 2024. **43**(4): p. 114005.
38. Clipperton-Allen, A.E. and D.T. Page, *Pten haploinsufficient mice show broad brain overgrowth but selective impairments in autism-relevant behavioral tests.* Hum Mol Genet, 2014. **23**(13): p. 3490-505.
39. Chen, Y., et al., *Pten Mutations Alter Brain Growth Trajectory and Allocation of Cell Types through Elevated β-Catenin Signaling.* J Neurosci, 2015. **35**(28): p. 10252-67.
40. Fernandez, A., et al., *Altered primary somatosensory neuron development in a Pten heterozygous model for autism spectrum disorder.* bioRxiv, 2025.

41. Poleg-Polsky, A., H. Ding, and J.S. Diamond, *Functional Compartmentalization within Starburst Amacrine Cell Dendrites in the Retina.* Cell Rep, 2018. **22**(11): p. 2898-2908.
42. Ding, H., et al., *Species-specific wiring for direction selectivity in the mammalian retina.* Nature, 2016. **535**(7610): p. 105-10.
43. Ing-Esteves, S. and J.L. Lefebvre, *Gamma-protocadherins regulate dendrite self-recognition and dynamics to drive self-avoidance.* Curr Biol, 2024. **34**(18): p. 4224-4239.e4.
44. Veldman, M.B., et al., *Brainwide Genetic Sparse Cell Labeling to Illuminate the Morphology of Neurons and Glia with Cre-Dependent MORF Mice.* Neuron, 2020. **108**(1): p. 111-127.e6.
45. Kosillo, P., et al., *Dopamine neuron morphology and output are differentially controlled by mTORC1 and mTORC2.* Elife, 2022. **11**.
46. Ferrer-Vaquer, A., et al., *A sensitive and bright single-cell resolution live imaging reporter of Wnt/ß-catenin signaling in the mouse.* BMC Dev Biol, 2010. **10**: p. 121.
47. Briggman, K.L., M. Helmstaedter, and W. Denk, *Wiring specificity in the direction-selectivity circuit of the retina.* Nature, 2011. **471**(7337): p. 183-8.
48. Beier, K.T., et al., *Circuit Architecture of VTA Dopamine Neurons Revealed by Systematic Input-Output Mapping.* Cell, 2015. **162**(3): p. 622-34.
49. Koizumi, A., et al., *Organotypic culture of physiologically functional adult mammalian retinas.* PLoS One, 2007. **2**(2): p. e221.
50. Ford, K.J. and M.B. Feller, *Assembly and disassembly of a retinal cholinergic network.* Vis Neurosci, 2012. **29**(1): p. 61-71.
51. Pei, Z., et al., *Conditional Knock-Out of Vesicular GABA Transporter Gene from Starburst Amacrine Cells Reveals the Contributions of Multiple Synaptic Mechanisms Underlying Direction Selectivity in the Retina.* J Neurosci, 2015. **35**(38): p. 13219-32.
52. Kostadinov, D. and J.R. Sanes, *Protocadherin-dependent dendritic self-avoidance regulates neural connectivity and circuit function.* Elife, 2015. **4**.
53. Yao, X., et al., *Gap Junctions Contribute to Differential Light Adaptation across Direction-Selective Retinal Ganglion Cells.* Neuron, 2018. **100**(1): p. 216-228.e6.
54. Liu, W. and A. Cvekl, *Six3 in a small population of progenitors at E8.5 is required for neuroretinal specification via regulating cell signaling and survival in mice.* Dev Biol, 2017. **428**(1): p. 164-175.
55. Marquardt, T., et al., *Pax6 is required for the multipotent state of retinal progenitor cells.* Cell, 2001. **105**(1): p. 43-55.
56. Rowan, S. and C.L. Cepko, *Genetic analysis of the homeodomain transcription factor Chx10 in the retina using a novel multifunctional BAC transgenic mouse reporter.* Dev Biol, 2004. **271**(2): p. 388-402.
57. Garcia-Junco-Clemente, P. and P. Golshani, *PTEN: A master regulator of neuronal structure, function, and plasticity.* Commun Integr Biol, 2014. **7**(1): p. e28358.
58. Jaworski, J., et al., *Control of dendritic arborization by the phosphoinositide-3'-kinase-Akt-mammalian target of rapamycin pathway.* J Neurosci, 2005. **25**(49): p. 11300-12.
59. Arafa, S.R., et al., *Self-reinforcing effects of mTOR hyperactive neurons on dendritic growth.* Exp Neurol, 2019. **311**: p. 125-134.

60. Getz, S.A., et al., *PTEN Regulates Dendritic Arborization by Decreasing Microtubule Polymerization Rate.* J Neurosci, 2022. **42**(10): p. 1945-1957.
61. Urwyler, O., et al., *Branch-restricted localization of phosphatase Prl-1 specifies axonal synaptogenesis domains.* Science, 2019. **364**(6439).
62. Feliciano, D.M., et al., *Single-cell Tsc1 knockout during corticogenesis generates tuber-like lesions and reduces seizure threshold in mice.* J Clin Invest, 2011. **121**(4): p. 1596-607.
63. Tariq, K., et al., *Disruption of mTORC1 rescues neuronal overgrowth and synapse function dysregulated by Pten loss.* Cell Rep, 2022. **41**(5): p. 111574.
64. Zhou, F.Q., et al., *NGF-induced axon growth is mediated by localized inactivation of GSK-3beta and functions of the microtubule plus end binding protein APC.* Neuron, 2004. **42**(6): p. 897-912.
65. Ziak, J., et al., *Microtubule-binding protein MAP1B regulates interstitial axon branching of cortical neurons via the tubulin tyrosination cycle.* Embo j, 2024. **43**(7): p. 1214-1243.
66. Meyer Zu Reckendorf, S., et al., *Motoneuron-Specific PTEN Deletion in Mice Induces Neuronal Hypertrophy and Also Regeneration after Facial Nerve Injury.* J Neurosci, 2022. **42**(12): p. 2474-2491.
67. Park, K.K., et al., *Promoting axon regeneration in the adult CNS by modulation of the PTEN/mTOR pathway.* Science, 2008. **322**(5903): p. 963-6.
68. Christie, K.J., et al., *PTEN inhibition to facilitate intrinsic regenerative outgrowth of adult peripheral axons.* J Neurosci, 2010. **30**(27): p. 9306-15.
69. Liu, K., et al., *PTEN deletion enhances the regenerative ability of adult corticospinal neurons.* Nat Neurosci, 2010. **13**(9): p. 1075-81.
70. Sun, F., et al., *Sustained axon regeneration induced by co-deletion of PTEN and SOCS3.* Nature, 2011. **480**(7377): p. 372-5.
71. Santos, J.R., et al., *Predicting the Regenerative Potential of Retinal Ganglion Cells Based on Developmental Growth Trajectories.* bioRxiv, 2025.
72. Yoshida, K., et al., *A key role of starburst amacrine cells in originating retinal directional selectivity and optokinetic eye movement.* Neuron, 2001. **30**(3): p. 771-80.
73. Amthor, F.R., K.T. Keyser, and N.A. Dmitrieva, *Effects of the destruction of starburst-cholinergic amacrine cells by the toxin AF64A on rabbit retinal directional selectivity.* Vis Neurosci, 2002. **19**(4): p. 495-509.
74. Vlasits, A.L., et al., *Visual stimulation switches the polarity of excitatory input to starburst amacrine cells.* Neuron, 2014. **83**(5): p. 1172-84.
75. Euler, T., P.B. Detwiler, and W. Denk, *Directionally selective calcium signals in dendrites of starburst amacrine cells.* Nature, 2002. **418**(6900): p. 845-52.
76. Lee, S. and Z.J. Zhou, *The synaptic mechanism of direction selectivity in distal processes of starburst amacrine cells.* Neuron, 2006. **51**(6): p. 787-99.
77. Morrie, R.D. and M.B. Feller, *A Dense Starburst Plexus Is Critical for Generating Direction Selectivity.* Curr Biol, 2018. **28**(8): p. 1204-1212.e5.
78. Williams, M.R., et al., *Hyperactivity of newborn Pten knock-out neurons results from increased excitatory synaptic drive.* J Neurosci, 2015. **35**(3): p. 943-59.
79. Rossi, J., et al., *Melanocortin-4 receptors expressed by cholinergic neurons regulate energy balance and glucose homeostasis.* Cell Metab, 2011. **13**(2): p. 195-204.

80. Furuta, Y., et al., *Retina- and ventral forebrain-specific Cre recombinase activity in transgenic mice.* Genesis, 2000. **26**(2): p. 130-2.
81. Backman, S.A., et al., *Deletion of Pten in mouse brain causes seizures, ataxia and defects in soma size resembling Lhermitte-Duclos disease.* Nat Genet, 2001. **29**(4): p. 396-403.
82. Madisen, L., et al., *A robust and high-throughput Cre reporting and characterization system for the whole mouse brain.* Nat Neurosci, 2010. **13**(1): p. 133-40.
83. Li, S., et al., *IPLaminator: an ImageJ plugin for automated binning and quantification of retinal lamination.* BMC Bioinformatics, 2016. **17**: p. 36.

STAR★METHODS

Resource Availability

Lead contact

Further information and requests for resources and reagents should be directed to and will be fulfilled by the Lead Contact, Dr. Kevin Wright (wrighke@ohsu.edu)

Materials Availability

Transgenic mouse lines used in this study are available upon request or in a central repository (Jackson Laboratory). All antibodies and reagents are commercially available.

Data availability

Data available upon request to lead contact.

Experimental Models and Subject Details

Animals and Animal Procedures

All animal procedures were approved by the Oregon Health and Science Institutional Animal Care and Use Committee (IACUC). The following mouse lines were used: *ChAT*^{Cre} [79], *Six3*^{Cre} [80], *Pten*^{flox} [81], *Ai9* [82], *TIGRE-MORF/Ai166* [44], *TCF/Lef:H2B/GFP* [46]. All lines were maintained on a *C57BL/6J* background. Mice of both sexes were used for experiments.

Intravitreal injections were performed on mice at P2 or P28. P2 mice were anesthetized through indirect contact with ice and brought back to body temperature through contact with a warm glove. Mice were injected with a 30psi pulse for 30ms. P28 mice were anesthetized using isoflurane at a flow rate of 3%, and maintained at a flow rate of 1.5%. After deeply anesthetized, animals were placed on a Kopf stereotaxic injection rig (Model 1900 Stereotaxic Alignment system). 0.5% proparacaine hydrochloride ophthalmic solution was applied as a topical anesthetic to the eye, followed by 1% tropicamide ophthalmic solution for dilation. Gentle-eye lubricant was added to both eyes, and a micro vessel clamp was used to push the globe outwards. Needles were pulled on a Sutter Instrument micropipette puller (P-97 Flaming/Brown Micropipette Puller) and beveled with sandpaper. Animals were injected with *AAV8-FLEx-tdTomato-CAAX* at a titer of $2.6x10^{11}$ or *AAV1-FLEx-mGFP-2A-Synaptophysin-mRuby* at a titer of 1.8×10^{12} [48].

Method Details

Tissue Processing and Immunohistochemistry

Mouse eyes were enucleated and drop fixed in 4% EM-grade PFA for 30 minutes. For *TIGRE-MORF* mice, retinas were instead fixed with a solution of 9% Glyoxal 8% Acetic Acid at pH = 4.0, as this improved resolution of the Tigre-GFP signal. After fixation eyes were washed in PBS. Eyes were then pierced with a 30G ½ inch needle and the cornea was cut away with microdissection scissors.

For retinal flat mounts, the retina was isolated and then transferred to an Eppendorf tube and blocked and permeabilized with a blocking solution (2% normal donkey serum, 0.2% Triton X-

100, 0.002% Sodium Azide) for 1 hour. After blocking, retinas were stained with primary antibodies and left shaking at 4ºC for 3-4 days. Retinas were then washed overnight in PBS. Retinas were then stained with secondary antibodies and left shaking at 4ºC for 1 day. Four cuts were made into the retina to allow it to lay flat on glass microscope slides. Retinas were mounted with Fluoromount-G and sealed with nail polish. All antibody dilutions are listed on the Key Resource Table.

For retinal cross-sections, the retina and lens were left in the eye cup and cryoprotected in 15% sucrose overnight. The next day, the lens was removed, eyes were placed in Neg-50, and the eyes were frozen in the eye cup in 2-methylbutane. Eyes were cryosectioned on a Leica cryostat (CM3050 S) at 20µm sections. The edges of the slide were then coated with a hydrophobic barrier using an ImmEdge pen. The slide was washed with PBS to remove any remaining Neg-50 attached to the slide. Retinas were then stained with primary antibody at 4ºC overnight. The next day, retinas were washed with PBS three times for 15 minutes. Secondary antibody was applied and the retinas were left at room temperature for 2 hours. Hoechst was then applied to the retinas for 10 minutes, followed by three 15-minute PBS washes. Retinas were mounted with Fluoromount-G and sealed with nail polish. Antibody dilutions were the same as in flat mounts.

Fluorescence Image Acquisition

Retinal sections were imaged on a Zeiss Axio Imager M2 upright microscope equipped with an ApoTome2 using a 20x objective. Retinal flat mounts imaged for cell density, somal quantification, mosaic analysis, pS6, and β-catenin quantification were also imaged with these settings. Retinal flat mounts imaged for single cell morphology and synaptophysin labeling were

imaged on a Zeiss LSM 900 confocal microscope using a 40x water objective with NA = 1.2. Images were acquired using the Zeiss Zen Imaging software for both microscopes.

Multi-Electrode Array Recordings

Tissue from mouse retinae were placed RGC side down on a 3Brain Accura HD-MEA connected to a BiocCAM DupleX recording system (3Brain AG, Wädenswil, Switzerland). The Accura HD-MEA contains 4096 electrodes in a 3.8 x 3.8 mm area, where each electrode is 21 µm x 21 µm spaced 60 µm apart. The internal diameter of the reservoir is 25mm, with a 7 mm height. Retinae were dissected off the choroid and the vitreous was then carefully dissected from the tissue prior to mounting the tissue photoreceptor-side down on Millicell polytetrafluoroethylene membrane cell culture insert (Millipore Sigma; PICM0RG50). To adhere the retina to the membrane, the Ames medium was removed from the insert and gentle suction was applied using a gas stone connected to a vacuum chamber with filter paper between the stone and the membrane. The insert was then placed back into Ames' medium and the membrane trimmed to outside the edges of the retinae. The retinae/insert was placed RGC-side down on the MEA surface in Ames' medium and the Ames medium was removed from the reservoir to facilitate connectivity with the electrodes. A platinum harp was placed over the insert to hold the retinae in place, the reservoir was filled with Ames, the MEA was transferred to the BioCAM DupleX, and the reservoir was continuously superfused with Ames' medium @ 32°C.

Visual stimuli were generated using custom software generated in Python (PyStim; https://github.com/SivyerLab/pystim) and presented on a LightCrafter 4500 projector (Texas Instruments, USA) modified by removing the focusing optics. Projector light was captured with

a TV lens, passed through neutral density filters and an Olympus MVX10 fluorescence microscope system with a MVPLAPO 2XC (0.5 numerical aperture) objective. A 1.5 mm coverslip was mounted onto the reservoir to reduce diffraction caused by the air/Ames interface. Visual stimuli presented used either the green (LE CG Q9WP; 520 nm peak) or blue LEDs (LE B Q9WP; 455 nm peak) and were presented full field at a range of light intensities between 6.2e11 photons/cm2/s and 8.9e13 photons/cm2/s. Stimuli consisted of green full field chirp responses used to isolate rod and cone mediated inputs to RGCs, ON and OFF responses, and temporal and spatial frequency tuning properties. Moving stimuli consisted of gratings moving in 12 directions for 3 seconds each direction.

Quantification and Statistical Analysis

SAC Population Analyses (Cell Counting, Soma Size, Mosaic Spacing, and pS6 and β-catenin)

Retina flat mounts were immunostained for either tdTomato or ChAT. Three regions were imaged per retina per animal. GCL and INL images were captured from the same regions of the retina, avoiding the center and far periphery. Every $Pten^{cKO}$ animal included had at least one $Pten^{cHet}$ littermate control. The tdTomato or ChAT channel was binarized in ImageJ using either the Otsu or Huang thresholding algorithm and ImageJ's "Analyze Particles" function was used to perform cell counts. As part of this process, we generated individual regions of interest (ROIs) for every cell, an ROI consisting of every cell and an inverse ROI consisting of the background.

As part of cell density quantification, the size of the particles and the xy coordinates of the center of SAC somas were collected for soma size and mosaic spacing analysis. These xy coordinates were then entered into WinDRP, a program designed to calculate the regularity of cells using a

density recovery profile (Rodieck 1991). From this, a regularity index ratio was calculated, which defines how mosaically spaced a population of cells are compared a random distribution.

The same image acquisition and ImageJ pipeline for cell counting was used to analyze pS6 and β-catenin fluorescence. ImageJ's "Analyze Particles" function was used to obtain ROIs for the SACs within an image and the inverse ROI representing background signal. The pS6 and β-catenin fluorescent signals were then measured in both these ROIs. The SAC ROI was then normalized to the background ROI to obtain a normalized fluorescence intensity signal.

IPLaminator Analysis

Lamination was quantified in P28 retina cross-sections stained for tdTomato and DAPI using IPLaminator. IPLaminator is an ImageJ plugin designed to bin and quantify retinal lamination [83]. DAPI was used to define the area of the IPL, then tdTomato fluorescence was measured by IPLaminator. For every image, the IPL was divided into 20 equal sections and measured along the depth of the IPL to normalize any variance in IPL thickness.

Imaris Reconstructions and Morphometric Analysis

SACs were reconstructed manually using the Imaris Filaments module. Briefly, the soma was assigned as a dendrite beginning point and dendrites were traced from there using the AutoPath tool. From these reconstructions, data including total dendrite length, number of branch points, and Sholl intersections were collected. Sholl data was generated from Imaris at 1µm intervals. Sholl data was normalized to the radial distance of the cell by averaging the number of Sholl intersections along every 10% of the radial distance. Dendrite field area was measured in ImageJ by taking the convex hull of the fluorescent area covered by a SAC. The number of self-crossings at P21 was manually counted in ImageJ by counting dendrite branch intersections in single z-

planes across a z-stack. Dendrite caliber was measure in ImageJ by drawing a line perpendicular to the dendrite and measuring its length. Any dendrite greater than 1µm in caliber was considered a hypertrophic dendrite.

Synaptophysin Analysis

Synaptophysin puncta were quantified in Imaris using the Surfaces module. Briefly, surfaces were generated for all putative synaptophysin puncta, which were then filtered based on fluorescence of the membrane bound GFP signal to exclude noise outside the SAC. Puncta smaller than 0.5µm were also excluded. The number of puncta, size of the puncta, and distance from the soma of every puncta was obtained through Imaris.

Spike Sorting

Herding Spikes 2 (HS2), via SpikeInterface[2] Python framework, was used for spike detection and sorting. HS2 uses a mixed approach of spike spatial and prominent waveform features combined with a mean shift clustering algorithm to identify individual cells and their corresponding spikes on the array. The spike sorting scripts were executed on a high-performance computing cluster (exacloud).

The following HS2 parameters were used:

Parameter	Value
mea_pitch	60
electrode_width	21
clustering_bandwidth	20
clustering_alpha	5.5
clustering_n_jobs	-1
clustering_bin_seeding	true
clustering_min_bin_freq	16

clustering_subset	null
left_cutout_time	0.3
right_cutout_time	1.8
detect_threshold	20
probe_masked_channels	[]
probe_inner_radius	100
probe_neighbor_radius	129
probe_event_length	0.26
probe_peak_jitter	0.2
t_inc	100000
num_com_centers	1
maa	12
ahpthr	11
out_file_name	"HS2_detected"
decay_filtering	false
save_all	false
amp_evaluation_time	0.4
spk_evaluation_time	1.0
pca_ncomponents	2
pca_whiten	true
freq_min	300.0
freq_max	6000.0
filter	true
pre_scale	true
pre_scale_value	20.0
filter_duplicates	true

DSGC Classification and Statistical Analysis

Post spike sort, subsequent analysis in MATLAB R2023a (Mathworks) was performed for further cell classification based on light responses. Responses from individual units were assessed for each presented direction of light. Units without a minimum of 400 total spikes were filtered out. Remaining units had their direction selectivity ($\frac{Preferred\ Direction - Null\ Direction}{Preferred\ Direction + Null\ Direction}$) and von Mises fit calculated [53]. Units with a DSI greater than 0.37 and a von Mises fit greater than 0.5, were classified as putative DSGCs. Additional filtering was then performed to make sure the units had a minimum of 10 average spikes in their preferred direction across the epochs. Once DSGCs were determined, the average number of spikes per stimulus window (epoch) and the average number of spikes in their preferred direction were measured. Tuning width was calculated by using the full width at half maximum (FWHM) [53].

Statistics

For each experiment and time point, a minimum of three mice per condition were analyzed. For single cell morphological analysis, a minimum of 6 cells were analyzed, with most conditions having at least 8 cells. For all datasets, the variance was reported as mean ± SEM. For analysis between two groups, a Student's t-test was performed. For analysis between three groups, an ANOVA with Tukey's multiple comparison was performed. For comparisons of distributions, a Kruskal-Wallis test was performed. For Sholl Analysis, an area under the curve (AUC) analysis was performed, where AUC statistics (mean, SEM, n) were computed, then analyzed via a Student's t-test. For comparison of the ratio of SACs with a hypertrophic dendrite, Fisher's exact test was used. All statistical tests were performed in GraphPad Prism 9.

Key Resources Table

REAGENT or RESOURCE	SOURCE	IDENTIFIER
Antibodies		
Goat anti-ChAT (1:500, IHC)	Millipore	Cat #: AB144P RRID: AB_11214092
Goat anti-tdTomato (1:1000, IHC)	Biorbyt	Cat #: orb182397 RRID: AB_2687917
Rabbit anti-pS6 Ser235/236 (1:100, IHC)	Cell Signaling	Cat #: 81736 RRID: AB_2938546
Rabbit anti-pS6 Ser240/244 (1:800, IHC)	Cell Signaling	Cat #: 35708 RRID: AB_2938547
Rabbit anti-Pten (1:500, IHC)	Cell Signaling	Cat #: 9559S RRID: AB_10695541
Rabbit anti-GFP (1:1000, IHC)	Abcam	Cat #: ab6556 RRID: AB_305564
Chicken anti-GFP (1:500, IHC)	Abcam	Cat #:ab13970 RRID:AB_300798
anti-Goat Alexa 546 (1:500, IHC)	Thermo Fisher Scientific	Cat #: A-11056 RRID: AB_142628
anti-Rabbit Alexa 488 (1:500, IHC)	Thermo Fisher Scientific	Cat #: A-21206 RRID: AB_2535792
anti-Rabbit Alexa 647 (1:500, IHC)	Thermo Fisher Scientific	Cat #: A-31573 RRID: AB_2536183
anti-Chicken Alexa 488 (1:500, IHC)	Thermo Fisher Scientific	Cat #: A78948 RRID: AB_2921070
Bacterial and virus strains		
AAV8-FLEx-tdTomato-CAAX		
AAV1-FLEx-mGFP-2A-Synaptophysin-mRuby (Beier et al. 2015)	Addgene	Plasmid #: 71760-AAV1 RRID: Addgene_71760
Chemicals, peptides, and recombinant proteins		
16% Paraformaldehyde	Fisher	Cat #: 50-980-487
Glyoxal	Fisher	Cat #: AC156225000
Sodium Azide	Fisher	Cat #: S227I-100
Triton X-100	Fisher	Cat #: BP151-100
Agarose	Fisher	Cat #: BP1356-500
Ethidium Bromide 1% Solution	Fisher	Cat #: BP1302-10
Normal Donkey Serum	Fisher	Cat #: 017-000-121
DreamTaq	Fisher	Cat #: FERK1082
Fluoromount-G	Fisher	Cat #: OB100-01
Neg-50	Fisher	Cat #: 22-046-511
2-methylbutane	Fisher	Cat #: AA19387AY
Sucrose	Fisher	Cat #: BP220-1
Acetic Acid, Glacial	Fisher	Cat #: A35-500
Hoechst 33342 (1:5000 IHC)	Fisher	Cat #: H3570
Ames' Medium	Sigma	Cat #: A1420-10X1L
Experimental models: Organisms/strains		
Mus Musculus: **C57BL/6J**	The Jackson Laboratory	Strain #: 000664 RRID: IMSR_JAX:000664
ChAT^{Cre} (Rossi et al. 2011) **B6.129S-*Chat*$^{tm1(cre)Lowl}$/MwarJ**	The Jackson Laboratory	Strain #: 031661 RRID: IMSR_JAX:031661

Six3^{Cre} (Furuta et al. 2000) **Tg(Six3-cre)69Frty/GcoJ**	The Jackson Laboratory	Strain #: 019755 RRID: IMSR_JAX:019755
Pten^{flox} (Backman et al. 2001) **B6.129S4-*Pten*^{tm1Hwu}/J**	The Jackson Laboratory	Strain #: 006440 RRID: IMSR_JAX:006440
Ai9 (Madisen et al. 2010) **B6.Cg-*Gt(ROSA)26Sor*$^{tm9(CAG-tdTomato)Hze}$/J**	The Jackson Laboratory	Strain #: 007909 RRID: IMSR_JAX:007909
TIGRE-MORF (Veldman et al. 2020) **B6;129S-*Igs7*$^{tm166(tetO-EGFP*,CAG-tTA2)Hze}$/XwyJ**	The Jackson Laboratory	Strain #: 035404 RRID: IMSR_JAX:035404
TCF/Lef:H2B/GFP (Ferrer-Vaquer et al. 2010) **Tg(TCF/Lef1-HIST1H2BB/EGFP)61Hadj/J**	The Jackson Laboratory	Strain #: 013752 RRID: IMSR_JAX:013752
Oligonucleotides		
Genotyping primers: Cre Forward 5'-tgccacgaccaagtgacagcaatg-3' and Cre Reverse 5'-accagagacggaaatccatcgctc-3'	Integrated DNA Technologies	N/A
Genotyping primers: Pten Flox Forward 5'-CAAGCACTCTGCGAACTGAG-3' and Pten Flox Reverse 5'-AAGTTTTTGAAGGCAAGATGC-3'	Integrated DNA Technologies	N/A
Genotyping primers: GFP Forward 5'-CTACGGCGTGCAGTGCTTC-3' and GFP Reverse 5'-CTGGGTGCTCAGGTAGTG-3'	Integrated DNA Technologies	N/A
Genotyping primers: MORF3 WT Forward 5'-CTGGCTTCTGAGGACCG-3' and MORF3 WT Reverse 5'-AATCTGTGGGAAGTCTTGTCC-3'	Integrated DNA Technologies	https://www.jax.org/Protocol?stockNumber=035403&protocolID=39963
Genotyping primers: MORF3 MUT Forward 5'-ACCACTATCAGCAGAATACGC-3' and MORF3 MUT Reverse 5'-AATTCGGCCATGTTGTTGTC-3'	Integrated DNA Technologies	https://www.jax.org/Protocol?stockNumber=035403&protocolID=39963
Software and algorithms		
Fiji (ImageJ)	Schindelin et al. 2012	https://imagej.net/software/fiji/ RRID: SCR_002285
Graphpad Prism 9	Graphpad Software	https://www.graphpad.com/ RRID: SCR_002798
Imaris 10.2.0	Bitplane	https://imaris.oxinst.com/ RRID: SCR_007370
IPLaminator	Li et al. 2016	https://isoptera.lcsc.edu/IPLaminator/
WinDRP	Rodieck 1991	N/A
MATLAB	MathWorks	RRID:SCR_001622
ZEN Blue	Zeiss	RRID: SCR_013672

Chapter 3: Troubleshooting

As part of this dissertation work, I attempted to implement methods to manipulate the timing of *Pten* deletion, assess the role of relevant proteins downstream of PTEN, and label postsynaptic sites in SACs. These experiments either did not work for technical reasons or produced inconclusive results. In this Chapter, I will cover the rationale and outcome of each of these series of experiments.

Timing of *Pten* Deletion

SAC-specific embryonic deletion of *Pten*

The ability to control when *Pten* is deleted from SACs would allow me to more directly address the developmental roles of PTEN during discrete time windows. My findings show that PTEN does not cell-autonomously regulate SAC density, mosaic spacing, or lamination when deleted from SACs beginning at P1 (Chapter 2 Figure 2.2). This differs from results seen in prior studies, which have deleted *Pten* from all retinal progenitor cells beginning at E8.5 (Sakagami et al. 2012; Cantrup et al. 2012). To conclusively show whether or not PTEN is cell-autonomously involved in these early developmental processes in SACs, the ideal experiment would be to delete *Pten* exclusively in retinal progenitor cells fated to be SACs at E8.5. This is not currently possible as retinal progenitor cells are practically indistinguishable from each other, and the factors that define what neuronal class a progenitor will give rise to is not fully understood (Cepko 2014). I attempted to instead delete *Pten* from SACs using a $Megf10^{Cre}$ which turns on in SACs as they finish their radial migration starting around E16.5 (Kay et al. 2012; Ray et al. 2018). Unfortunately, I found that $Megf10^{Cre};Pten^{cKO}$ mice died at birth. I took newborn mice at P0 and performed immunohistochemistry in retinal cross sections to examine their somal lamination

(Chapter 3 Figure 3.1A-D). *Megf10*^{Cre};*Pten*^{cKO} retinas appear grossly normal, with SACs properly organized in the INL and GCL (Chapter 3 Figure 3.1A-D). From this preliminary data, it appears that *Pten* deletion beginning at E16.5 is insufficient to disrupt SAC somal lamination by P0, and it is not possible to investigate how this manipulation affects SACs in adulthood. I concluded that using *Megf10*^{Cre} as a method of embryonic deletion of *Pten* in SACs is not viable for postnatal inquiries, as the mice die at birth.

Using *ChAT*^{CreER} to control timing of postnatal *Pten* deletion

In addition to deleting *Pten* embryonically, I also attempted to control the timing of postnatal *Pten* deletion using a *ChAT*^{CreER} line, in which Cre is only active when tamoxifen is administered. *ChAT*^{Cre};*Pten*^{cKO} SACs appear morphologically normal at P14, but have nearly double the number of dendritic branches by P21. This raises the question of whether PTEN activity is largely dispensable prior to P14. Additionally, between P21 and P60 the total number of dendritic branches does not change, suggesting a

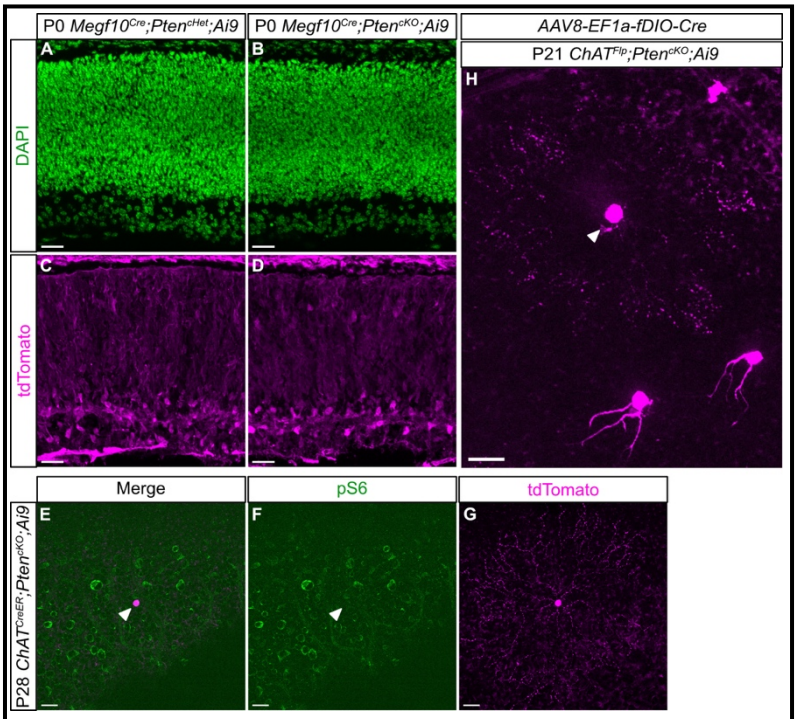

Figure 3.1 Controlling the timing of SAC *Pten* deletion
A-D. Using a *Megf10*^{Cre} line to delete *Pten* in SACs starting at E16.5 shows no changes to gross structure of the retina (A, B) or somal lamination of SACs (C, D) at P0. **E-G.** Attempt to use a *ChAT*^{CreER} line to control the timing of *Pten* deletion and sparsely label SACs. SAC somas labeled with tdTomato (E) show no indication an increase in pS6 levels (F). White arrow shows location of SAC soma. SACs are able to be successfully sparsely labeled for reconstruction (G), but without confirmation of *Pten* deletion cannot be used experimentally. **H.** Example of sparse SAC labeling through a *ChAT*^{Flp} line approach. Pups were injected at P1 with *AAV8-EF1a-fDIO-Cre* and immunostained for tdTomato. While an individual SAC was detected, off target retinal ganglion cells were also labeled through this approach.

critical window for SAC dendritic development between P14 and P21. By deleting *Pten* at P14 and P21, I could address whether PTEN is required at specific developmental timepoints to regulate dendritic branching. I performed intraperitoneal administration of tamoxifen at P5 in *ChAT^{CreER};Pten^{cKO};Ai9* mice to confirm sparse labeling of SACs and consistent *Pten* deletion. It is critical to validate both tdTomato expression and *Pten* loss as recombination of one genetic locus in a CreER line does not guarantee recombination of the other (Schmidt-Supprian and Rajewsky 2007; Fernández-Chacón et al. 2019). While I was able to achieve sparse labeling of SACs through the *ChAT^{CreER}* line, I could not confirm the loss of *Pten* through pS6 staining (Chapter 3 Figure 3.1E-G). To address this weakness of CreER lines, another group developed an iSuRe-Cre mouse line, which turns on a constitutively active Cre when dosed with Tamoxifen (Fernández-Chacón et al. 2019). Unfortunately, these mice were not available at Jax laboratories and I was unable to get in contact with any of the labs who have published studies using these mice. Due to the inability to confirm loss of *Pten* in *ChAT^{CreER};Pten^{cKO}* mice, I did not move forward with experiments using this line.

Using a novel *ChAT^{Flp}* approach delete *Pten* in SACs postnatally

Using the iSuRe-Cre line as inspiration, I pioneered a novel approach for temporally controlled, constitutive Cre expression in SACs. Intersectional approaches combining Cre and Flp, a recombinase like Cre that recognizes mutually exclusive DNA sequences, have been utilized to achieve specific targeting of neuronal subtypes that would otherwise be inaccessible (Sadowski 1995; Kwan 2002). Similar to CreER lines which require tamoxifen for activity, I developed an approach where constitutive Cre activity was gated by the presence of Flp. To do so, I combined a *ChAT^{Flp}* line with injection of an AAV for a Flp-dependent Cre, *AAV8-EF1a-fDIO-*

Cre (Schneeberger et al. 2019). In this experimental paradigm, only infected Flp^+ cells will express Cre, allowing for cell type-specific targeting of SACs in the retina and temporal control of Cre expression through viral injection. I generated *ChAT^{Flp};Pten$^{f/f}$;Ai9* mice, which will only delete *Pten* and express tdTomato in the presence of Cre, and injected them at P1 with *AAV8-EF1a-fDIO-Cre*. In my preliminary trials, I was able to detect a sparsely labeled SAC (Chapter 3 Figure 3.1H). However, I also saw non-specific labeling of other retinal neurons, suggesting either leaky expression of Cre from the virus or non-specific Flp expression from the mouse line. While this approach is not truly cell-autonomous due to the leaky expression, this method still enables temporally controlled postnatal deletion of *Pten* in SACs.

Attempts to manipulate the PI3K Pathway

One of my project goals was to determine which proteins in the PI3K pathway were involved in the branching phenotype seen in *ChAT^{Cre};Pten^{cKO}* SACs. I attempted this with two approaches, utilizing mouse genetics to delete *Tsc2*, an upstream regulator of mTOR, and virally injecting constitutively active AKT (CA-AKT) and dominant negative GSK3β (DN-GSK3β). Together, these approaches would reveal to the relative contributions of mTOR, AKT, and GSK3β to SAC dendritic branching phenotype seen in *ChAT^{Cre};Pten^{cKO}* mice. Unfortunately, I was unable to confirm the efficacy of these methods in successfully manipulating key aspects of the PI3K pathway.

Mouse genetic approach to discern downstream mechanisms of *Pten* deletion in SACs

Hamartin (TSC1) and tuberin (TSC2) function together downstream of AKT to regulate mTOR, a major signaling protein that forms two complexes, mTORC1 and mTORC2 (van Slegtenhorst et al. 1998; Inoki et al. 2002; Inoki et al. 2003). Studies in cortex, olfactory bulb,

and dentate gyrus have shown that deletion of *Tsc1* or *Tsc2* causes upregulation of mTOR activity and changes in neuronal morphology (Feliciano et al. 2011; Feliciano et al. 2012; Kowalczyk et al. 2025). Manipulations of either mTORC1 or mTORC2 are sufficient to cause changes in neuronal morphology, and the effects are different depending on which complex is affected (Kosillo et al. 2022). mTOR hyperactivation largely recapitulates the general phenotypes of *Pten* deletion and inhibition of mTOR is sufficient to rescue the morphological effects of *Pten* loss in dentate granule neurons (Nguyen et al. 2024; Tariq et al. 2022; Cullen et al. 2023; Dhaliwal et al. 2024). Therefore, we sought to answer whether *ChAT*^{Cre}-mediated loss of *Tsc2* was sufficient to recapitulate our *Pten* deletion in SACs.

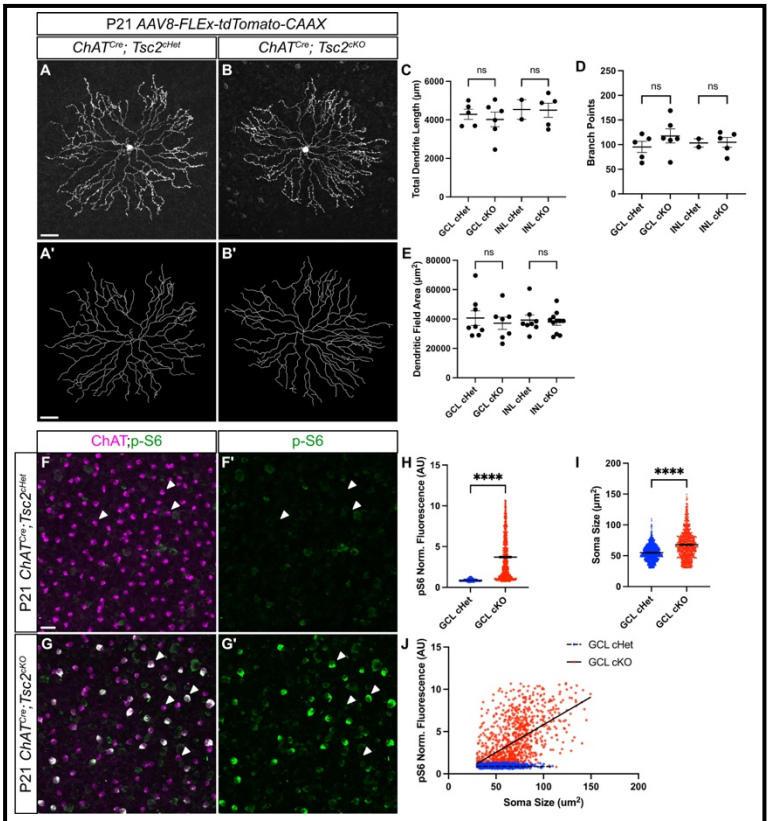

Figure 3.2 *ChAT^{Cre};Tsc2^{cKO}* SACs show inconsistent elevation of pS6
A, B. Sparsely labeled *ChAT^{Cre};Tsc2^{cHet}* and *ChAT^{Cre};Tsc2^{cKO}* SACs at P21. **A', B'.** Imaris reconstructions of the SACs from A and B. **C-E.** Quantification of total dendrite length, number of branch points, and dendritic field area reveal no change in and *ChAT^{Cre};Tsc2^{cKO}* SACs. **F-G'.** pS6 labeling of *ChAT^{Cre};Tsc2^{cHet}* and *ChAT^{Cre};Tsc2^{cKO}* SACs reveals that only a subpopulation of *ChAT^{Cre};Tsc2^{cKO}* SACs have elevated levels of pS6. **H.** Quantification of pS6 levels reveal differences in populations of *ChAT^{Cre};Tsc2^{cHet}* and *ChAT^{Cre};Tsc2^{cKO}* SACs, but many individual cells do not show any elevation in the *ChAT^{Cre};Tsc2^{cKO}* condition. **I.** Quantification of soma size reveals an increase *ChAT^{Cre};Tsc2^{cKO}* SACs. **J.** Comparing the pS6 levels and soma sizes of individual SACs reveals a moderately strong correlation between the two in *ChAT^{Cre};Tsc2^{cKO}* SACs, and no correlation in *ChAT^{Cre};Tsc2^{cHet}* SACs.

As with *ChAT^{Cre};Pten^{cKO}* mice, *ChAT^{Cre};Tsc2^{cKO}* animals were intravitreally injected at P2 with *AAV8-FLEx-tdTomato-CAAX* and retinas were collected for analysis at P21. Sparse labeling

followed by reconstruction in Imaris revealed *ChAT^{Cre};Tsc2^{cKO}* SACs showed no differences in dendritic length, branch points, an dendritic field area compared to controls (Chapter 3 Figure 3.2A-E). To validate deletion of the *Tsc2* flox allele and increased mTOR activation, retinas were stained with pS6 (Chapter 3 Figure 3.2F-G'). While there were SACs with very clear elevation of pS6, many cells exhibited no apparent increase (Chapter 3 Figure 3.2H). The same appeared to be true for soma size (Chapter 3 Figure 3.2I). Notably, there was a correlation between the levels of pS6 an individual SAC was expressing and its soma size in *ChAT^{Cre};Tsc2^{cKO}* animals (Chapter 3 Figure 3.2J).

In using the *ChAT^{Cre};Tsc2^{cKO}*, I discovered an unusual phenotype where approximately half of the SAC population showed robust upregulation of pS6 activity and the other half showed no change. This finding is quite surprising as *ChAT^{Cre};Pten^{cKO}* SACs have consistent upregulation of pS6 in the entire population, suggesting this isn't due to a lack of Cre expression in SACs. TSC1 and TSC2 are both required to function in the tuberous sclerosis complex and are insufficient to compensate for loss of the other (van Slegtenhorst et al. 1998). One possibility is the *Tsc2* locus is very resistant to Cre-mediated recombination, however other studies have used this *Tsc2$^{f/f}$* allele with no indication of inconsistency (Hernandez et al. 2007; Ren et al. 2016; Wong and Beirowski 2018). This phenotype may also be due to a spurious mutation in the mice and backcrossing back to a C57BL/6J background may resolve it. How this phenotype came about or why it affects only half of the SAC population is currently unknown.

Despite the inconsistency of pS6 upregulation, this line could still be used to evaluate the effect mTOR activation alone has on SAC morphology. By combining sparse labeling of SACs with immunostaining of pS6, one could evaluate the two population of SACs, high in pS6 and

low in pS6, separately. One could then compare each population within the same animal to see if pS6 activity results in a difference of morphology.

Viral Approaches of Manipulating the PI3K Pathway

I aimed to test the contribution to SAC morphology of other proteins downstream of PTEN through viral manipulation. Prior studies have utilized different versions of a CA-AKT to recapitulate hypertrophy similar to *Pten* deletion (Flores et al. 2008; Zheng et al. 2008; Fedder-Semmes and Appel 2021). In these studies, three primary variants of CA-AKT are used, (1) a CA-AKT that is myristoylated, localizing it to the membrane and increasing its activity tenfold, (2) a CA-AKT with two point mutations at Thr^{308} and Ser^{473} to aspartic acid leading to full activation of AKT, and (3) a combination of manipulations 1 and 2 (Kotani et al. 1999; Flores et al. 2008; Fedder-Semmes and Appel 2021). I produced an *AAV8-FLEx-myrAKT-DD-T2A-eGFP* construct that expresses a CA-AKT that is myristoylated and has two mutated aspartates at Thr^{308} and Ser^{473}. Using this AAV, I was able to successfully get GFP labeling in SACs at P21 (Chapter 3 Figure 3.3A, B). However, while individual SACs were very clearly GFP positive, I was unable to detect a noticeable increase in pS6 levels, unlike in $Pten^{cKO}$

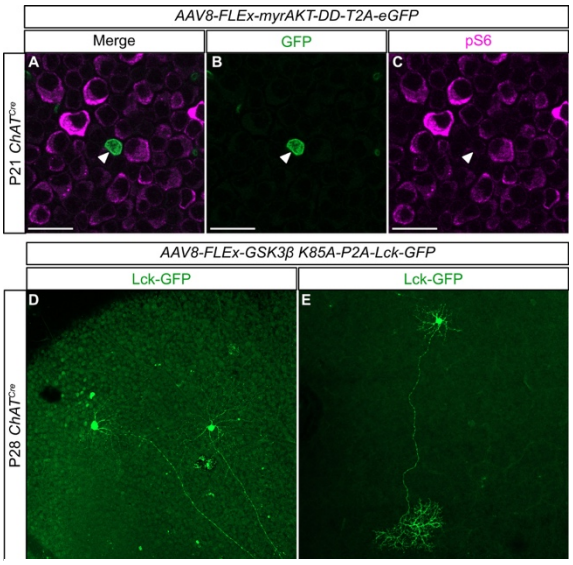

Figure 3.3 Viral Approaches to Manipulating the PI3K Pathway
A-C. Example image showing a P21 SAC infected with *AAV8-FLEx-myrAKT-DD-T2A-eGFP* and immunostained for pS6 (A). While the cell is GFP^+ (B), indicating expression of CA-AKT, there is no indication of pS6 upregulation (C). Therefore, I am unable to validate efficacy of the CA-AKT construct. **D, E.** Example images of retinas injected with *AAV8-FLEx-GSK3β K85A-P2A-Lck-GFP*. The Lck-GFP shows membraned localized staining of retinal neurons but is not specific for SACs. A couple of retinal ganglion cells (D) and a horizontal cell (E) were labeled, while no SACs were found. The construct shows both non-specific labeling in Cre^- cells and a lack of expression in Cre^+ cells.

SACs (Chapter 3 Figure 3.3C). Without a readout of the construct's efficacy, I decided not to move forward with single cell reconstruction.

With TSC2 experiments in progress to test the role of mTOR, I wanted to also examine how GSK3β activity might be contributing SAC morphology. Since PTEN activity results in activation of GSK3β, I developed a construct, *AAV8-FLEx-GSK3β K85A-P2A-Lck-GFP*, which produces a kinase dead version of GSK3β that inhibits endogenous GSK3β in a dominant negative manner (Guo et al. 2016). GSK3β is known to have a key role in axonogenesis and microtubule polarity, and its inhibition has also been shown to facilitate regeneration in RGC axons (Jiang et al. 2005; Yoshimura et al. 2005; Guo et al. 2016). I attempted to test whether inhibiting GSK3β would have a specific effect on SAC morphology as they are purely dendritic. Similar to CA-AKT, I developed a DN-GSK3β AAV FLeX vector with a *syn* promoter, and a T2A linked Lck-GFP to enable reconstruction. Unfortunately, when tested, I saw misexpression in Cre- cells within the retina, notably retinal ganglion cells and horizontal cells (Chapter 3 Figure 3.2D, E). Additionally, I was unable to find any infected SACs. Due to the lack of specificity of this construct, I decided to forgo this experiment.

Labeling of SAC postsynaptic sites

While *Pten*^{cKO} SACs had increases in branch density, it was unknown whether they would also upregulate the number of synapses they formed along these branches. To test this, I attempted to label their synaptic inputs and outputs using fluorescently tagged PSD-95 and synaptophysin, respectively. To label synaptophysin, I utilized an *AAV1-FLEx-mGFP-2A-Synaptophysin-mRuby* vector which expresses mRuby-tagged synaptophysin and a membrane bound GFP (Beier et al. 2015). This allowed for efficient visualization of SAC synaptic outputs

while also providing the cell's morphology to filter synaptophysin puncta (Chapter 2 Figure 2.7A, B). I attempted to recapitulate this with PSD-95, however, it is such a large protein that it barely fits in an AAV capsid alongside a fluorescent reporter. PSD-95 is a 724 amino acid protein with about 2.2 kilo base pairs (kb) and AAV packaging capacity is approximately 4.7kb, leaving not enough room for a T2A and fluorescent protein (Dong et al. 1996). I opted to dual inject AAVs, an *AAV-EF1a-DIO-PSD95-EGFP-WPRE* expressing GFP-tagged PSD-95 at high titer, and an *AAV8-FLEx-tdTomato-CAAX* virus used previously at low titer (Sun et al. 2019; Chapter 2 Figure 2.3). This would result in many SACs having GFP-tagged PSD-95 and a few SACs expressing tdTomato that can be used to filter the PSD-95 signal. I was able to successfully label tdTomato SACs, but none of them had any GFP signal. While I was unable to detect any GFP from the viral construct in neurons, I did see labeling in microglia (Chapter 3 Figure 3.4A, B). I additionally, attempted to label PSD-95 using immunohistochemistry. I utilized a PSD-95 antibody that our lab has validated in cerebellum but was unable to detect any signal in the retina (Chapter 3 Figure 3.4C, D). While I was unable to label PSD-95 in SACs, based on my

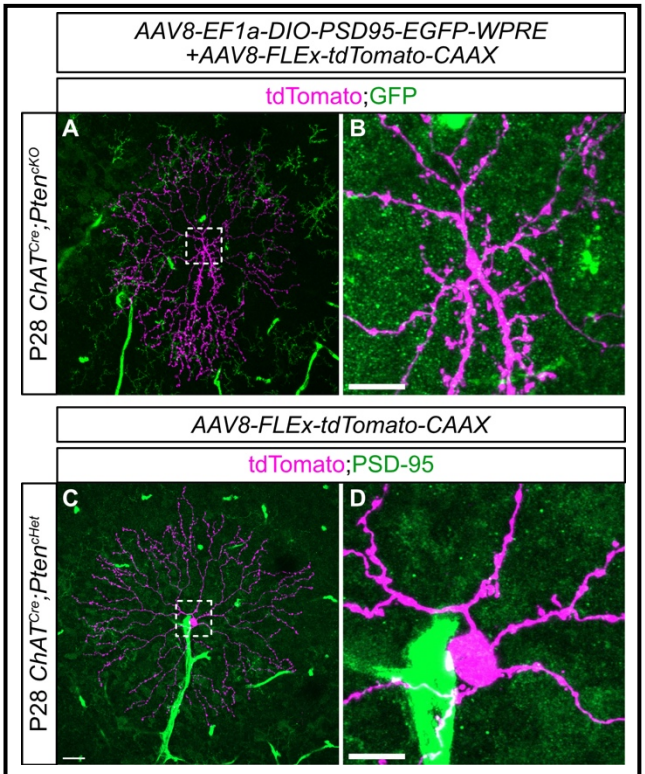

Figure 3.4 Attempts at PSD-95 Labeling in SACs
A, B. Mice were injected with *AAV8-EF1a-DIO-PSD95-EGFP-WPRE* and *AAV8-FLEx-tdTomato-CAAX* to express eGFP-tagged PSD95 alongside a membrane localized tdTomato. No PSD-95 was detected within the SAC arbors (A, B). For unknown reasons, microglia appeared to be labeled in GFP. The soma was omitted from the z-stack to prevent excessive photobleaching. **C, D.** SACs were sparsely labeled with *AAV8-FLEx-tdTomato-CAAX* and then stained for PSD-95. PSD-95 antibody staining looked non-specific across the retina, and showed no overlap with SAC dendritic arbors (C, D).

synaptophysin findings and studies in *Amigo2 KO* SACs showing PSD-95 localization is independent of cell size, I would hypothesize that postsynaptic sites do not have changes in their size, density, or localization in *Pten-null* SACs (Soto et al. 2019).

The troubleshooting work presented here taught me the importance and difficulty of validating methods and approaches. Many good ideas do not work out for technical reasons.

Chapter 4: Discussion

Summary of Results

First discovered in 1980, the starburst amacrine cell (SAC) was aptly named due to its "starburst-like" dendrites (Famiglietti and Siegfried 1980). Since then, SACs have been studied in a host of mammalian model organisms, helping uncover the evolutionary conservation of their morphology (Wässle and Boycott 1991). Their form is directly tied to their functional role in conferring direction-selectivity in the retina and they accomplish this task by providing inhibitory input in the null-direction to direction-selective retinal ganglion cells (DSGCs) (Fried et al. 2002; Taylor and Smith 2012). Additionally, SACs are incredibly amenable to cell-autonomous manipulation, as they are the only cholinergic neuron in the retina, and are therefore genetically tractable through use of a *ChAT*^{Cre} line (Masland 2005; Rossi et al. 2011). These features have made SACs an ideal model to study the principles of morphological development. A handful of transmembrane proteins have been shown to regulate discrete aspects of SAC development, including self-avoidance, arbor size, and lamination of the IPL (Lefebvre et al. 2012; Sun et al. 2013; Ray et al. 2018; Soto et al. 2019; Prigge et al. 2023). However, little is known about what intracellular signaling follows downstream of these transmembrane proteins. The lipid phosphatase activity of PTEN is a likely candidate, as it is an established regulator of neuronal growth and is known to be downstream of transmembrane protein Plexin during growth cone collapse (Chadborn et al. 2006). Pan-retinal *Pten* deletion causes developmental deficits in the cell density, mosaic spacing, and lamination of SACs (Sakagami et al. 2012; Cantrup et al. 2012). However, these studies did not address whether

SAC morphology is affected following *Pten* deletion nor utilize a SAC-specific approach to delete *Pten*. This led us to ask the following questions:

(1) How does PTEN cell-autonomously regulate SAC morphology over the course of development?

(2) What signaling downstream of PTEN in the PI3K-AKT pathway is responsible for modulating SAC morphology?

(3) What are the functional consequences of PTEN-dependent changes in morphology?

In Chapter 2, I showed that a SAC-specific deletion of *Pten* (*ChAT^{Cre};Pten^{cKO}*) results in a near doubling of dendritic branches in SACs by P21. This genetic manipulation avoids the effects of non-cell autonomous *Pten* deletion (*Six3^{Cre};Pten^{cKO}*) on SAC specification, migration, or lamination. Despite the stark increase in branching, SAC dendritic field areas were unchanged, and total dendrite length minorly increased in GCL SACs. Dendritic branching was normal prior to P14, meaning this phenotype manifests during a discrete developmental window between P14 and P21. Increased dendritic branching is still present at P60 but does not worsen. Instead, P60 SACs showed the presence of a single hypertrophic dendritic branch and a shrinking dendritic field area.

I next interrogated what signaling was occurring downstream of *Pten* following its deletion and found that pS6 levels were upregulated while β-catenin signaling remained unchanged. This selective upregulation of pS6 indicated that mTOR signaling is likely one of the primary drivers of increased branching in *Pten-null* SACs (Chapter 1 Figure 1.4). mTOR activity can be directly inhibited via rapamycin or increased by suppressing either of its upstream inhibitors, Tsc1 and Tsc2. I performed a conditional deletion of tuberin (*Tsc2*) in SACs using a

ChAT^{Cre}*;Tsc2*$^{f/f}$ mouse to test whether direct manipulation of mTOR activity was sufficient to phenocopy *Pten* deletion (van Slegtenhorst et al. 1998; Chapter 3 Figure 3.2). Initially, I was unable to detect any morphological changes in *Tsc2-null* SACs. Upon further investigation, SACs showed inconsistent upregulation of pS6 following *Tsc2* deletion, with only half the population showing an appreciable increase. It is unclear why the *Tsc2* and *Pten* deletions differ in the number of SACs affected, as *ChAT*^{Cre} should be active in every cell and *Tsc1* is insufficient to compensate for loss of *Tsc2* (Rossi et al. 2011; van Slegtenhorst et al. 1998). It is possible the *Tsc2*$^{f/f}$ allele does not consistently recombine, but this has not been reported previously in the literature (Hernandez et al. 2007; Ren et al. 2016; Wong and Beirowski 2018). To truly tease out the specific role of mTOR in SACs using this genetic approach, I would sparsely label SACs for morphometric analysis and quantify pS6 levels to assess the degree of mTOR activation. I could then classify SACs into different groups based on pS6 activation and determine whether SACs with high pS6 levels phenocopy *Pten-null* SACs. Due to reduced survivability in *Tsc2* line, I instead focused on the timing of pS6 activation during SAC development. I found that pS6 is active in wildtype SACs at P7 and this signal is mostly gone by P14. In *Pten-null* SACs, the pS6 signal is unchanged at P7, but remains high at P14 and onwards. These results suggest loss of *Pten* in SACs produces no phenotype earlier in development due to naturally high levels of pS6 but causes a phenotype after P14 when pS6 levels normally drop.

In attempting to discern the functional consequences of *Pten* loss in SACs, I found no effect on their synaptic outputs or the direction-selectivity of downstream direction-selective ganglion cells (DSGCs). Sparse labeling of synaptophysin in SACs revealed no changes in the density, volume, or localization of their synaptic outputs. Despite large increases in dendritic

branching, the machinery transporting synaptophysin to synapses seemed unaffected. Multielectrode array (MEA) analysis showed no changes in the relative distribution of DSGCs in the retina nor their functional properties, such as direction-selective index, tuning width, or average firing rate. This indicates that, at a circuit level, *Pten* loss in SACs does not seem to impact their function.

Working Model of *Pten* loss in SAC Morphological Development

Based on the findings in this dissertation, the working model for how PTEN regulates SAC dendritic development involves controlled suppression of PTEN activity during a dynamic growth stage followed by robust activation of PTEN when transitioning into a more stable state (Chapter 4 Figure 4.1). At P7 SACs are in a period of exuberant dendritic growth and express high levels of pS6 (Ing-Esteves and Lefebvre 2024; Chapter 2 Figure 2.6A). By P14, SACs have begun transitioning to a more stable state and show low levels of pS6 (Chapter 2 Figure 2.6C). However, at both P7 and P14, *Pten-null* SACs appear morphologically normal (Chapter 2 Figure S2.1). This finding suggests that prior to P14 PTEN is largely dispensable. *Pten* loss does cause an increase of pS6 level at P14 but does not affect dendritic morphology (Chapter 2 Figure 2.6D; Appendix A Figure A.1). By P21, a near doubling of dendritic branching occurs in the absence of *Pten* (Chapter 2 Figure 2.3). This presents a well-defined time window from P14 to P21 where PTEN activity is necessary for stereotyped morphological development (Chapter 4 Figure 4.1). *Pten* loss continues to impact SACs at P60, as they develop a hypertrophic dendrite and show shrinkage of their dendritic arbor. Still, there remain many unanswered questions that would provide more clarity to the model.

PTEN's role in Regulating SAC Dendrite Dynamics

One of the greatest limitations in attempting to understand a developmental process is that tissue imaging techniques are often static. Live imaging enables evaluation of dynamic cellular processes and can provide fundamental mechanistic insights with higher temporal resolution (Smith et al. 2010; Ing-Esteves and Lefebvre 2021). Ing-Esteves and Lefebvre have shown that it is possible to capture dendrite dynamics of *ex vivo* SACs, which morphologically appear to reliably match *in vivo* SACs (Ing-Esteves and Lefebvre 2021; Ing-Esteves and Lefebvre 2024). Recapitulating these experiments using *Pten*-

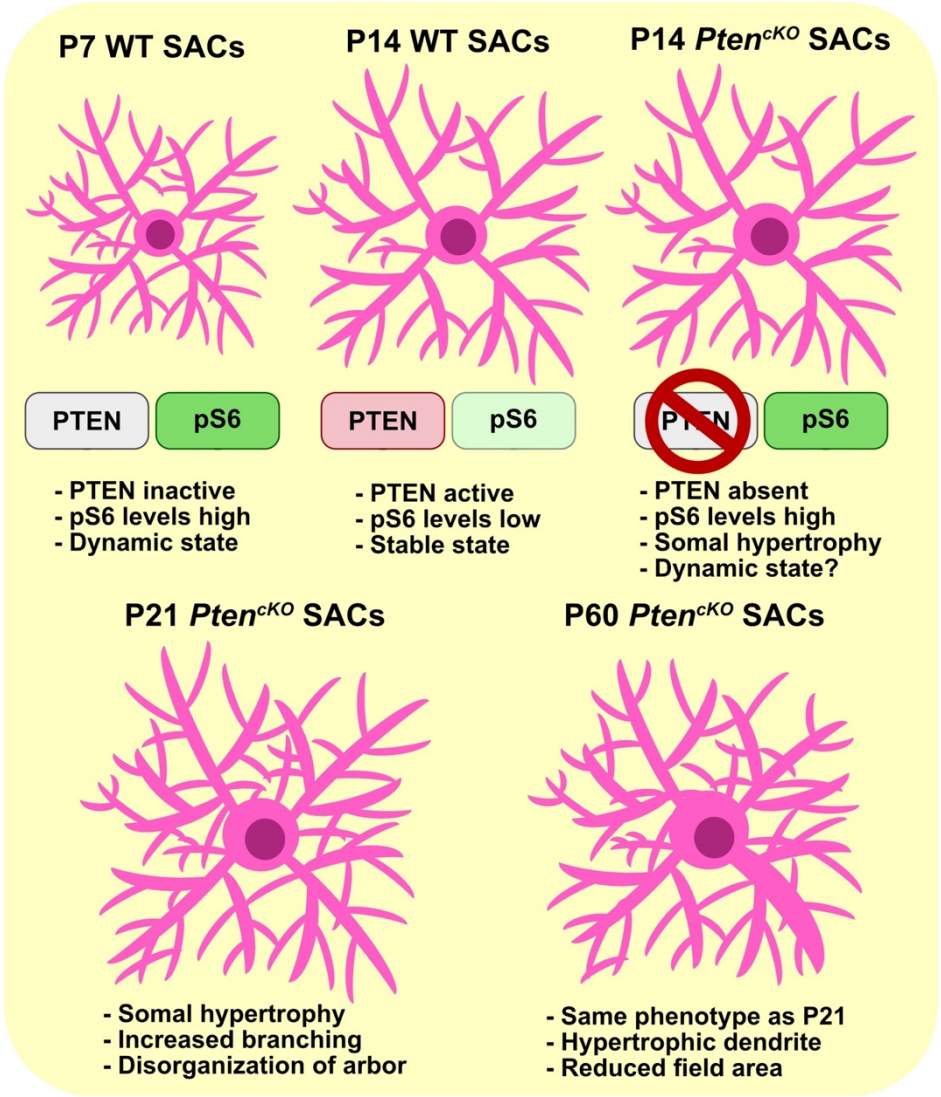

Figure 4.1 Working model of *Pten* function and deletion in SACs.
At an early developmental timepoint (P7), SACs have high levels of pS6, indicating PTEN activity is low. By P14 pS6 levels significantly decrease, suggesting that PTEN is active by this timepoint. The timing of PTEN activity inversely correlates with when SACs are in more dynamic or stable developmental states. When *Pten* is deleted from SACs, P14 SACs continue to show high pS6 levels, indicating they may still be in a dynamic developmental state. At P21, *Pten-null* SACs show increased dendritic branching and a more disorganized arbor, indicating morphological differences from wildtype SACs arise between P14 and P21. At P60, *Pten-null* SACs additionally show a hypertrophic dendrite and reduced field area.

null SACs would answer many key developmental questions such as (1) Does *Pten* loss affect SAC dendrite dynamics prior to P14? And (2) Do *Pten-null* SACs continue to have dynamic filopodial protrusions and retractions after P14? Unfortunately, live imaging of the retina is a technically challenging protocol, as it is difficult to keep the retina alive and healthy *ex vivo* for an extended period of time to get representative data (Ing-Esteves and Lefebvre 2024). In order to capture meaningful changes in dendrite dynamics, the retina must be kept healthy for 30 to 60 minutes while being fluorescently imaged (Ing-Esteves and Lefebvre 2024). Additionally, Ing-Esteves and Lefebvre did not use *ex vivo* tissue past P14, as difficulty maintaining *ex vivo* tissue increases with age. Performing live imaging at P21, or even P60, would add to the degree of difficulty, but could directly elucidate the nature of how *Pten* loss affects SAC dendrite dynamics at later ages. Thus, while technically challenging, these experiments could define how PTEN activity shapes the developmental processes SACs undergo to achieve their stereotyped morphology.

Outside of live imaging, there are alternative ways to partially address the mechanism of increased dendritic branching in *Pten-null* SACs. From P21 to P60, the number of dendritic branches in *Pten-null* SACs does not change. One possibility is that the increase in branching is confined between P14 and P21. SACs decrease their branch points by about 33% from P14 to P21, and increased branching in *Pten-null* SACs may result from a failure to retract these branches. It is also possible that SACs never transition out of their dynamic period of growth, instead reaching a steady state of extension and retraction with *Pten* loss. Performing a temporally controlled deletion of *Pten* after P21 would help to resolve these possibilities. Normal morphology at P60 would indicate the increased branching from *Pten* loss largely stems

from an inability to prune dendritic arbors from P14 to P21. If P60 SACs show the same phenotype in both conditions, this would support the hypothesis that *Pten-null* SACs maintain a dynamic state into maturity and continuously extend and retract dendrites until they reach a steady state. The reality is likely a combination of both mechanisms.

Timing of PTEN Activity

While PTEN's impact on cell morphology has been assessed in a variety of neurons, few studies have established a true developmental time course outlining morphological changes due to *Pten* loss (Kwon et al. 2006; Cupolillo et al. 2016; Gallent and Steward 2018; Chen et al. 2021). Most PTEN research utilizes genetic knockout in adults, precluding earlier developmental timepoints from analysis (Luikart et al. 2011; Santos et al. 2017; Getz et al. 2022). Consequently, such studies may miss that inactivation of PTEN could be a critical part of neuronal development. In SACs, PTEN does not appear to be required for proper dendritic morphology prior to P14 (Chapter 2 Figure S2.1; Chapter 4 Figure 4.1). It is still unknown whether early developmental PTEN activity is truly dispensable, or PTEN serves a critical role prior to P14 but the phenotype manifests later in SACs. Future experiments pinpointing the timing of PTEN activation in SACs followed by rescue experiments would clarify the developmental role of PTEN in neuronal morphology.

It is still unclear precisely when PTEN activity begins in SAC morphological development. I evaluated SAC morphology at three discrete developmental timepoints and was able to determine critical time windows where PTEN was either non-essential or required. However, mapping out the exact postnatal days of PTEN activity onset and pS6 inactivation would

enhance the granularity of the model. This could be achieved by performing ChAT and pS6 co-labeling between P7 and P14, elucidating the precise timing of PTEN activation in SACs. This experiment would allow for the integration of PTEN activity with changes in SAC dendrite dynamics during development. While SACs are broadly dynamic from P2 to P14, the nature of their contacts changes during this developmental window (Ing-Esteves and Lefebvre 2024). The number of self-contacting dendritic protrusions peaks from P4 to P8 while non-self-contacting protrusions remain steady from P6 to P14. Studying PTEN's timing of activation may reveal a correlation with this change in protrusion dynamics.

My current findings suggest PTEN protein must either be absent or inhibited prior to P14 during normal SAC development, but the mechanism is unknown. Since PTEN activity is low at P7, confirming the presence of PTEN in SACs through immunostaining would address this question. Phosphorylation via casein kinase 2 (CK2) is known to render PTEN inactive (Das et al. 2003; Vazquez et al. 2001; Litchfield 2003; Torres and Pulido 2001). If PTEN is present at P7, immunostaining for phosphorylated PTEN could confirm its inactivity. The presence of primarily inactive PTEN early in SAC development would be a novel finding and provide a target for further manipulation. A conditional deletion of CK2, which is expressed in SACs, could decrease the amount of phosphorylated PTEN and derepress PTEN activity (Yan et al. 2020; Rebholz et al. 2013). If CK2 is an upstream inhibitor of PTEN and the conditional deletion is successful, this model could be used to effectively study PTEN overactivation from P2 to P14 and confirm the necessity of PTEN inhibition for normal SAC development.

Rescue experiments are an excellent way to address exactly how critical PTEN signaling is during specific periods of SAC development. Reintroduction of PTEN before and after

branching phenotypes emerge would further resolve the critical window of PTEN signaling. A *Cre*-dependent AAV that induces expression of PTEN can be intravitreally injected alongside a fluorescent label into *ChAT^{Cre};Pten$^{f/f}$* mice to rescue PTEN activity and perform morphometric analysis. This approach would address whether PTEN is truly dispensable prior to P14 and if reintroduction of PTEN after P21 can correct its aberrant branching morphology. If PTEN rescue at P14 corrects the branching phenotype of *Pten-null* SACs, I would conclude that PTEN is largely dispensable prior to P14. If expressing PTEN after P21 reduces the amount of branching by P60, especially of small protrusions, this would suggest that *Pten-null* SACs retain a somewhat dynamic state into maturity unless PTEN signaling is present to inhibit this process. To successfully perform these experiments precise timing of viral expression in SACs is key and would need to be defined, as AAVs usually take 3-7 days to begin expressing and 1-2 weeks to reach maximal expression in murine neurons (Reimsnider et al. 2007; Zincarelli et al. 2008; Dang et al. 2017; Hollidge et al. 2022). Another caveat is that expression of genes through an AAV may be differentially regulated than the native genetic locus. If SACs appear to have reduced dendritic complexity, this may be indicative of excessive PTEN activity. These experiments would address the effects of PTEN during discrete time windows.

The Interactions Between Transmembrane Proteins and PTEN in SACs

Cell-autonomous deletion of *Pten* from SACs did not appear to be primarily responsible for any of the phenotypes observed in prior deletions of cell surface proteins (Chapter 1 Figure 1.3). The only known signaling component downstream of transmembrane proteins important for SAC morphology is the RasGAP domain of PlexA2 (James et al. 2024). Deletion of the

RasGAP domain from PlexA2 presented a milder phenotype than full PlexA2 deletion, indicating RasGAP signaling is only partially responsible for PlexA2 downstream function. In contexts of growth cone collapse, PTEN activity is known to follow Plexin and Semaphorin signaling via RasGAP activity (Chadborn et al. 2006; Oinuma et al. 2010). My results show that a lack of PTEN activity disrupts the stereotyped organization of the SAC dendritic arbor, much like in *PlexA2-null* SACs, quantified by an increase in dendritic self-crossings (Sun et al. 2013). While both *PlexA2* and *Pten* deletions cause dendritic disorganization, SACs lacking PlexA2 show no indications of increased dendritic branching. PTEN activity may still be acting downstream of PlexA2 and Sema6A signaling in SACs to prevent dendritic self-crossings, but it does not seem to serve a primary role in causing the phenotype of *PlexA2-null* SACs.

In SACs, the clustered g-protocadherins (Pcdhgs) serve a critical role in dendritic self-avoidance, but nothing about their downstream signaling is known (Lefebvre et al. 2012). Live imaging studies have revealed that SACs are dynamically self-contacting and retracting their dendrites from P2-P14, and the Pcdhgs are essential for this process (Ing-Esteves and Lefebvre 2024). Deletion of the *Pcdhg*s in SACs causes morphological changes that can be seen as early as P0 and leads to a significant amount of dendritic overlap and excess fasciculation in mature SACs. Developing *Pcdhg-null* SACs fail to retract self-contacting dendrites and form more persistent dendritic loops from P2-P8. Interestingly, this period of dynamic dendritic growth is anti-correlated with PTEN activity, which appears low at P7 and more active by P14 (Chapter 2 Figure 2.6). The amount of dendritic self-contacts decreases substantially by P14, suggesting that Pcdhg signaling may decrease as well. It is unclear whether any sort of direct modulation of PTEN activity occurs downstream of the Pcdhgs. One possibility is the Pcdhgs suppress PTEN

activity, and while SACs are dynamically self-contacting PTEN activity is low. However, this does not explain how the number of contacts begin to diminish in the first place, nor how they rise from P4 to P8 (Ing-Esteves et al. 2024). A more parsimonious explanation is that these two processes do not directly interact, and other processes modulate PTEN activity, which allows for and then inhibits this critical period of dynamic dendritic growth.

PTEN signaling does not seem to directly follow from AMIGO2, MEGF10, FLRT2, or UNC5, as their phenotypes following deletion are completely different. SACs lacking AMIGO2 show a controlled increase in dendritic field area but maintain a normal branch structure (Soto et al. 2019). *Pten-null* SACs have a near twofold increase of branching but an unchanged field area, the inverse of *Amigo2* deletion. In SACs, AMIGO2 controls elongation between dendritic branches, while PTEN dictates the likelihood of branch formation. While there is evidence in other cell types that PI3K-AKT signaling is downstream of AMIGO2, this does not appear to be the case in SACs (Park et al. 2015). Similarly, loss of *Megf10*, *Flrt2*, and *Unc5* are all characterized by defects in SAC lamination of the IPL and ectopic projections, none of which occur in *Pten-null* SACs (Ray et al. 2018; Prigge et al. 2023). PTEN does not appear to be directly involved in ensuring dendritic growth occurs in a planar manner. In summary, *Pten-null* SACs did not strongly phenocopy any established manipulations of SAC morphology and instead present a novel dendritic branching phenotype.

Intracellular Signaling Downstream of PTEN in SACs

It is still largely unclear how individual signaling molecules impact SAC morphology in the context of *Pten* deletion. I attempted to perform a *Tsc2* deletion via *ChAT*^{Cre} to isolate the

role of mTORC1 activity on SAC morphology, but the results were inconclusive (Chapter 3 Figure 3.2). An alternative approach would be to intravitreally inject AAVs inducing expression of shRNA and knockdown proteins downstream of PTEN (Hu et al. 2014; Cideciyan et al. 2018; Dong et al. 2023). This methodology is easily scalable, as a single mouse line can be used to test several shRNAs targeted to different genes in the PI3K pathway, though the caveat to this approach is timing. *ChAT*^{Cre} expression begins at P1, meaning any manipulation occurs early in development (Ray et al. 2018). By contrast, the earliest mice can be intravitreally injected is P1, and AAVs can take anywhere from 3-7 days to begin expression (Zincarelli et al. 2008; Dang et al. 2017; Hollidge et al. 2022). However, if PTEN activity is non-essential before P14, this time discrepancy is less critical (Chapter 4 Figure 4.1). shRNA knockdown experiments could provide meaningful insight as to what signaling molecules are involved in SAC dendrite development.

Pten deletion in SACs leads to an upregulation in mTOR and no change in GSK3β activity, suggesting mTOR activation may drive SAC branching. This aligns with work done in cortical pyramidal neurons, where manipulations of *Tsc1*, *Rheb*, and mTOR all had effects comparable to *Pten* deletion on neuronal morphology (Nguyen et al. 2024). Other studies have shown that the morphological phenotypes of *Pten* deletion can be rescued through inhibition of mTORC1 or mTORC2 (Tariq et al. 2022; Cullen et al. 2023). Similarly, performing conditional deletion or shRNA knockdown of *Tsc1* or *Tsc2* could assess whether mTORC1 activation recapitulates *Pten* loss in SACs. Conversely, knockdown of *raptor*, an adaptor protein required for mTORC1 assembly, in conjunction with *Pten* deletion could be used to see if mTORC1 activity is required for the phenotype of *Pten-null* SACs (Tariq et al. 2022). In midbrain dopamine neurons, mTORC2 and mTORC1 both regulate neuronal morphology, but suppression of mTORC1 decreases

branching while suppression of mTORC2 increases proximal branching (Kosillo et al. 2022). Using the same approach, deleting *rictor*, the adaptor protein required for mTORC2 assembly, would confirm if mTORC2 inhibition is also sufficient to rescue the phenotype of *Pten* loss in SACs (Cullen et al. 2023). These experiments would clarify the role of mTOR in the context of *Pten* deletion and allow for future studies establishing the developmental role of mTOR in SACs.

It is still unclear what causes cytoskeletal reorganization in *Pten-null* SACs. PTEN has been shown to co-localize with and post-translationally modify microtubules (Chadborn et al. 2006; Kreis et al. 2014; Cupolillo et al. 2016; Kath et al. 2018) In dentate granule neurons lacking *Pten*, treatment of vinblastine to reduce microtubule polymerization rates was sufficient to rescue dendritic hypertrophy (Getz et al. 2022). Genetically targeting microtubule dynamics is challenging as many proteins are involved and capable of compensating for one another (Lasser et al. 2018; Kelliher et al. 2019; Lian and Lin 2024). MAP1B, EB1, and EB3 would be good initial targets for shRNA knockdown in the context of *Pten* deletion as these proteins are known play a role in neurite elongation and microtubule extension (Tortosa et al. 2013; Yang et al. 2017).

PTEN activity also regulates the actin cytoskeleton through modulation of PIP2 and PIP3 (Goberdhan et al. 1999; Kreis et al. 2014). PIP3 itself is a master regulator the Rho family of GTPases, which have an established role in actin cytoskeletal remodeling (Luo 2000; Hawkins et al. 2006; Kreis et al. 2014). I would begin by targeting RhoA and Rac1, as these small GTPases are associated with PTEN and the PI3K pathway and interact with each other to induce change in the actin cytoskeleton (Kwon et al. 2000; Li et al. 2005; Sanchez et al. 2005; Stankiewicz and Linesman 2014; Cao et al. 2015; Campa et al. 2015). RasGAP would be another candidate to

target using shRNA, as it is important for PlexA2 function in SACs and has been shown to regulate PTEN activity in growth cone collapse (James et al. 2024; Oinuma et al. 2010). Ultimately, an shRNA knockdown approach in combination with *Pten* deletion could provide immense insight into the downstream mechanisms of dendrite regulation in SACs.

Defining the True Cell-Autonomous Role of PTEN

While deletions targeting a specific subtype of neurons are generally referred to as "cell-autonomous," these experiments would more accurately be called "population-autonomous." Determining true cell-autonomy would require deletion of a gene from a single cell. Population-wide deletion of *TrkC* in Purkinje neurons causes no morphological changes, but sparse deletion leads to hypotrophy in *TrkC-null* cells, highlighting how competition between a population of neurons can regulate morphology (Joo et al. 2014). Contacts between neighboring SACs are required for proper lamination of the IPL and isolated SACs fail to do so (Ray et al. 2018). With a *ChAT*^{Cre}-mediated *Pten* deletion, all SACs lack PTEN and are equally matched when it comes to dendrite development. However, it is unknown whether SACs compete with each other for space and dendritic coverage. SACs have a defined coverage factor of 30, meaning any point in the retina contains dendrites from approximately 30 SACs (Keeley et al. 2007). This begs the question: if a single *Pten-null* SAC was surrounded by wildtype SACs, would their dendritic arbor be any different from a context where all SACs lack *Pten*? As SACs coordinate to form an even plexus, it is possible SACs may provide inhibitory cues to one another to modulate their dendritic field areas (Morrie and Feller 2018). If sparsely deleted *Pten-null* SACs show increases

in dendritic length or arbor size, it could indicate continuous communication between SACs throughout development to modulate their dendritic field areas.

This experiment could theoretically be performed by using a *ChAT*^{CreER} line, however, ensuring recombination of the *Pten*$^{f/f}$ allele is unreliable, as *Cre* is only transiently expressed while tamoxifen is present (Fernández-Chacón et al. 2019). When I attempted to conditionally delete *Pten* in this manner, I was unable to confirm loss of *Pten* and upregulation of pS6 (Chapter 3 Figure 3.1). Instead, I combined a *ChAT*^{Flp} line with injection of a *Flp*-dependent *Cre* AAV to enable continuous *Cre* expression in a sparse population of SACs (Allaway et al. 2020). This would ensure recombination of the *Pten*$^{f/f}$ allele and facilitate the study of true cell-autonomy. Using this method, I was able to detect sparsely labeled SACs, but also saw other neuronal cell types labeled, limiting the ability to claim a truly cell-autonomous manipulation. Another limitation of this approach is the timing, as AAV-mediated gene expression can take 3-7 days to express, meaning *Pten* deletion would occur later than in a *ChAT*^{Cre} mouse (Zincarelli et al. 2008; Dang et al. 2017; Hollidge et al. 2022). Since *Pten* loss of function does not appear to elicit a phenotype prior to P14, this is a minor caveat. This experimental approach would thus define which aspects *ChAT*^{Cre}-mediated *Pten* deletion are "population autonomous" and which are truly "cell-autonomous."

SAC Physiology in *Pten* Deletion

While the compartmentalization of SAC synaptic outputs and the direction-selectivity of DSGCs remain normal, it is unclear if *Pten* loss affects the intrinsic functionality of SACs. When *Pten* is deleted, dentate granule neurons become hyperexcitable, while Purkinje neurons

become hypoexcitable (Luikart et al. 2011; Cupolillo et al. 2016). Mechanistically, *Pten-null* dentate granule neurons develop more spines, suggesting a postsynaptic change may be increasing their excitatory input (Luikart et al. 2011). In *Pten-null* Purkinje neurons, the amplitude of EPSCs (excitatory postsynaptic currents) from the parallel fiber synapse increase, while the climbing fiber synapses show a decrease, resulting in an incorrect balance between the synapses and a hypoexcitable Purkinje neuron (Cupolillo et al. 2016). I attempted to quantify changes in *Pten-null* SAC synapses by labeling PSD-95 and Synaptophysin, but I was unable to visualize postsynaptic sites and saw no changes in the density, size, or localization of presynaptic sites (Chapter 3 Figure 3.4, Chapter 2 Figure 2.7). While it is likely that electrophysiological properties of SACs are perturbed, it is unclear how, necessitating validation via single cell patch clamp recordings (Lee and Zhou 2006; Morrie and Feller 2018). Doing so would inform how the rest of the circuit compensates to maintain normal DS responsiveness. While requiring incredible expertise, this has been done on individual SAC varicosities (Morrie and Feller 2018). It would be fascinating to see if individual varicosities on SACs maintain their organized direction-selectivity with respect to the orientation of their dendrites (Morrie and Feller 2018). This experiment would tie together changes in morphology with function in *Pten-null* SACs.

Starburst Amacrine Cell: Compartmentalization of Morphology

The starburst amacrine cell has provided many insights into the compartmentalization of developmental processes. Previous work has shown how the processes of self-avoidance, cell-cell contact, lamination, and elongation are all controlled through discrete transmembrane

proteins (Lefebvre et al. 2012; Sun et al. 2013; Ray et al. 2018; Soto et al. 2019; Prigge et al. 2023). My work identifies a novel role for the intracellular signaling molecule PTEN in regulating dendritic branching, while leaving other developmental processes unaffected. In *Pten-null* SACs, synaptic outputs labeled by synaptophysin do not change in their number, size, or relative localization. Similarly, work in *Amigo2-null* mice showed that despite elongation of the dendritic arbor, the number and relative localization of synaptic inputs labeled via PSD95 remained unchanged. This suggests discrete processes are responsible for the initial spatial configuration of dendritic arbors and the subsequent compartmentalization of synapses.

It is unclear why *Pten* deletion in SACs causes specific morphological changes rather than generalized hypertrophy. In hippocampal dentate granule, serotonergic raphe, and cortical neurons, *Pten* deletion causes broad increases in the length, amount of branching, and size or their arbors (Kwon et al. 2006; Chen et al. 2021; Gallent and Steward 2018). In contrast, the dorsocentral neurons of *Drosophila* present a localized increase in branching rather than broad hypertrophy in response to *Pten* deletion, likely due to subcellular compartmentalization and regulation of PI3K-PTEN signaling by phosphatase Prl-1 (Urwyler et al. 2019). Similarly, SACs resemble these neurons as total dendritic length and field area remain largely unchanged following *Pten* deletion. While it is clear that PTEN is required for control of SAC branching, other parameters may be modulated through parallel pathways that supersede PTEN signaling. Since the dendritic coverage and receptive field size of neurons is so critical to their function in the retina, the density of the SAC plexus is tightly regulated (Keeley et al. 2007; Morrie and Feller 2018). Regulation of coverage factor is likely also a discrete process that dictates the

dendritic field area of SACs and may constrain generalized hypertrophy in *Pten-null* SACs by limiting the space SACs can occupy.

Conclusion

In this dissertation I show that PTEN has a specific role in regulating the branching dynamics of starburst amacrine cells. I identify a developmental time window (P14-P21) in SAC development where PTEN activity is essential for regulating the number of dendritic branches. During this time, PTEN suppresses mTOR activity and reduces dendritic branching. These findings increase our understanding of the mechanisms guiding the morphological identity of neurons and provide valuable insights to the field of developmental neuroscience.

References

Albeg, A., Smith, C. J., Chatzigeorgiou, M., Feitelson, D. G., Hall, D. H., Schafer, W. R., ... & Treinin, M. (2011). C. elegans multi-dendritic sensory neurons: morphology and function. *Molecular and Cellular Neuroscience*, *46*(1), 308-317.

Allaway, K. C., Muñoz, W., Tremblay, R., Sherer, M., Herron, J., Rudy, B., Machold, R., & Fishell, G. (2020). Cellular birthdate predicts laminar and regional cholinergic projection topography in the forebrain. *eLife*, *9*, e63249.

Amthor, F. R., Keyser, K. T., & Dmitrieva, N. A. (2002). Effects of the destruction of starburst-cholinergic amacrine cells by the toxin AF64A on rabbit retinal directional selectivity. *Visual neuroscience*, *19*(4), 495–509.

Armañanzas, R., & Ascoli, G. A. (2015). Towards the automatic classification of neurons. *Trends in neurosciences*, *38*(5), 307–318.

Azeredo da Silveira, R., & Roska, B. (2011). Cell types, circuits, computation. *Current opinion in neurobiology*, *21*(5), 664–671.

Backman, S. A., Stambolic, V., Suzuki, A., Haight, J., Elia, A., Pretorius, J., Tsao, M. S., Shannon, P., Bolon, B., Ivy, G. O., & Mak, T. W. (2001). Deletion of Pten in mouse brain causes seizures, ataxia and defects in soma size resembling Lhermitte-Duclos disease. *Nature genetics*, *29*(4), 396–403.

Beier, K. T., Steinberg, E. E., DeLoach, K. E., Xie, S., Miyamichi, K., Schwarz, L., Gao, X. J., Kremer, E. J., Malenka, R. C., & Luo, L. (2015). Circuit Architecture of VTA Dopamine Neurons Revealed by Systematic Input-Output Mapping. *Cell*, *162*(3), 622–634.

Blochlinger, K., Bodmer, R., Jan, L. Y., & Jan, Y. N. (1990). Patterns of expression of cut, a protein required for external sensory organ development in wild-type and cut mutant Drosophila embryos. *Genes & development*, *4*(8), 1322–1331.

Bodmer, R., & Jan, Y. N. (1987). Morphological differentiation of the embryonic peripheral neurons in Drosophila. *Roux's archives of developmental biology : the official organ of the EDBO*, *196*(2), 69–77.

Bononi, A., & Pinton, P. (2015). Study of PTEN subcellular localization. *Methods (San Diego, Calif.)*, *77-78*, 92–103.

Brand, A. H., & Perrimon, N. (1993). Targeted gene expression as a means of altering cell fates and generating dominant phenotypes. *Development (Cambridge, England)*, *118*(2), 401–415.

Branda, C. S., & Dymecki, S. M. (2004). Talking about a revolution: The impact of site-specific recombinases on genetic analyses in mice. *Developmental Cell*, 6(1), 7–28.

Briggman, K. L., Helmstaedter, M., & Denk, W. (2011). Wiring specificity in the direction-selectivity circuit of the retina. *Nature*, *471*(7337), 183–188.

Butler, M. G., Dasouki, M. J., Zhou, X. P., Talebizadeh, Z., Brown, M., Takahashi, T. N., Miles, J. H., Wang, C. H., Stratton, R., Pilarski, R., & Eng, C. (2005). Subset of individuals with autism spectrum disorders and extreme macrocephaly associated with germline PTEN tumour suppressor gene mutations. *Journal of medical genetics*, *42*(4), 318–321.

Campa, C. C., Ciraolo, E., Ghigo, A., Germena, G., & Hirsch, E. (2015). Crossroads of PI3K and Rac pathways. *Small GTPases*, *6*(2), 71–80.

Cantrup, R., Dixit, R., Palmesino, E., Bonfield, S., Shaker, T., Tachibana, N., Zinyk, D., Dalesman, S., Yamakawa, K., Stell, W. K., Wong, R. O., Reese, B. E., Kania, A., Sauvé, Y., & Schuurmans, C. (2012). Cell-type specific roles for PTEN in establishing a functional retinal architecture. *PloS one*, *7*(3), e32795.

Cao, X., Kaneko, T., Li, J. S., Liu, A. D., Voss, C., & Li, S. S. (2015). A phosphorylation switch controls the spatiotemporal activation of Rho GTPases in directional cell migration. *Nature communications*, *6*, 7721.

Cepko C. (2014). Intrinsically different retinal progenitor cells produce specific types of progeny. *Nature reviews. Neuroscience*, *15*(9), 615–627.

Chadborn, N. H., Ahmed, A. I., Holt, M. R., Prinjha, R., Dunn, G. A., Jones, G. E., & Eickholt, B. J. (2006). PTEN couples Sema3A signalling to growth cone collapse. *Journal of cell science*, *119*(Pt 5), 951–957.

Chen, L., Gong, W. K., Yang, C. P., Shao, C. C., Song, N. N., Chen, J. Y., Zhou, L. Q., Zhang, K. S., Li, S., Huang, Z., Richter-Levin, G., Xu, L., & Ding, Y. Q. (2021). Pten is a key intrinsic factor regulating raphe 5-HT neuronal plasticity and depressive behaviors in mice. *Translational psychiatry*, *11*(1), 186.

Christensen, R., de la Torre-Ubieta, L., Bonni, A., & Colón-Ramos, D. A. (2011). A conserved PTEN/FOXO pathway regulates neuronal morphology during C. elegans development. *Development (Cambridge, England)*, *138*(23), 5257–5267.

Cideciyan, A. V., Sudharsan, R., Dufour, V. L., Massengill, M. T., Iwabe, S., Swider, M., Lisi, B., Sumaroka, A., Marinho, L. F., Appelbaum, T., Rossmiller, B., Hauswirth, W. W., Jacobson, S. G., Lewin, A. S., Aguirre, G. D., & Beltran, W. A. (2018). Mutation-independent rhodopsin gene therapy by knockdown and replacement with a single AAV vector. *Proceedings of the National Academy of Sciences of the United States of America*, *115*(36), E8547–E8556.

Cullen, E. R., Tariq, K., Shore, A. N., Luikart, B. W., & Weston, M. C. (2023). mTORC2 Inhibition Improves Morphological Effects of PTEN Loss, But Does Not Correct Synaptic Dysfunction or Prevent Seizures. *The Journal of neuroscience : the official journal of the Society for Neuroscience*, *43*(5), 827–845.

Cupolillo, D., Hoxha, E., Faralli, A., De Luca, A., Rossi, F., Tempia, F., & Carulli, D. (2016). Autistic-Like Traits and Cerebellar Dysfunction in Purkinje Cell PTEN Knock-Out Mice. *Neuropsychopharmacology : official publication of the American College of Neuropsychopharmacology*, *41*(6), 1457–1466.

Dang, C. H., Aubert, M., De Silva Feelixge, H. S., Diem, K., Loprieno, M. A., Roychoudhury, P., Stone, D., & Jerome, K. R. (2017). In vivo dynamics of AAV-mediated gene delivery to sensory neurons of the trigeminal ganglia. *Scientific reports*, *7*(1), 927.

Das, S., Dixon, J. E., & Cho, W. (2003). Membrane-binding and activation mechanism of PTEN. *Proceedings of the National Academy of Sciences of the United States of America*, *100*(13), 7491–7496.

De Robertis, E. D., & Bennett, H. S. (1955). Some features of the submicroscopic morphology of synapses in frog and earthworm. *The Journal of Cell Biology*, *1*(1), 47-58.

Dhaliwal, N. K., Weng, O. Y., Dong, X., Bhattacharya, A., Ahmed, M., Nishimura, H., Choi, W. W. Y., Aggarwal, A., Luikart, B. W., Shu, Q., Li, X., Wilson, M. D., Moffat, J., Wang, L. Y., Muffat, J., & Li, Y. (2024). Synergistic hyperactivation of both mTORC1 and mTORC2

underlies the neural abnormalities of PTEN-deficient human neurons and cortical organoids. *Cell reports*, *43*(5), 114173.

Díaz-Balzac, C. A., Rahman, M., Lázaro-Peña, M. I., Hernandez, L. A. M., Salzberg, Y., Aguirre-Chen, C., ... & Bülow, H. E. (2016). Muscle-and skin-derived cues jointly orchestrate patterning of somatosensory dendrites. *Current Biology*, *26*(17), 2379-2387.

Dong, J. Y., Fan, P. D., & Frizzell, R. A. (1996). Quantitative analysis of the packaging capacity of recombinant adeno-associated virus. *Human gene therapy*, *7*(17), 2101–2112.

Dong, L., Zhang, R. H., Wu, H. T., Li, H. Y., Zhou, W. D., Shi, X. H., Yu, C. Y., Li, Y. T., Li, Y. F., Jonas, J. B., & Wei, W. B. (2023). Intravitreal Short-Hairpin RNA Attenuated Adeno-Associated Virus-Induced Knockdown of Amphiregulin and Axial Elongation in Experimental Myopia. *Investigative ophthalmology & visual science*, *64*(4), 11.

Dong, X., Liu, O. W., Howell, A. S., & Shen, K. (2013). An extracellular adhesion molecule complex patterns dendritic branching and morphogenesis. *Cell*, *155*(2), 296-307.

Dong, Y., Sui, L., Yamaguchi, F., Kamitori, K., Hirata, Y., Hossain, M. A., Suzuki, A., Holley, M. C., & Tokuda, M. (2010). Phosphatase and tensin homolog deleted on chromosome 10 regulates sensory cell proliferation and differentiation of hair bundles in the mammalian cochlea. *Neuroscience*, *170*(4), 1304–1313.

Famiglietti E. V. (1987). Starburst amacrine cells in cat retina are associated with bistratified, presumed directionally selective, ganglion cells. *Brain research*, *413*(2), 404–408.

Famiglietti Jr, E. V. (1983a). On and off pathways through amacrine cells in mammalian retina: the synaptic connections of “starburst” amacrine cells. *Vision research*, *23*(11), 1265-1279.

Famiglietti Jr, E. V. (1983b). ‘Starburst’ amacrine cells and cholinergic neurons: mirror-symmetric ON and OFF amacrine cells of rabbit retina. *Brain research*, *261*(1), 138-144.

Famiglietti, E. V., & Siegfried, E. C. (1980). The amacrine cells of rabbit retina. *Invest. Ophthalmol*, *19*, 70-71.

Fedder-Semmes, K. N., & Appel, B. (2021). The Akt-mTOR Pathway Drives Myelin Sheath Growth by Regulating Cap-Dependent Translation. *The Journal of neuroscience : the official journal of the Society for Neuroscience*, *41*(41), 8532–8544.

Feliciano, D. M., Quon, J. L., Su, T., Taylor, M. M., & Bordey, A. (2012). Postnatal neurogenesis generates heterotopias, olfactory micronodules and cortical infiltration following single-cell Tsc1 deletion. *Human molecular genetics*, *21*(4), 799–810.

Feliciano, D. M., Su, T., Lopez, J., Platel, J. C., & Bordey, A. (2011). Single-cell Tsc1 knockout during corticogenesis generates tuber-like lesions and reduces seizure threshold in mice. *The Journal of clinical investigation*, *121*(4), 1596–1607.

Fernández-Chacón, M., Casquero-García, V., Luo, W., Francesca Lunella, F., Ferreira Rocha, S., Del Olmo-Cabrera, S., & Benedito, R. (2019). iSuRe-Cre is a genetic tool to reliably induce and report Cre-dependent genetic modifications. *Nature communications*, *10*(1), 2262.

Fernández-Chacón, M., Casquero-García, V., Luo, W., Francesca Lunella, F., Ferreira Rocha, S., Del Olmo-Cabrera, S., & Benedito, R. (2019). iSuRe-Cre is a genetic tool to reliably induce and report Cre-dependent genetic modifications. *Nature communications*, *10*(1), 2262.

Fernandez, A., Sarn, N., Eng, C., & Wright, K. M. (2025). Altered primary somatosensory neuron development in a *Pten* heterozygous model for autism spectrum disorder. *bioRxiv : the preprint server for biology*, 2023.08.04.552039.

Fire, A. (1986). Integrative transformation of Caenorhabditis elegans. *The EMBO journal*, *5*(10), 2673.

Flores, A. I., Narayanan, S. P., Morse, E. N., Shick, H. E., Yin, X., Kidd, G., Avila, R. L., Kirschner, D. A., & Macklin, W. B. (2008). Constitutively active Akt induces enhanced myelination in the CNS. *The Journal of neuroscience : the official journal of the Society for Neuroscience*, *28*(28), 7174–7183.

Ford, K. J., & Feller, M. B. (2012). Assembly and disassembly of a retinal cholinergic network. *Visual neuroscience*, *29*(1), 61–71.

Fried, S. I., Münch, T. A., & Werblin, F. S. (2002). Mechanisms and circuitry underlying directional selectivity in the retina. *Nature*, *420*(6914), 411–414.

Fruman, D. A., Chiu, H., Hopkins, B. D., Bagrodia, S., Cantley, L. C., & Abraham, R. T. (2017). The PI3K Pathway in Human Disease. *Cell*, *170*(4), 605–635.

Gallent, E. A., & Steward, O. (2018). Neuronal PTEN deletion in adult cortical neurons triggers progressive growth of cell bodies, dendrites, and axons. *Experimental neurology*, *303*, 12–28.

Galli-Resta, L., Resta, G., Tan, S. S., & Reese, B. E. (1997). Mosaics of islet-1-expressing amacrine cells assembled by short-range cellular interactions. *The Journal of neuroscience : the official journal of the Society for Neuroscience*, *17*(20), 7831–7838.

Getz, S. A., Tariq, K., Marchand, D. H., Dickson, C. R., Howe Vi, J. R., Skelton, P. D., Wang, W., Li, M., Barry, J. M., Hong, J., & Luikart, B. W. (2022). PTEN Regulates Dendritic Arborization by Decreasing Microtubule Polymerization Rate. *The Journal of neuroscience : the official journal of the Society for Neuroscience*, *42*(10), 1945–1957.

Goberdhan, D. C., Paricio, N., Goodman, E. C., Mlodzik, M., & Wilson, C. (1999). Drosophila tumor suppressor PTEN controls cell size and number by antagonizing the Chico/PI3-kinase signaling pathway. *Genes & development*, *13*(24), 3244–3258.

Goffin, A., Hoefsloot, L. H., Bosgoed, E., Swillen, A., & Fryns, J. P. (2001). PTEN mutation in a family with Cowden syndrome and autism. *American journal of medical genetics*, *105*(6), 521–524.

Golgi, C. (1873). *Sulla struttura della sostanza grigia del cervello*. Gazzetta Medica Italiana Lombardia, 33, 244–246.

Grove, J., Ripke, S., Als, T. D., Mattheisen, M., Walters, R. K., Won, H., Pallesen, J., Agerbo, E., Andreassen, O. A., Anney, R., Awashti, S., Belliveau, R., Bettella, F., Buxbaum, J. D., Bybjerg-Grauholm, J., Bækvad-Hansen, M., Cerrato, F., Chambert, K., Christensen, J. H., Churchhouse, C., … Børglum, A. D. (2019). Identification of common genetic risk variants for autism spectrum disorder. *Nature genetics*, *51*(3), 431–444.

Grueber, W. B., Jan, L. Y., & Jan, Y. N. (2002). Tiling of the Drosophila epidermis by multidendritic sensory neurons. *Development (Cambridge, England)*, *129*(12), 2867–2878.

Grueber, W. B., Jan, L. Y., & Jan, Y. N. (2003). Different levels of the homeodomain protein cut regulate distinct dendrite branching patterns of Drosophila multidendritic neurons. *Cell*, *112*(6), 805–818.

Gu, H., Zou, Y. R., & Rajewsky, K. (1993). Independent control of immunoglobulin switch recombination at individual switch regions evidenced through Cre-loxP-mediated gene targeting. *Cell*, 73(6), 1155–1164.

Guo, X., Snider, W. D., & Chen, B. (2016). GSK3β regulates AKT-induced central nervous system axon regeneration via an eIF2Bε-dependent, mTORC1-independent pathway. *eLife*, *5*, e11903.

Gupta, C., Jogdand, D. S., & Kumar, M. (2022). Reviewing the Impact of Social Media on the Mental Health of Adolescents and Young Adults. *Cureus*, *14*(10), e30143.

Hawkins, P. T., Anderson, K. E., Davidson, K., & Stephens, L. R. (2006). Signalling through Class I PI3Ks in mammalian cells. *Biochemical Society transactions*, *34*(Pt 5), 647–662. Kwon, T., Kwon, D. Y., Chun, J., Kim, J. H., & Kang, S. S. (2000). Akt protein kinase inhibits Rac1-GTP binding through phosphorylation at serine 71 of Rac1. *The Journal of biological chemistry*, *275*(1), 423–428.

Hayden, S. A., Mills, J. W., & Masland, R. M. (1980). Acetylcholine synthesis by displaced amacrine cells. *Science (New York, N.Y.)*, *210*(4468), 435–437.

Hernandez, O., Way, S., McKenna, J., 3rd, & Gambello, M. J. (2007). Generation of a conditional disruption of the Tsc2 gene. *Genesis (New York, N.Y. : 2000)*, *45*(2), 101–106.

His, W. (1889). *Die Neuroblasten und deren Entstehung im embryonalen Mark* (Vol. 15). S. Hirzel.

Hollidge, B. S., Carroll, H. B., Qian, R., Fuller, M. L., Giles, A. R., Mercer, A. C., Danos, O., Liu, Y., Bruder, J. T., & Smith, J. B. (2022). Kinetics and durability of transgene expression after intrastriatal injection of AAV9 vectors. *Frontiers in neurology*, *13*, 1051559.

Horvitz, H. R., & Sternberg, P. W. (1982). Nematode postembryonic cell lineages. *Journal of Nematology*, *14*(2), 240.

Hu, B., Zhang, Y., Zeng, Q., Han, Q., Zhang, L., Liu, M., & Li, X. (2014). Intravitreal injection of ranibizumab and CTGF shRNA improves retinal gene expression and microvessel ultrastructure in a rodent model of diabetes. *International journal of molecular sciences*, *15*(1), 1606–1624.

Ing-Esteves, S., & Lefebvre, J. L. (2024). Gamma-protocadherins regulate dendrite self-recognition and dynamics to drive self-avoidance. *Current biology : CB*, *34*(18), 4224–4239.e4.

Inoki, K., Li, Y., Zhu, T., Wu, J., & Guan, K. L. (2002). TSC2 is phosphorylated and inhibited by Akt and suppresses mTOR signalling. *Nature cell biology*, *4*(9), 648–657.

Inoki, K., Zhu, T., & Guan, K. L. (2003). TSC2 mediates cellular energy response to control cell growth and survival. *Cell*, *115*(5), 577–590.

James, R. E., Hamilton, N. R., Huffman, L. N., Brown, M. P., Neckles, V. N., Pasterkamp, R. J., Goff, L. A., & Kolodkin, A. L. (2024). Retinal ganglion cell-derived semaphorin 6A segregates starburst amacrine cell dendritic scaffolds to organize the mouse inner retina. *Development (Cambridge, England)*, *151*(22), dev204293.

Jan, Y. N., & Jan, L. Y. (2003). The control of dendrite development. *Neuron*, *40*(2), 229-242.

Jiang, H., Guo, W., Liang, X., & Rao, Y. (2005). Both the establishment and the maintenance of neuronal polarity require active mechanisms: critical roles of GSK-3beta and its upstream regulators. *Cell*, *120*(1), 123–135.

Jinushi-Nakao, S., Arvind, R., Amikura, R., Kinameri, E., Liu, A. W., & Moore, A. W. (2007). Knot/Collier and cut control different aspects of dendrite cytoskeleton and synergize to define final arbor shape. *Neuron*, *56*(6), 963–978.

Jo, H. S., Kang, K. H., Joe, C. O., & Kim, J. W. (2012). Pten coordinates retinal neurogenesis by regulating Notch signalling. *The EMBO journal*, *31*(4), 817–828.

Joo, W., Hippenmeyer, S., & Luo, L. (2014). Neurodevelopment. Dendrite morphogenesis depends on relative levels of NT-3/TrkC signaling. *Science (New York, N.Y.)*, *346*(6209), 626–629.

Kath, C., Goni-Oliver, P., Müller, R., Schultz, C., Haucke, V., Eickholt, B., & Schmoranzer, J. (2018). PTEN suppresses axon outgrowth by down-regulating the level of detyrosinated microtubules. *PloS one*, *13*(4), e0193257.

Kay, J. N., Chu, M. W., & Sanes, J. R. (2012). MEGF10 and MEGF11 mediate homotypic interactions required for mosaic spacing of retinal neurons. *Nature*, *483*(7390), 465–469.

Keeley, P. W., Whitney, I. E., Raven, M. A., & Reese, B. E. (2007). Dendritic spread and functional coverage of starburst amacrine cells. *The Journal of comparative neurology*, *505*(5), 539–546.

Kelliher, M. T., Saunders, H. A., & Wildonger, J. (2019). Microtubule control of functional architecture in neurons. *Current opinion in neurobiology*, *57*, 39–45.

Kilo, L., Stürner, T., Tavosanis, G., & Ziegler, A. B. (2021). Drosophila Dendritic Arborisation Neurons: Fantastic Actin Dynamics and Where to Find Them. *Cells*, *10*(10), 2777.

Kim, H. J., Woo, H. M., Ryu, J., Bok, J., Kim, J. W., Choi, S. B., Park, M. H., Park, H. Y., & Koo, S. K. (2013). Conditional deletion of pten leads to defects in nerve innervation and neuronal survival in inner ear development. *PloS one*, *8*(2), e55609.

Kim, I. J., Zhang, Y., Yamagata, M., Meister, M., & Sanes, J. R. (2008). Molecular identification of a retinal cell type that responds to upward motion. *Nature*, *452*(7186), 478–482.

Kosillo, P., Ahmed, K. M., Aisenberg, E. E., Karalis, V., Roberts, B. M., Cragg, S. J., & Bateup, H. S. (2022). Dopamine neuron morphology and output are differentially controlled by mTORC1 and mTORC2. *eLife*, *11*, e75398.

Kostadinov, D., & Sanes, J. R. (2015). Protocadherin-dependent dendritic self-avoidance regulates neural connectivity and circuit function. *eLife*, *4*, e08964.

Kotani, K., Ogawa, W., Hino, Y., Kitamura, T., Ueno, H., Sano, W., Sutherland, C., Granner, D. K., & Kasuga, M. (1999). Dominant negative forms of Akt (protein kinase B) and atypical protein kinase Clambda do not prevent insulin inhibition of phosphoenolpyruvate carboxykinase gene transcription. *The Journal of biological chemistry*, *274*(30), 21305–21312.

Kowalczyk, M., Lee, Y. J., & Huang, W. H. (2025). TSC2-mTORC1 axis regulates morphogenesis and neurological function of $Gli1^{+}$ adult-born dentate granule cells. *Molecular biology of the cell*, *36*(1), br1.

Kreis, P., Leondaritis, G., Lieberam, I., & Eickholt, B. J. (2014). Subcellular targeting and dynamic regulation of PTEN: implications for neuronal cells and neurological disorders. *Frontiers in molecular neuroscience*, *7*, 23.

Kwan K. M. (2002). Conditional alleles in mice: practical considerations for tissue-specific knockouts. *Genesis (New York, N.Y. : 2000)*, *32*(2), 49–62.

Kwon, C. H., Luikart, B. W., Powell, C. M., Zhou, J., Matheny, S. A., Zhang, W., Li, Y., Baker, S. J., & Parada, L. F. (2006). Pten regulates neuronal arborization and social interaction in mice. *Neuron*, *50*(3), 377–388.

Kwon, C. H., Zhu, X., Zhang, J., Knoop, L. L., Tharp, R., Smeyne, R. J., Eberhart, C. G., Burger, P. C., & Baker, S. J. (2001). Pten regulates neuronal soma size: a mouse model of Lhermitte-Duclos disease. *Nature genetics*, *29*(4), 404–411.

Kwon, T., Kwon, D. Y., Chun, J., Kim, J. H., & Kang, S. S. (2000). Akt protein kinase inhibits Rac1-GTP binding through phosphorylation at serine 71 of Rac1. *The Journal of biological chemistry*, *275*(1), 423–428.

Lasser, M., Tiber, J., & Lowery, L. A. (2018). The Role of the Microtubule Cytoskeleton in Neurodevelopmental Disorders. *Frontiers in cellular neuroscience*, *12*, 165.

Lee, S., & Zhou, Z. J. (2006). The synaptic mechanism of direction selectivity in distal processes of starburst amacrine cells. *Neuron*, *51*(6), 787–799.

Lee, T., & Luo, L. (1999). Mosaic analysis with a repressible cell marker for studies of gene function in neuronal morphogenesis. *Neuron*, *22*(3), 451–461.

Lefebvre, J. L., Kostadinov, D., Chen, W. V., Maniatis, T., & Sanes, J. R. (2012). Protocadherins mediate dendritic self-avoidance in the mammalian nervous system. *Nature*, *488*(7412), 517–521.

Lefebvre, J. L., Sanes, J. R., & Kay, J. N. (2015). Development of dendritic form and function. *Annual review of cell and developmental biology*, *31*(1), 741-777.

Li, J., Yen, C., Liaw, D., Podsypanina, K., Bose, S., Wang, S. I., Puc, J., Miliaresis, C., Rodgers, L., McCombie, R., Bigner, S. H., Giovanella, B. C., Ittmann, M., Tycko, B., Hibshoosh, H., Wigler, M. H., & Parsons, R. (1997). PTEN, a putative protein tyrosine phosphatase gene mutated in human brain, breast, and prostate cancer. *Science (New York, N.Y.)*, *275*(5308), 1943–1947.

Li, L., Liu, F., Salmonsen, R. A., Turner, T. K., Litofsky, N. S., Di Cristofano, A., Pandolfi, P. P., Jones, S. N., Recht, L. D., & Ross, A. H. (2002). PTEN in neural precursor cells: regulation of migration, apoptosis, and proliferation. *Molecular and cellular neurosciences*, *20*(1), 21–29.

Li, W., Wang, F., Menut, L., & Gao, F. B. (2004). BTB/POZ-zinc finger protein abrupt suppresses dendritic branching in a neuronal subtype-specific and dosage-dependent manner. *Neuron*, *43*(6), 823–834.

Li, Z., Dong, X., Wang, Z., Liu, W., Deng, N., Ding, Y., Tang, L., Hla, T., Zeng, R., Li, L., & Wu, D. (2005). Regulation of PTEN by Rho small GTPases. *Nature cell biology*, *7*(4), 399–404.

Li, Z., Dong, X., Wang, Z., Liu, W., Deng, N., Ding, Y., Tang, L., Hla, T., Zeng, R., Li, L., & Wu, D. (2005). Regulation of PTEN by Rho small GTPases. *Nature cell biology*, *7*(4), 399–404.

Lian, Y. L., & Lin, Y. C. (2024). The emerging tools for precisely manipulating microtubules. *Current opinion in cell biology*, *88*, 102360.

Litchfield D. W. (2003). Protein kinase CK2: structure, regulation and role in cellular decisions of life and death. *The Biochemical journal*, *369*(Pt 1), 1–15.

Liu, I. S., Chen, J. D., Ploder, L., Vidgen, D., van der Kooy, D., Kalnins, V. I., & McInnes, R. R. (1994). Developmental expression of a novel murine homeobox gene (Chx10): evidence for roles in determination of the neuroretina and inner nuclear layer. *Neuron*, *13*(2), 377–393.

Liu, O. W., & Shen, K. (2012). The transmembrane LRR protein DMA-1 promotes dendrite branching and growth in C. elegans. *Nature neuroscience*, *15*(1), 57-63.

Liu, W., & Cvekl, A. (2017). Six3 in a small population of progenitors at E8.5 is required for neuroretinal specification via regulating cell signaling and survival in mice. *Developmental biology*, *428*(1), 164–175.

López-Muñoz, F., Boya, J., & Alamo, C. (2006). Neuron theory, the cornerstone of neuroscience, on the centenary of the Nobel Prize award to Santiago Ramón y Cajal. *Brain research bulletin*, *70*(4-6), 391–405.

Luikart, B. W., Schnell, E., Washburn, E. K., Bensen, A. L., Tovar, K. R., & Westbrook, G. L. (2011). Pten knockdown in vivo increases excitatory drive onto dentate granule cells. *The Journal of neuroscience : the official journal of the Society for Neuroscience*, *31*(11), 4345–4354.

Luo L. (2000). Rho GTPases in neuronal morphogenesis. *Nature reviews. Neuroscience*, *1*(3), 173–180.

Manning, B. D., & Toker, A. (2017). AKT/PKB Signaling: Navigating the Network. *Cell*, *169*(3), 381–405.

Mariotto, S., Bentivoglio, M., Cotrufo, T., Berzero, A., Monaco, S., Mazzarello, P., & Ferrari, S. (2018). Clinical Neuropathology image 1-2018: Golgi silver staining, the black reaction. *Clinical neuropathology*, *37*(1), 4–5.

Masland, R. H. (2005). The many roles of starburst amacrine cells. *Trends in Neurosciences*, *28*(8), 395-396.

Meyer Zu Reckendorf, S., Moser, D., Blechschmidt, A., Joga, V. N., Sinske, D., Hegler, J., Deininger, S., Catanese, A., Vettorazzi, S., Antoniadis, G., Boeckers, T., & Knöll, B. (2022). Motoneuron-Specific PTEN Deletion in Mice Induces Neuronal Hypertrophy and Also Regeneration after Facial Nerve Injury. *The Journal of neuroscience : the official journal of the Society for Neuroscience*, *42*(12), 2474–2491.

Minsky, M. (1988). Memoir on inventing the confocal scanning microscope. *Scanning*, 10(4), 128–138.

Misra, S., Ghosh, G., Chowdhury, S. G., & Karmakar, P. (2021). Non-canonical function of nuclear PTEN and its implication on tumorigenesis. *DNA repair*, *107*, 103197.

Morrie, R. D., & Feller, M. B. (2018). A Dense Starburst Plexus Is Critical for Generating Direction Selectivity. *Current biology : CB*, *28*(8), 1204–1212.e5.

Nguyen, L. H., Xu, Y., Nair, M., & Bordey, A. (2024). The mTOR pathway genes *MTOR*, *Rheb*, *Depdc5*, *Pten*, and *Tsc1* have convergent and divergent impacts on cortical neuron development and function. *eLife*, *12*, RP91010.

Oinuma, I., Ito, Y., Katoh, H., & Negishi, M. (2010). Semaphorin 4D/Plexin-B1 stimulates PTEN activity through R-Ras GTPase-activating protein activity, inducing growth cone collapse in hippocampal neurons. *The Journal of biological chemistry*, *285*(36), 28200–28209.

Oren-Suissa, M., Hall, D. H., Treinin, M., Shemer, G., & Podbilewicz, B. (2010). The fusogen EFF-1 controls sculpting of mechanosensory dendrites. *Science*, *328*(5983), 1285-1288.

Palade, G. E., Palay, S.L. (1954). Electron microscope observations of interneuronal and neuromuscular synapses. *Anat Rec*, *118*, 335-336.

Palavalli, A., Tizón-Escamilla, N., Rupprecht, J. F., & Lecuit, T. (2021). Deterministic and Stochastic Rules of Branching Govern Dendrite Morphogenesis of Sensory Neurons. *Current biology : CB*, *31*(3), 459–472.e4.

Park, H., Lee, S., Shrestha, P., Kim, J., Park, J. A., Ko, Y., Ban, Y. H., Park, D. Y., Ha, S. J., Koh, G. Y., Hong, V. S., Mochizuki, N., Kim, Y. M., Lee, W., & Kwon, Y. G. (2015). AMIGO2, a novel membrane anchor of PDK1, controls cell survival and angiogenesis via Akt activation. *The Journal of cell biology*, *211*(3), 619–637.

Parrish, J. Z., Kim, M. D., Jan, L. Y., & Jan, Y. N. (2006). Genome-wide analyses identify transcription factors required for proper morphogenesis of Drosophila sensory neuron dendrites. *Genes & development*, *20*(7), 820–835.

Peng, Y. R., James, R. E., Yan, W., Kay, J. N., Kolodkin, A. L., & Sanes, J. R. (2020). Binary Fate Choice between Closely Related Interneuronal Types Is Determined by a Fezf1-Dependent Postmitotic Transcriptional Switch. *Neuron*, *105*(3), 464–474.e6. https://doi.org/10.1016/j.neuron.2019.11.002

Prigge, C. L., Dembla, M., Sharma, A., El-Quessny, M., Kozlowski, C., Paisley, C. E., Miltner, A. M., Johnson, T. M., Della Santina, L., Feller, M. B., & Kay, J. N. (2023). Rejection of inappropriate synaptic partners in mouse retina mediated by transcellular FLRT2-UNC5 signaling. *Developmental cell*, *58*(20), 2080–2096.e7.

Rademacher, S., & Eickholt, B. J. (2019). PTEN in Autism and Neurodevelopmental Disorders. *Cold Spring Harbor perspectives in medicine*, *9*(11), a036780.

Ramón y Cajal, S. (1888). *Estructura de los centros nerviosos de las aves*.

Ramón y Cajal, S. (1923). *Recuerdos de mi vida*. Proyecto Gutemberg.

Ray, T. A., Roy, S., Kozlowski, C., Wang, J., Cafaro, J., Hulbert, S. W., Wright, C. V., Field, G. D., & Kay, J. N. (2018). Formation of retinal direction-selective circuitry initiated by starburst amacrine cell homotypic contact. *eLife*, *7*, e34241.

Rebholz, H., Zhou, M., Nairn, A. C., Greengard, P., & Flajolet, M. (2013). Selective knockout of the casein kinase 2 in d1 medium spiny neurons controls dopaminergic function. *Biological psychiatry*, *74*(2), 113–121.

Reimsnider, S., Manfredsson, F. P., Muzyczka, N., & Mandel, R. J. (2007). Time course of transgene expression after intrastriatal pseudotyped rAAV2/1, rAAV2/2, rAAV2/5, and rAAV2/8 transduction in the rat. *Molecular therapy : the journal of the American Society of Gene Therapy*, *15*(8), 1504–1511.

Ren, S., Luo, Y., Chen, H., Warburton, D., Lam, H. C., Wang, L. L., Chen, P., Henske, E. P., & Shi, W. (2016). Inactivation of Tsc2 in Mesoderm-Derived Cells Causes Polycystic Kidney Lesions and Impairs Lung Alveolarization. *The American journal of pathology*, *186*(12), 3261–3272.

Rodieck R. W. (1989). Starburst amacrine cells of the primate retina. *The Journal of comparative neurology*, *285*(1), 18–37. https://doi.org/10.1002/cne.902850104

Rossi, J., Balthasar, N., Olson, D., Scott, M., Berglund, E., Lee, C. E., Choi, M. J., Lauzon, D., Lowell, B. B., & Elmquist, J. K. (2011). Melanocortin-4 receptors expressed by cholinergic neurons regulate energy balance and glucose homeostasis. *Cell metabolism*, *13*(2), 195–204.

Sadowski P. D. (1995). The Flp recombinase of the 2-microns plasmid of Saccharomyces cerevisiae. *Progress in nucleic acid research and molecular biology*, *51*, 53–91.

Sakagami, K., Chen, B., Nusinowitz, S., Wu, H., & Yang, X. J. (2012). PTEN regulates retinal interneuron morphogenesis and synaptic layer formation. *Molecular and cellular neurosciences*, *49*(2), 171–183.

Sanchez, T., Thangada, S., Wu, M. T., Kontos, C. D., Wu, D., Wu, H., & Hla, T. (2005). PTEN as an effector in the signaling of antimigratory G protein-coupled receptor. *Proceedings of the National Academy of Sciences of the United States of America*, *102*(12), 4312–4317.

Santos, V. R., Pun, R. Y. K., Arafa, S. R., LaSarge, C. L., Rowley, S., Khademi, S., Bouley, T., Holland, K. D., Garcia-Cairasco, N., & Danzer, S. C. (2017). PTEN deletion increases hippocampal granule cell excitability in male and female mice. *Neurobiology of disease*, *108*, 339–351.

Satterstrom, F. K., Kosmicki, J. A., Wang, J., Breen, M. S., De Rubeis, S., An, J. Y., Peng, M., Collins, R., Grove, J., Klei, L., Stevens, C., Reichert, J., Mulhern, M. S., Artomov, M., Gerges, S., Sheppard, B., Xu, X., Bhaduri, A., Norman, U., Brand, H., … Buxbaum, J. D. (2020). Large-Scale Exome Sequencing Study Implicates Both Developmental and Functional Changes in the Neurobiology of Autism. *Cell*, *180*(3), 568–584.e23.

Schmidt-Supprian, M., & Rajewsky, K. (2007). Vagaries of conditional gene targeting. *Nature immunology*, *8*(7), 665–668.

Schmidt, M., Humphrey, M. F., & Wässle, H. (1987). Action and localization of acetylcholine in the cat retina. *Journal of neurophysiology*, *58*(5), 997–1015.

Schneeberger, M., Parolari, L., Das Banerjee, T., Bhave, V., Wang, P., Patel, B., Topilko, T., Wu, Z., Choi, C. H. J., Yu, X., Pellegrino, K., Engel, E. A., Cohen, P., Renier, N., Friedman, J. M., & Nectow, A. R. (2019). Regulation of Energy Expenditure by Brainstem GABA Neurons. *Cell*, *178*(3), 672–685.e12.

Sethuramanujam, S., McLaughlin, A. J., deRosenroll, G., Hoggarth, A., Schwab, D. J., & Awatramani, G. B. (2016). A Central Role for Mixed Acetylcholine/GABA Transmission in Direction Coding in the Retina. *Neuron*, *90*(6), 1243–1256.

Sherrington, C.S. (1906). The integrative action of the nervous system. New Haven, CT. *Yale University Press*.

Shree, S., Sutradhar, S., Trottier, O., Tu, Y., Liang, X., & Howard, J. (2022). Dynamic instability of dendrite tips generates the highly branched morphologies of sensory neurons. *Science Advances*, *8*(26), eabn0080.

Skelton, P. D., Stan, R. V., & Luikart, B. W. (2020). The Role of PTEN in Neurodevelopment. *Molecular neuropsychiatry*, *5*(Suppl 1), 60–71.

Smith, C. J., Watson, J. D., Spencer, W. C., O'Brien, T., Cha, B., Albeg, A., ... & Miller III, D. M. (2010). Time-lapse imaging and cell-specific expression profiling reveal dynamic branching and molecular determinants of a multi-dendritic nociceptor in C. elegans. *Developmental biology*, *345*(1), 18-33.

Soto, F., Tien, N. W., Goel, A., Zhao, L., Ruzycki, P. A., & Kerschensteiner, D. (2019). AMIGO2 Scales Dendrite Arbors in the Retina. *Cell reports*, *29*(6), 1568–1578.e4.

Spinelli, L., Black, F. M., Berg, J. N., Eickholt, B. J., & Leslie, N. R. (2015). Functionally distinct groups of inherited PTEN mutations in autism and tumour syndromes. *Journal of medical genetics*, *52*(2), 128–134.

Stankiewicz, T. R., & Linseman, D. A. (2014). Rho family GTPases: key players in neuronal development, neuronal survival, and neurodegeneration. *Frontiers in cellular neuroscience*, *8*, 314.

Steck, P. A., Pershouse, M. A., Jasser, S. A., Yung, W. K., Lin, H., Ligon, A. H., Langford, L. A., Baumgard, M. L., Hattier, T., Davis, T., Frye, C., Hu, R., Swedlund, B., Teng, D. H., &

Tavtigian, S. V. (1997). Identification of a candidate tumour suppressor gene, MMAC1, at chromosome 10q23.3 that is mutated in multiple advanced cancers. *Nature genetics*, *15*(4), 356–362.

Sugimura, K., Satoh, D., Estes, P., Crews, S., & Uemura, T. (2004). Development of morphological diversity of dendrites in Drosophila by the BTB-zinc finger protein abrupt. *Neuron*, *43*(6), 809–822.

Sulston, J. E., & Horvitz, H. R. (1977). Post-embryonic cell lineages of the nematode, Caenorhabditis elegans. *Developmental biology*, *56*(1), 110-156.

Sun, L. O., Jiang, Z., Rivlin-Etzion, M., Hand, R., Brady, C. M., Matsuoka, R. L., Yau, K. W., Feller, M. B., & Kolodkin, A. L. (2013). On and off retinal circuit assembly by divergent molecular mechanisms. *Science (New York, N.Y.)*, *342*(6158), 1241974.

Sun, Y. J., Espinosa, J. S., Hoseini, M. S., & Stryker, M. P. (2019). Experience-dependent structural plasticity at pre- and postsynaptic sites of layer 2/3 cells in developing visual cortex. *Proceedings of the National Academy of Sciences of the United States of America*, *116*(43), 21812–21820.

Sundararajan, L., Stern, J., & Miller III, D. M. (2019). Mechanisms that regulate morphogenesis of a highly branched neuron in C. elegans. *Developmental Biology*, *451*(1), 53-67.

Tachibana, N., Cantrup, R., Dixit, R., Touahri, Y., Kaushik, G., Zinyk, D., Daftarian, N., Biernaskie, J., McFarlane, S., & Schuurmans, C. (2016). Pten Regulates Retinal Amacrine Cell Number by Modulating Akt, Tgfβ, and Erk Signaling. *The Journal of neuroscience : the official journal of the Society for Neuroscience*, *36*(36), 9454–9471.

Tariq, K., Cullen, E., Getz, S. A., Conching, A. K. S., Goyette, A. R., Prina, M. L., Wang, W., Li, M., Weston, M. C., & Luikart, B. W. (2022). Disruption of mTORC1 rescues neuronal overgrowth and synapse function dysregulated by Pten loss. *Cell reports*, *41*(5), 111574.

Tauchi, M., & Masland, R. H. (1984). The shape and arrangement of the cholinergic neurons in the rabbit retina. *Proceedings of the Royal Society of London. Series B, Biological sciences*, *223*(1230), 101–119.

Taylor, W. R., & Smith, R. G. (2012). The role of starburst amacrine cells in visual signal processing. *Visual neuroscience*, *29*(1), 73-81.

Torres, J., & Pulido, R. (2001). The tumor suppressor PTEN is phosphorylated by the protein kinase CK2 at its C terminus. Implications for PTEN stability to proteasome-mediated degradation. *The Journal of biological chemistry*, *276*(2), 993–998.

Tortosa, E., Galjart, N., Avila, J., & Sayas, C. L. (2013). MAP1B regulates microtubule dynamics by sequestering EB1/3 in the cytosol of developing neuronal cells. *The EMBO journal*, *32*(9), 1293–1306.

Touahri, Y., Hanna, J., Tachibana, N., Okawa, S., Liu, H., David, L. A., Olender, T., Vasan, L., Pak, A., Mehta, D. N., Chinchalongporn, V., Balakrishnan, A., Cantrup, R., Dixit, R., Mattar, P., Saleh, F., Ilnytskyy, Y., Murshed, M., Mains, P. E., Kovalchuk, I., … Schuurmans, C. (2024). Pten regulates endocytic trafficking of cell adhesion and Wnt signaling molecules to pattern the retina. *Cell reports*, *43*(4), 114005.

Tsalik, E. L., Niacaris, T., Wenick, A. S., Pau, K., Avery, L., & Hobert, O. (2003). LIM homeobox gene-dependent expression of biogenic amine receptors in restricted regions of the C. elegans nervous system. *Developmental biology*, *263*(1), 81-102.

Urwyler, O., Izadifar, A., Vandenbogaerde, S., Sachse, S., Misbaer, A., & Schmucker, D. (2019). Branch-restricted localization of phosphatase Prl-1 specifies axonal synaptogenesis domains. *Science (New York, N.Y.)*, *364*(6439), eaau9952.

van Slegtenhorst, M., Nellist, M., Nagelkerken, B., Cheadle, J., Snell, R., van den Ouweland, A., Reuser, A., Sampson, J., Halley, D., & van der Sluijs, P. (1998). Interaction between hamartin and tuberin, the TSC1 and TSC2 gene products. *Human molecular genetics*, *7*(6), 1053–1057.

Vazquez, F., Grossman, S. R., Takahashi, Y., Rokas, M. V., Nakamura, N., & Sellers, W. R. (2001). Phosphorylation of the PTEN tail acts as an inhibitory switch by preventing its recruitment into a protein complex. *The Journal of biological chemistry*, *276*(52), 48627–48630.

Veldman, M. B., Park, C. S., Eyermann, C. M., Zhang, J. Y., Zuniga-Sanchez, E., Hirano, A. A., Daigle, T. L., Foster, N. N., Zhu, M., Langfelder, P., Lopez, I. A., Brecha, N. C., Zipursky, S. L., Zeng, H., Dong, H. W., & Yang, X. W. (2020). Brainwide Genetic Sparse Cell Labeling to Illuminate the Morphology of Neurons and Glia with Cre-Dependent MORF Mice. *Neuron*, *108*(1), 111–127.e6.

Voigt T. (1986). Cholinergic amacrine cells in the rat retina. *The Journal of comparative neurology*, *248*(1), 19–35.

Voinescu, P. E., Kay, J. N., & Sanes, J. R. (2009). Birthdays of retinal amacrine cell subtypes are systematically related to their molecular identity and soma position. *The Journal of comparative neurology*, *517*(5), 737–750.

Waldeyer, W. (1891). Ueber einige neuere Forschungen im Gebiete der Anatomie des Centralnervensystems1. *DMW-Deutsche Medizinische Wochenschrift*, *17*(44), 1213-1218.

Wässle, H., & Boycott, B. B. (1991). Functional architecture of the mammalian retina. *Physiological reviews*, *71*(2), 447-480.

Way, J. C., & Chalfie, M. (1989). The mec-3 gene of Caenorhabditis elegans requires its own product for maintained expression and is expressed in three neuronal cell types. *Genes & development*, *3*(12a), 1823-1833.

White, J. G., Horvitz, H. R., & Sulston, J. E. (1982). Neurone differentiation in cell lineage mutants of Caenorhabditis elegans. *Nature*, *297*(5867), 584-587.

Wit, C. B., & Hiesinger, P. R. (2023, January). Neuronal filopodia: From stochastic dynamics to robustness of brain morphogenesis. In *Seminars in Cell & Developmental Biology* (Vol. 133, pp. 10-19). Academic Press.

Wong, K. M., & Beirowski, B. (2018). Multiple lines of inhibitory feedback on AKT kinase in Schwann cells lacking TSC1/2 hint at distinct functions of mTORC1 and AKT in nerve development. *Communicative & integrative biology*, *11*(1), e1433441.

Worby, C. A., & Dixon, J. E. (2014). PTEN. *Annual review of biochemistry*, *83*, 641–669.

Yan, W., Laboulaye, M. A., Tran, N. M., Whitney, I. E., Benhar, I., & Sanes, J. R. (2020). Mouse retinal cell atlas: molecular identification of over sixty amacrine cell types. *Journal of Neuroscience*, *40*(27), 5177-5195.

Yang, C., Wu, J., de Heus, C., Grigoriev, I., Liv, N., Yao, Y., Smal, I., Meijering, E., Klumperman, J., Qi, R. Z., & Akhmanova, A. (2017). EB1 and EB3 regulate microtubule minus end organization and Golgi morphology. *The Journal of cell biology*, *216*(10), 3179–3198.

Yoshida, K., Watanabe, D., Ishikane, H., Tachibana, M., Pastan, I., & Nakanishi, S. (2001). A key role of starburst amacrine cells in originating retinal directional selectivity and optokinetic eye movement. *Neuron*, *30*(3), 771–780.

Yoshimura, T., Kawano, Y., Arimura, N., Kawabata, S., Kikuchi, A., & Kaibuchi, K. (2005). GSK-3beta regulates phosphorylation of CRMP-2 and neuronal polarity. *Cell*, *120*(1), 137–149.

Zeng, H., & Sanes, J. R. (2017). Neuronal cell-type classification: challenges, opportunities and the path forward. *Nature Reviews Neuroscience*, *18*(9), 530-546.

Zheng, J., Shen, W. H., Lu, T. J., Zhou, Y., Chen, Q., Wang, Z., Xiang, T., Zhu, Y. C., Zhang, C., Duan, S., & Xiong, Z. Q. (2008). Clathrin-dependent endocytosis is required for TrkB-dependent Akt-mediated neuronal protection and dendritic growth. *The Journal of biological chemistry*, *283*(19), 13280–13288.

Zincarelli, C., Soltys, S., Rengo, G., & Rabinowitz, J. E. (2008). Analysis of AAV serotypes 1-9 mediated gene expression and tropism in mice after systemic injection. *Molecular therapy : the journal of the American Society of Gene Therapy*, *16*(6), 1073–1080.

Zori, R. T., Boyar, F. Z., Williams, W. N., Gray, B. A., Bent-Williams, A., Stalker, H. J., Rimer, L. A., Nackashi, J. A., Driscoll, D. J., Rasmussen, S. A., Dixon-Wood, V., & Williams, C. A. (1998). Prevalence of 22q11 region deletions in patients with velopharyngeal insufficiency. *American journal of medical genetics*, *77*(1), 8–11.

Zou, W., Shen, A., Dong, X., Tugizova, M., Xiang, Y. K., & Shen, K. (2016). A multi-protein receptor-ligand complex underlies combinatorial dendrite guidance choices in C. elegans. *Elife*, *5*, e18345.